University of Padova

Department of Phyisics and Astronomy, Galileo Galilei

Master Thesis in Physics

Production of Thermal Axions across the ElectroWeak Phase Transition

Supervisor
Prof. Francesco D'Eramo
University of Padova

Master Candidate
Camilla Mupo

Student ID
2090446

Academic Year 2023-2024

A mamma, papà e Paola

Contents

Introduction

Theoretical frameworks for axion-like particles address outstanding questions in the physics of fundamental interactions. An astonishing experimental effort paves the way toward discoveries that could lead to remarkable advancements in the understanding of both particle interactions and the composition of our universe. Indeed the QCD axion provides an elegant solution to two well-known drawbacks of the standard model (SM) of particle physics: the strong CP problem and the observed dark matter abundance.

The introductory part of this thesis will present the strong CP problem and how the Peccei-Quinn mechanism provides a solution to these two open questions. The core of this work will be to investigate a complementary manifestation of the axion on cosmological scales. In particular, we will study an additional dark radiation component in the form of relativistic axions generated at high temperatures in the Early Universe, specifically around the ElectroWeak Phase Transition (EWPT). Thermal production could lead to a potentially observable axion contribution to the cosmic energy budget, conventionally parameterized by an effective number of additional neutrinos (Δ_{Neff}).

The main goal of this thesis is to predict the axion contribution to Δ_{Neff}. We will consider the relevant processes for the thermal production of axions and derive explicit expressions for cross-sections. We will compute them above and below the EWPT and will connect the results across this threshold. With these quantities then we feed the Boltzmann equations to derive Δ_{Neff}.

The last part of this research work involves the possibility of investigating the thermal production of axion dark radiation in momentum space. More specifically, we will introduce a new formalism based entirely on phase space analysis, presented in a model-independent way in [1]. We will apply this general formalism to axion dark radiation and outline the necessary steps needed for a phase-space analysis. So we provide the frameworks for future works meant to extract more accurate predictions for Δ_{Neff}. Current observations align with the SM prediction for Δ_{Neff}, yet upcoming experiments promise to refine bounds on this parameter and potentially discover deviations from the SM. In this context, the implications of our findings could be a significant step towards a more accurate prediction of the axion dark radiation impact on the effective number of neutrinos. If detected, this contribution could help to validate the axion's role in the ongoing exploration of physics beyond the SM.

In Chapter 1, we present the Strong CP Problem, a fundamental issue in Quantum Chromodynamics (QCD), which is our model for strong interactions. The problem arises from a contradiction between experimental results and theoretical expectations: the apparent violation of CP symmetry in the QCD Lagrangian, quantified by the θ term, is not detected experimentally, and one has to invoke a surprisingly small θ parameter to account for experimental bounds.

In Chapter 2, the axion is presented as a solution to this problem. The key ingredient is a new scalar field, a, introduced within an effective field theory (EFT) framework, characterised by a suppressing energy scale f_a which sets the limit to its validity. The low-energy behavior of the axion potential drives the field to the CP-conserving minimum, effectively setting the θ term to zero, thereby dynamically solving the Strong CP Problem. We complete the discussion with the main features of some candidate models in the search for an axion Quantum Field Theory (QFT) that could serve as the high-energy completion of the axion effective Lagrangian.

Some cosmological implications of the axion are briefly explored in Chapter 3. In particular, its production as a cold relic through the misalignment mechanism, which makes the axion a viable dark matter candidate, is presented. Furthermore, axion interactions with thermal bath particles can lead to a population of axions that, if the mass is small enough, can still be relativistic around recombination and contribute as an additional component to the radiation at the stage of CMB formation—this is known as axion dark radiation.

Chapter 4 is devoted to exploring the thermal production of axions across the electroweak phase transition (EWPT). Starting from the axion Lagrangian, we derive the necessary couplings and collect the relevant scattering processes involving third-generation fermions (top and bottom quarks). Explicit expressions for the cross sections both above and below the EWPT are provided and analytically matched at this threshold.

In Chapter 5 we solve the Boltzmann equations for axion (comoving) number density using the canonical approach. First, thermally averaged cross sections are evaluated both above and below the EWPT and then smoothly connected. Then, the numerical solution is derived and connected to ΔN_{eff}. The results are summed up in some plots showing ΔN_{eff} as a function of the axion scale f_a for top and bottom couplings.

The last chapter (6) is devoted to the perspective of a phase-space anlysis. We present the steps to build an integro-differential system that allows tracking the phase-space distribution function's evolution in an expanding Universe, while accounting for the feedback on the thermal bath as well. This formalism, when adapted to the case of axion dark radiation, serves as the foundation for a phase-space analysis aimed at providing a more detailed and accurate predic-

tion of axion production across the EWPT. In particular, we implement a code using Python in order to numerically integrate the Boltzmann system. Given this, new preliminary results for ΔN_{eff} are derived.

Finally this work is complemented by four appendices that have been useful for writing the thesis and are meant to be a support in its reading. They cover different aspects: a brief summary on the Standard Model (A), detailed calculations for the scattering cross sections (B), the derivation of the Boltzmann equation in the number density approach (C), and some hints of the code that we employed to solve the phase-space evolution (D).

1

Strong CP Problem

The Standard Model of particle physics serves as a powerful tool for explaining experimental observations, yet it is affected by the presence of some theoretical shortcomings related to the appearance of small numbers, leading to 'naturalness issues'. Among these challenges lies the strong CP problem, which question the absence of significant violation of CP simmetry in QCD despite theoretical expectations. The axion emerges as the most valued solution to such inconsistency.

In the first paragraph 1.1 we present the QCD Lagrangian in its CP invariant form which is generally used to get experimental predictions. Then we sum up the topics of discrete symmetries with the remarkable result of CPT theorem (1.1.1) and of global symmetries (1.1.2) in the SM.

In the second part 1.2 we introduce the two CP violating terms in the Lagrangian showing how they can be related and reduced to the single 'topological' term, whose relevance is enlightened: despite being initially considered negligible, its significance emerged through the discovery of instanton solutions, that we briefly sketch in 1.2.1.

The most important observations supporting the existence of the strong CP problem is the remarkably small neutron electric dipole moment (nEDM). This experimental result, that constraints the possible violation of CP symmetry within QCD, is shortly presented in the last paragraph 1.2.2.

1.1 QCD Lagrangian part I

Quantum chromodynamics (QCD) is the theory of strong interactions. Its Lagrangian, in the form that is usually engaged in the experimental sector, reads:

$$L_{QCD} = \sum_q \bar{q}(i\gamma_\mu D^\mu - m_q)q - \frac{1}{4}G^{a\mu\nu}G^a_{\mu\nu} \tag{1.1}$$

This expression is invariant under CP symmetry, reflecting what is empirically observed for QCD. Before diving further in this aspect is useful to address the topic of discrete and global symmetries in Particle Physics. The main reference for this part is [2].

1.1.1 Discrete symmetries

Let's sketch how quantum fields behave under the discrete space-time transformations of parity, i.e. space inversion $\vec{x} \to -\vec{x}$, time reversal $t \to -t$, and charge conjugation, which physically corresponds to reversing the sign of all charges $e \to -e$.

Parity

From classical considerations[1] we recover the transformation properties of the electromagnetic fields under the parity induced unitary operator, then we require scalar and pseudo-scalar fields to be respectively even and odd under parity and, finally, the behavior of spinors can be deduced requiring Dirac equation be invariant under it. We obtain:

$$\begin{aligned}
U(P)A^\mu(\vec{x},t)U(P)^{-1} &= \eta(\mu)A^\mu(-\vec{x},t)\\
U(P)S(\vec{x},t)U(P)^{-1} &= S(-\vec{x},t)\\
U(P)P(\vec{x},t)U(P)^{-1} &= -P(-\vec{x},t)\\
U(P)\psi(\vec{x},t)U(P)^{-1} &= \gamma_0\psi(-\vec{x},t)
\end{aligned}$$

with $\eta(\mu) = 1$ for $\mu = 0$ and $\eta(\mu) = -1$ otherwise. Given these, one deduces the transformation rules of fermion-antifermion bilinears and applies them to the currents in A.2.2. It turns that the electro-weak sector is parity violating: electromagnetism is parity invariant while, since

[1] The Lorentz force $\vec{F} = \frac{d\vec{p}}{dt} = q(\vec{E} + \vec{v} \times \vec{B})$ has to change sign under parity transformation, since $p \to -p$ as reversing the space coordinates.

parity exchange chiral fields, weak interactions are not. The strong interactions, however, are invariant under Parity.

Charge Conjugation

Charge conjugation phisically sends the electric charge $e \to -e$, this coincides for the vector potential to transform as:

$$U(C)A^{\mu}(x)U(C)^{-1} = -A^{\mu}(x)$$

Instead for Dirac fields, since charge conjugation should transform particles into antiparticles, this operation essentially corresponds to Hermitian conjugation:

$$U(C)\psi(x)U(C)^{-1} = C\psi(x)^{\dagger}$$

where C is defined requiring invariance of Dirac equation by the condition $C\gamma^{\mu *}C^{-1} = -\gamma^{\mu}$, and so depends on the form of the γ matrices used: in the Majorana base $C = 1$, whereas in the Dirac formalism $C = \gamma^2$. Again, deriving the transformation of fermionic bilinears we have that electromagnetic interactions are C-invariant. To guarantee invariance of the quark gluon interaction terms, since $SU(3)$ matrices λ_a get transposed in the bilinears, it is necessary to assume that the charge conjugation properties of the gluon fields themselves vary according to which component one is dealing with. We get:

$$U(C)A^{\mu}_{a}(x)U(C)^{-1} = -\eta(a)A^{\mu}_{a}(x)$$

where $\eta(a) = 1$ for the symmetric generators, $\eta(a) = -1$ for the anti-symmetric ones. Finally, the transformation properties of $SU(2)$ matrices imply that

$$U(C)\,W^{\mu}_{\pm}U(C)^{-1} = -\,W^{\mu}_{\mp}$$

Nevertheless, even so, as it is experimentally verified, the simultaneous presence of vector and pseudo-vector parts in the weak interacting currents, which are affected by C in different ways, drives us to conclude that they violate also charge conjugation.

Time reversal

Classically, temporal invariance means that the very same equations of motion describe both a particle going from A to B along a path than from B to A, that is the time reversed motion. In

quantum mechanics, time reversal, and so effectively the interchange of incoming and outgoing states, is implemented by an anti-unitary operator $U(T) = V(T)K$, being $V(T)$ unitary while K complex conjugates any number quantity it acts on[2]. The transformation property of the electromagnetic field can be deduced again from the classical case, instead for spinor fields this is derived by asking that the action of $U(T)$ on $\psi(\vec{x}, t)$ produce another solution of the Dirac equation. We have:

$$U(T)A^{\mu}(\vec{x}, t)U(T)^{-1} = \eta(\mu)A^{\mu}(\vec{x}, -t)$$
$$U(T)\psi(\vec{x}, t)U(P)^{-1} = T\psi(\vec{x}, -t)$$

The form of the matrix T also depends on which representation is used as long as it satisfies the conditions to get the invariance of the Dirac equation: $T\gamma^{0*}T^{-1} = \gamma^0$ and $T\gamma^{i*}T^{-1} = \gamma^i$. In the Majorana base $T = \gamma^0\gamma^5$. Remembering that $U(T)$ complex conjugates c-numbers, transformation properties for fermion-antifermion bilinears appearing in SM currents can be deduced. So one sees that both QCD and electroweak interactions in A.2.2 turn to be invariant, provided that the gauge fields transform according to the fact that for $SU(3)$ only λ_2, λ_5 and λ_7 are imaginary, and for $SU(2)$ only σ_2 is imaginary:

$$U(T)A_a^{\mu}(\vec{x}, t)U(T)^{-1} = -\eta(\mu)\eta(a)A_a^{\mu}(\vec{x}, -t)$$

However T violation emerges in the Yukawa sector because of the complex nature of the Yukawa couplings as presented in A.2.3. Here we show that, after diagonalization, the source of T violation can be transferred to the electroweak sector expressed in the mass basis and encoded in the complex phase of the CKM matrix.

CPT theorem implications

It turns out that if nature is described by a relativistic quantum field theory, with a local Lorentz invariant and hermitian lagrangian, its action is always invariant under the combined application of a C, a P, and a T transformation. This result, known as the CPT Theorem, has deep implications. Indeed it is meant to hold when we have violation of the individual symmetries and it establish the substantial equivalence between a T transformation and a CP transformation, that is Parity and Charge Conjugation together. We can sketch how the CPT results

[2]The need for complex conjugation can be understood noticing that, provided that the Hamiltonian is real, the complex conjugation of the wave function plus the reversal in the direction of time $\psi^*(\vec{x}, t)$ is also a solution of the Schrodinger equation.

from the underlying complementary action of CP and T on operators $O(x)$ and complex numbers c in a hermitian lagrangian, i.e. in the form $L(x) = aO(x) + a^*O(x)^\dagger$. Under T the operator is unchanged and the c-number is complex conjugated: $O(\vec{x},t) \xrightarrow{T} O(\vec{x},-t)$ and $a \xrightarrow{T} a^*$. Under CP the first is replaced by its hermitian adjoint and the second stays the same: $O(\vec{x},t) \xrightarrow{CP} O(-\vec{x},t)^\dagger$ and $a \xrightarrow{CP} a$. Combing the two we see that $L(x) \xrightarrow{CPT} L(-x)$, and performing change of the space-time integration variable in the action, we see this is invariant.

1.1.2 Continuous global symmetries

Approximate global symmetries result from effectively neglecting certain parameters in our theory, otherwise a symmetry is exact. Both exact and approximate global symmetries can be manifest (Wigner-Weyl realized) or spontaneously broken (Nambu-Goldstone realized), depending on whether or not the vacuum state respects the symmetry. In the first case we will see degenerate multiplets of states in the spectrum of the theory, while if a symmetry group G is spontaneously broken to a subgroup H, then $n = dim G/H$ massless scalars appear, known as Nambu-Goldstone bosons.
QCD manifests an approximate global symmetry, rising from the fact that the lightest quark masses are much smaller than the dynamical scale of the theory $m_u, m_d << \Lambda_{QCD}$, and so negligible. In this limit, and considering only up and down quarks kinetic terms, QCD Lagrangian can be written in the following chiral representation:

$$L_{QCD} \supset \sum_{q=u,d} (\bar{q}_L \not{\partial} q_L + \bar{q}_R \not{\partial} q_R)$$

that is invariant under the rotation $\begin{pmatrix} u \\ d \end{pmatrix}_L \to e^{a\alpha_{iL}T_i} \begin{pmatrix} u \\ d \end{pmatrix}_L$ and $\begin{pmatrix} u \\ d \end{pmatrix}_R \to e^{a\alpha_{iR}T_i} \begin{pmatrix} u \\ d \end{pmatrix}_R$ with $T_i = (\tau_i, \mathbb{I})$. This is a global $U(2)_L \times U(2)_R = U(2)_V \times U(2)_A$ symmetry, that can be split in $SU(2)_A \times SU(2)_V \times U(1)_B \times U(1)_A$ and that is actually a symmetry of QCD at the classical level. It turns, indeed, that $U(1)_A$ is broken at quantum level. Among the others, only $SU(2)_V$ and $U(1)_B$ are manifest symmetries, whereas $SU(2)_A$ is spontaneously broken by the formation of u and d quark condensates $\langle \bar{u}u \rangle = \langle \bar{d}d \rangle \neq 0$, leading to the appearance of three Nambu-Goldstone bosons, which are identified as the pions. The manifest $SU(2)_V$ symmetry is the well-known isospin symmetry of the strong interactions, with the associated approximate nucleon $N = (p, n)$ and pion $\pi = (\pi_+, \pi_-, \pi_0)$ multiplets. Instead $U(1)_B$ is actually an exact global symmetry of QCD, corresponding to a common phase quark rotation. This is also a

symmetry of the electroweak sector, leading to the conserved quantity of the baryon number B. Furthermore in the Standard Model we can make a similar argument for leptons, entailing the lepton number L conservation. Nevertheless neither L or B are conserved at quantum level, while the only true global quantum symmetry is $B - L$. Finally we remark that in the limit of vanishing neutrino masses, separate conserved numbers referred to different fermion species L_i emerge at the classical level, while at the quantum level each $3L_i - B$ is conserved.

Quantum chiral anomaly

When a symmetry of a classical theory is not a symmetry at quantum level, it is said to be anomalous and the associated current will not be conserved. This is because certain 1-loop diagrams, as triangle diagrams, introduce anomalous terms which prevent the Ward identities from reproducing themselves at higher orders in the perturbative expansion.
The existence of the chiral $U(1)_A$ anomaly was formally explained by Adler Bell and Jackiw in this terms, pointing out that it is not possible to preserve both the axial and vector currents because of the singular behavior of the three-point functions involving them[3]. Such behaviour brings into the lagrangian a gauge field structure $\propto \tilde{F}^{a,\mu\nu} F^a_{\mu\nu} = \frac{1}{2}\varepsilon^{\mu\nu\alpha\beta} F^a_{\alpha\beta} F^a_{\mu\nu}$, that is C even, but both P and T odd, providing additional sources of CP violation.
This is common whenever there are fermions in our theory. Indeed it was later pointed out by Fujikawa[4] that the *ABJ* anomalous term could be recovered directly in the path-integral formalism as an extra Jacobian factor, since the measure for gauge invariant fermion theory is not invariant under the γ_5 transformation. As we will see, this will be crucial for QCD.

1.2 QCD Lagrangian part II

At experimental level QCD turns to be unexpectedly invariant under charge and parity transformation. Conversely QCD Lagrangian in its most general form can be written:

$$L_{QCD} = \sum_q \bar{q}(i\gamma_\mu D^\mu - m_q e^{i\theta_q \gamma_5}) q - \frac{1}{4} G^{a\mu\nu} G^a_{\mu\nu} + \theta \frac{g_s^2}{32\pi^2} G^{a\mu\nu} \tilde{G}^a_{\mu\nu} \tag{1.2}$$

This contains two potential sources of CP violation: the phases of the quark masses θ_q, and the 'topological term', proportional to θ, that we will address to as $G\tilde{G}$. Let's explore the connection between the two CP violating terms. We perform a global chiral transformation on a single quark field $q \to e^{i\gamma_5 \alpha} q$ sending the two chiral components $q_R \to e^{i\alpha} q_R$ and $q_L \to e^{-i\alpha} q_L$.

The associated axial current is not conserved for two reasons. First the quark mass term gets modified as $\theta_q \rightarrow \theta_q + 2\alpha$, and, as previously anticipated, this transformation is an anomaly, so the non-invariance of the path integral measure under the transformation rise a term in the action that is equivalent to the shift $\theta \rightarrow \theta - 2\alpha$. [3]
Generalizing to quark multiplet $q = (u, d, ...)^T$ with n_f flavours the mass term can be rearranged as:

$$\bar{q}_L M_q q_R + h.c.$$

where $M_q = diag(m_u, m_d, ...)$ and $Argdet M_q \rightarrow Argdet M_q + 2\alpha$. We see that performing a chiral rotation is possible to cancel one or the other CP violating term, for instance making θ the only source of CP violation in L_{QCD}.

The $U(1)_A$ problem

Historically the development of QCD, in the framework we presented in 1.1.1, was displaying a puzzling issue that we can deem being a forerunner of the Strong CP Problem.
Consider the quark sector of QCD Lagrangian in the reasonable limit of vanishing up and down quark masses ($m_{u,d} << \Lambda_{QCD}$). As seen, this has a large global symmetry: $U(2)_V \times U(2)_A$, broken spontaneously by quark condensates $\langle q\bar{q} \rangle$ and so one expects the emergence of Nambu-Goldstone bosons, that are associated light particles in the hadronic spetrum. What we find experimentally is that the vector symmetry, which can be decomposed as isospin times baryon number $U(2)_V = SU(2)_I \times U(1)_B$, is a good approximate symmetry of nature, but on the other hand we observe no light state that could correspond to the Goldstone boson of a $U(1)_A$. This is a puzzle that baffled physicists in the '70s, addressed as 'the $U(1)_A$ problem'. As pointed out in the previous section, the solution lays in the fact that no Goldstone boson must be expected since $U(1)_A$ is not a true symmetry but it is indeed an anomaly under the symmetry group of QCD, meaning that at level of path integral the measure is not invariant. From its transformation a term that resemble the $G\tilde{G}$ in 1.2 rise in the action. So the solution of the $U(1)_A$ problem turns into the question of why, despite this term, CP is not badly broken in QCD. This is the strong CP problem.

[3] from $DqD\bar{q} \rightarrow DqD\bar{q} \exp\left(-i\alpha \frac{g_S^2}{16\pi^2} G\tilde{G}\right)$

1.2.1 Meaning of the θ term

Let's now explore the role of the operator $G\tilde{G}$, once we suppose to encapsulate all source of CP violation in the θ term, to ensure that this must be included in the action. Indeed we have that $G\tilde{G}$ can be re-written as a total derivative:

$$G^{a\mu\nu}\tilde{G}^{a}_{\mu\nu} = \partial_\mu K^\mu = \partial_\mu \varepsilon^{\mu\nu\rho\sigma}(A_\nu G_{\rho\sigma} - \frac{g_s}{3} f^{abc} A^a_\nu A^b_\rho A^c_\sigma) \tag{1.3}$$

where K_μ is named Chern-Simons current. So one could argue that it has no physical relevance. But this is not actually true. Indeed if we use Gauss theorem to write the volume integral of the operator $G\tilde{G}$ as a surface integral, we can look for field configurations such that its contribution to the path integral is finite.

$$\int d^4x G^{a\mu\nu}\tilde{G}^{a}_{\mu\nu} = \int d^4x \partial_\mu K^\mu = \int_{S_3} d\sigma_\mu K^\mu \tag{1.4}$$

where S_3 denotes the three-sphere of infinite radius and element of hypersurface $d\sigma_\mu$. If K vanishes faster than $1/r^3$ at infinity, then this quantity will integrate to zero and θ cannot have any physical effect. It turns out that finite energy field configurations where $K \sim 1/r^3$ and the surface integral does not vanish at infinity exist. These are called instantons, alluding to field configurations localized in space and time. Let's look for them. Since we want a system with finite energy, to have finite action we require boundary conditions $\lim_{|x|\to\infty} G^a_{\mu\nu} = 0$. This is satisfied by $A^a_\mu|_{S_3} = 0$ on S_3, and all the other configurations that can be obtained from this by a gauge transformation, in the form of a pure gauge at the boundaries:

$$A'_\mu|_{S_3} = i\frac{1}{g} U^{-1}\partial_\mu U$$

We are interested in pure gauges for which U cannot be continuously deformed into the identity in group space. More precisely we ask whether the gauge configurations that A_μ goes to at infinity are all equivalent, or to phrase it in the parlance of a mathematician, whether the mappings between the gauge group, $SU(3)$, and the sphere at infinity, S_3, are all equivalent. It is worth to claim in general that if the homotopy group between the physical space and the group space for which the theory is invariant is not trivial then soliton solutions can exists. In particular, one can prove that $\pi_3(SU(3)) = \mathbb{Z}$[4]. This implies that all field configurations in their

[4]We can think at gauge configurations that the field can go to at infinity as characterized by an integer. Therefore, as integers are not smoothly connected, they cannot be smoothly deformed into each other. [5]

asymptotic behavior (i. e. $SU(3)$ mappings) are characterized by an integer n, typically called the winding number. It turns out that the winding number of any given gauge configuration can be determined by:

$$\frac{1}{32\pi^2}\int d^4x G^{a\mu\nu}\tilde{G}^a_{\mu\nu} = n_1 - n_2 \equiv \nu \tag{1.5}$$

where n_1 and n_2 are the winding numbers of the gauge field at the boundaries, and ν is the so called the Pontryagin index. One can build these gauge field configurations explicitly and show that their finite action corresponds to a minimum, which implies that they are solutions of the classical equation of motion in Euclidean space. In particular since these are self-dual $G^{a\mu\nu} = \tilde{G}^{a\mu\nu}$ we have $Tr(G\tilde{G}) = Tr(G^2)$ and we obtain the following contribution:

$$S_E = -\frac{1}{4}\int d^4x G^{a\mu\nu}G^a_{\mu\nu} = -\frac{1}{2}\int d^4x Tr(G^{\mu\nu}G_{\mu\nu}) = -\frac{8\pi^2}{g^2}\nu \tag{1.6}$$

Being of finite action, these gauge configurations are localised in all the four dimensions which justifies the name instantons. Thus, from 1.5, we can state that the instanton describes a solution of the gauge field equation tunnelling from one vacuum state (pure gauge, i.e. $G^a_{\mu\nu} = 0$)[5] to a gauge rotated one with different winding number. Since the action 1.6 is finite we have a non zero transition amplitude between this gauge rotated vacua. Taking all possible values n, one obtains an infinite number of homotopically inequivalent vacua, and the transition amplitude between them is non-zero. An important issue is that K_μ by itself is not gauge invariant, and so different n labelling the vacuum states have no real physical meaning: indeed the action of a gauge transformation on them corresponds to a relabelling $U|n_i\rangle = |n_{i+1}\rangle$. A proper definition for a gauge invariant vacumm is therefore:

$$|\theta\rangle = \sum_{-\infty}^{+\infty} e^{in\theta}|n\rangle \tag{1.7}$$

where θ is what is called a super-selection rule. One can show that states labelled by different θ are ground states of independent superselection sectors ($\langle\theta|O|\theta'\rangle = 0$ and any observables O connecting different vacua is zero), meaning that is impossible to transition from one value of θ to another. Therefore when defining a theory, one chooses a single value of θ and throws out all other values. Finally in field theories the θ-vacuum is tipically introduced as an additional

[5] All n states have the same energy. Each of these states is specified by how the gauge field falls off at infinity. The lowest energy state in each of these sectors is when the gauge field takes on its asymptotic value at all points in space time. Because the gauge field is pure gauge, they all have zero E and B fields and thus the same energy.[5]

term in the action entering the path integral, that is the familiar:

$$\frac{\theta}{32\pi^2}\int d^4x G^{a\mu\nu}\tilde{G}^a_{\mu\nu} = \nu\theta$$

1.2.2 The core of Strong CP Problem

As seen at the beginning of this section, to reach a physical basis where the quark masses are real, one must diagonalize the quark mass matrix M_q and in doing so one performs a chiral transformation which changes θ by $ArgdetM_q$. Besides $\bar{\theta} = \theta + ArgdetM_q$ is invariant under a quark chiral rotation, and therefore linked to physically observable quantities, from which we infer whether strong interactions violate CP. Among these, neutron electric dipole moment shows up as the most sensitive one. We can define nEDM in non-relativistic approach as the coupling with the electric field in the Hamiltonian $H = -d_n\hat{S}\cdot\vec{E}$. This can be thought as derived from a Lorentz invariant lagrangian operator:

$$L = -d_n\frac{i}{2}\bar{n}\sigma_{\mu\nu}\gamma_5 nF_{\mu\nu}$$

The dependence of d_n on θ can be estimated as [6]:

$$d_n \sim \frac{1}{8\pi^2}\frac{m_q}{m_n}\frac{\bar{\theta}e}{m_n} \approx 10^{-16}\bar{\theta}\, e\, cm$$

The current best measurement of the neutron eDM is $d_n \leq 10^{-26}\, e\, cm$, so to agree with experimental bounds we need $\theta \leq 10^{-10}$. This results in an incredibly small number, basically zero, whereas, being a dimensionless coupling, it is quite natural to expect it to be of order one. Why this should be so is a mystery. We are at the core of the strong CP problem.

[6] Being a dimension five operator, we naively expect its Wilson coefficient to be of $O(1/m_n)$ size. Then to compensate the imaginary unit we need the phase of a light quark mass $e^{i\theta} \approx 1 + i\theta$ (in a proper basis). Finally we insert two extra suppression factors for dipole loop. [6]

2

The Axion

The *axion* was so named after an American laundry detergent, to denote the particle that washes away the issue of CP violation in QCD, providing an efficient solution to the strong CP problem. It is introduced in EFT framework (which is discussed in the first section 2.1), and so it is associated to a suppressing scale f_a. Here we require axion coupling with the very same CP violating gluon term of QCD, so that the minimum of axion potential occurs when the coefficient of such term vanishes. Subsequently (2.1 and 2.1.1), we report model-independent properties, i.e. the axion mass and some couplings, than can be derived from a chiral Lagrangian formulation of axion potential. Finally, in the second paragraph we present the receipt to build a QFT that could match the axion effective lagrangian. Candidate models are indeed based on spontaneous breaking of a global Peccei-Quinn $U(1)$ symmetry at some high energy scale, and in this scenario, the axion emerges as a pseudo-Nambu Goldstone Boson.

2.1 Axion solution in chiral QCD

The key ingredient for the PQ solution is a new scalar field $a(x)$, called the axion field, whose effective Lagrangian is defined at energies far below a scale f_a and the electroweak scale and reads:

$$L_a = \frac{1}{2}(\partial_\mu a)^2 + L(\partial_\mu a, \psi) + \frac{g_s^2}{32\pi^2}\frac{a}{f_a}G\tilde{G} \tag{2.1}$$

where ψ generically denotes some other fields. We observe that the transformation $a \to a + \kappa f_a$ leaves this Langrangian invariant up to the $G\tilde{G}$ term: since κ is arbitrary, one can exploit this quasi shift simmetry to remove the $\bar{\theta}$ in L_{QCD} (in an appropriate basis where the CP violation is encapsulated by $G\tilde{G}$ term). Considering this theory at low energies, the CP violating term provides a potential, whose minumum lays at $a = 0$. In fact, a theorem of Vafa and Witten guarantees that the instanton potential is minimized at the CP conserving value, so we have $\langle a \rangle = 0$. [1]. Then once the axion relaxes to the minimum of its potential, the strong CP problem is dinamically solved. However the low energy behaviour of this theory is well described by chiral QCD and it is useful to look at the axion potential obtained in this framework, to investigate axion properties. One can define 'axion dressed' parameters and consider them in the chiral lagrangian, which describes the low energy non perturbative behaviour of QCD in terms of pions. We report here the main results of the derivation [6]. In particular, on the pion ground state, the chiral perturbation theory axion potential, coming from the non derivative part of the lagrangian, takes the form:

$$V(a) = -m_\pi^2 f_\pi^2 \sqrt{1 - \frac{4 m_u m_d}{(m_u + m_d)^2} \sin^2\left(\frac{a}{2 f_a}\right)}$$

Expanding this for $a/f_a << 1$ we can read the axion mass term $\frac{1}{2} m_a^2 a^2$ with:

$$m_a^2 = \frac{m_u m_d}{(m_u + m_d)^2} \frac{m_\pi^2 f_\pi^2}{f_a^2} \quad \longrightarrow \quad m_a = 5.7 \frac{10^{12}\ GeV}{f_a} \mu eV \tag{2.2}$$

2.1.1 Some axion couplings

We can include in 2.1 model depending terms accounting for the interaction of axion with other particles.
The interaction with a fermion has derivative structure (preseving invariance under shift), so we expect an axion-quark coupling of the kind:

$$L_{a,q} = \frac{C_{aq}}{2 f_a} \bar{q} \gamma^\mu \gamma_5 q \partial_\mu a$$

[1] or equivalently, not performing the κ shifting, the potential provided by the CP-violating term depending now on $\bar{\theta} + a/f_a$ drives to the CP-conserving minimum at $a = -\bar{\theta} f_a$

Here, q denotes the quark field, with mass m_q, and C_{aq} is a numerical coefficient[2]. Then, invoking again chiral perturbation theory, the derivative part of the axion chiral Lagrangian yields the axion-pion coupling:

$$L_{a\pi} = \frac{C_{a\pi}}{3f_a f_\pi}\partial^\mu a(2\partial_\mu\pi^0\pi^+\pi^- - \pi^0\partial_\mu\pi^+\pi^- - \pi^0\pi^+\partial_\mu\pi^-) + \frac{C_{a\pi}f_\pi}{2f_a}\partial_\mu a\partial_\mu\pi^0 \tag{2.3}$$

with $C_{a\pi} = \frac{m_u - m_d}{m_u + m_d} + C^0_{au} - C^0_{ad}$ where for completeness we added model-dependent couplings C^0_{au} and C^0_{ad}.
We can also think of a photon-axion interaction term included in 2.1:

$$L_{a,\gamma} = \frac{1}{4}g_{a\gamma}a\tilde{FF}$$

Indeed it is convenient to first eliminate in the axion QCD lagrangian the $aG\tilde{G}$ term via an a field-dependent axial transformation of the quark fields. In general this transformation is anomalous under QED, so it will affect the lagrangian adding a term $\propto \tilde{FF}$. Therefore supposing a model dependent coupling $g^0_{a\gamma}$ to which this effect is summing to, we obtain the axion-photon coupling (evaluated taking into accounts also contribution by axion-pion mixing) $g_{a,\gamma} = g^0_{a\gamma} + \frac{\alpha}{2\pi f_a}\frac{2}{3}\frac{4m_d + m_u}{m_u + m_d}$.

Finally we report the relevant term of axion interaction Lagrangian [6], where we included by completeness interaction with matter fields $f = n, p, e$ and the $nEDM$ operator:

$$L^{int}_a \supset \frac{1}{4}g_{a\gamma}a\tilde{FF} + \frac{C_{af}}{2f_a}\bar{f}\gamma^\mu\gamma_5 f\partial_\mu a + \frac{C_{a\pi}}{3f_a f_\pi}\partial_\mu a[\partial\pi\pi\pi]^\mu - \frac{a}{f_a}\frac{C_{an\gamma}}{m_n}\frac{i}{2}\bar{n}\sigma_{\mu\nu}\gamma_5 nF_{\mu\nu}$$

where $[\partial\pi\pi\pi]^\mu$ denotes a short form for the expression in 2.3.

2.2 Axion models

The Lagrangian 2.1 constitutes a non-renormalizable effective theory that breaks down at energies of the order of f_a. In the searching for a UV completition, we briefly consider three general types of QCD axion model, that share the common framework of a $U(1)_{PQ}$ spontaneously

[2] This very same form makes up axion coupling to a generic fermion and so to electron: indeed, additionally to possible model dependent tree level contribution, the axion-photon interaction implies a loop-induced axion-electron interaction.

broken with the axion being its pNBG. In Peccei-Quinn-Weinberg-Wilczek (PQWW) model f_a lays at the electroweak scale, so, since all axion couplings are suppressed by $1/f_a$ they are too large and therefore excluded by experiments. In the Kim-Shifman-Vainshtein-Zakharov (KSVZ) and Dine-Fischler-Srednicki-Zhitnitsky (DFSZ) models instead the scale f_a is an arbitrary parameter that can be properly adjusted. Both their axions are indeed known as invisible axions.

2.2.1 PQWW axion

The PQWW model introduces one additional complex scalar field to the Standard Model as a second Higgs doublet: we have one Higgs field giving mass to the up type quarks φ_1, while the other to the down type quarks φ_2. Then we can choose whatever to give mass to leptons (also a third field). So this new field couples to the standard model particles in the usual Yukawa terms rising the fermions mass.

$$L_{PQWW} = -\lambda_u^{ij}\bar{Q}_L^i\varphi_1 u_R^j - \lambda_d^{ij}\bar{Q}_L^i\varphi_2 d_R^j + h.c + V(\varphi_1,\varphi_2)$$

In unitary gauge:

$$\varphi_1 = \frac{v_1+\rho_1}{\sqrt{2}}e^{iax/v_F}\begin{pmatrix}1\\0\end{pmatrix} \qquad \varphi_2 = \frac{v_2+\rho_2}{\sqrt{2}}e^{ia/xv_F}\begin{pmatrix}0\\1\end{pmatrix}$$

where $v_F = \sqrt{v_1^2+v_2^2}$ and $x = v_2/v_1$. The axion is the common phase field a. We take the theory invariant under a global chiral $U(1)_{PQ}$ symmetry, that acts on φ_i as a shift in the angular part and the invariance of the Yukawa terms under global rotations fixes the $U(1)_{PQ}$ charges of the various fermions: $a \to a + \alpha v_F, u_R^j \to e^{i\alpha x}u_R^j, d_R^j \to e^{i\alpha/x}d_R^j$.
Symmetry breaking of φ_i occurs, akin the Higgs, at the electro-weak phase transition. The potential is the usual:

$$V(\varphi_i) = \lambda\big(|\varphi_i|^2 - \frac{v_i^2}{2}\big)^2$$

and φ_i acquires a vacuum expectation value $\langle\varphi_i\rangle = \frac{v_i}{\sqrt{2}}$. In the original Peccei-Quinn model $f_a \sim v_F \approx 250\ GeV$, so we can take for simplicity $x \approx 1$. So after SSB, having integrated out the radial part, we can parametrize $\varphi_i = \langle\varphi_i\rangle e^{ia/2f_a}$. The angular field a is the Goldstone boson of the spontaneously broken $U(1)_{PQ}$ symmetry and it coincides with the axion. The Yakawa

term reads:

$$-\frac{v_F e^{ia/2f_a}}{\sqrt{2}}(\lambda_u^{ij}\bar{u}_L^i u_R^j+\lambda_d^{ij}\bar{d}_L^i d_R^j)+h.c. \supset -m_u\frac{a}{f_a}i\bar{u}_L^i u_R^i - m_d\frac{a}{f_a}i\bar{d}_L^i d_R^i + h.c. = \sum_q m_q\frac{a}{f_a}i\bar{q}^i\gamma_5 q^i$$

Expanding $e^{ia/2f_a}\sim 1+ia/2f_a$ we got the couplings with quarks[3]. The chiral anomaly induces couplings to gauge bosons rising the term needed to solve the strong-CP problem, whereas the quarks tree level derivative couplings are obtained considering how the transformation affects the fermion kinetic terms. Since this model has been excluded, we now focus on the other two, remembering that however the procedure to get the axion effective couplings is quite general and applicable also to the PQWW axion.

2.2.2 KSVZ axion

The KSVZ axion model introduces, alongside with the scalar $\varphi\sim(1,1,0)$, a heavy quark doublet $Q\sim(3,2,0)$ of components Q_L, Q_R, that under chiral $U(1)_{PQ}$ transform as: $Q_{L,R}\to e^{\pm i\alpha/2}Q_{L,R}$, $\varphi\to e^{i\alpha}\varphi$. The simmetry is, again, spontaneously broken by the potential:

$$V(\varphi)=\lambda\big(|\varphi|^2-\frac{v_a^2}{2}\big)^2 \qquad and \qquad \varphi=\frac{v_a+\rho_a}{\sqrt{2}}e^{ia/v_a} \tag{2.4}$$

where the axion field a corresponds to the Goldstone mode. The scalar φ and the heavy quarks interact via the PQ-invariant Yukawa term in the Lagrangian:

$$L_{KSVZ}=(\partial_\mu\varphi)^2\bar{Q}i\not{\partial}Q-\lambda_Q\varphi\bar{Q}_L Q_R+h.c.-V(\varphi)$$

This provides the heavy quark mass $m_Q=v_a\lambda/\sqrt{2}$ in the broken phase, while the radial mode ρ_a acquires $m_{\rho_a}=\sqrt{2\lambda}v_a$. Setting v_a at large scale, the quark field is heavy and can be integrated out. On the other hand the operator $G\tilde{G}$ is produced by chiral anomaly and stays, at EFT level, as the only modification to SM Lagrangian. Indeed we have no other tree-level couplings to standard model matter fields. To see this, we look at the term:

$$-m_Q\bar{Q}_L Q_R e^{ia/v_a}+h.c.$$

[3] we have considered $q_{R,L}=\frac{(1\pm\gamma_5)}{2}q$, and summing with the h.c. only the part with γ_5 survives.

and perform an axial transformation $Q \to e^{-i\gamma_5 a/2v_a}Q$ that is equivalent to $Q_L \to e^{ia/2v_a}Q_L$ and $Q_R \to e^{-ia/2v_a}Q_R$. Being anomalous under QCD, the non-invariance of the path integral measure brings the additional term to the lagrangian $\delta L_{KSVZ} = \frac{g_s^2}{32\pi^2}\frac{a}{v_a}G\tilde{G}$, that is the required one with the identification $v_a = f_a$.
We can explore the KSVZ model in a more general scenario where the heavy fermions Q live in a generic reducible representation $\sum_Q (C_Q, I_Q, Y_Q)$ of the $SU(3)_c \times SU(2)_L \times U(1)_Y$ gauge group, where at least one C_Q is non trivial. Both a QCD and electromagnetic anomalous term will rise, parametrised by the coefficients $N = \sum_Q N_Q$ and $E = \sum_Q E_Q$, with N_Q and E_Q indicating the contributions to the anomalies of each irreducible representation[4]. After removing the axion field from the Yukawa Lagrangian via the chiral transformation, we obtain the effective anomalous interactions (with $\alpha_s = \frac{g_s^2}{4\pi^2}$ and $\alpha = \frac{e^2}{4\pi^2}$):

$$\delta L_{KSVZ} = \frac{\alpha_s}{4\pi}N\frac{a}{v_a}G\tilde{G} + \frac{\alpha}{4\pi}E\frac{a}{v_a}F\tilde{F}$$

Then setting $f_a = v_a/2N$ we rewrite:

$$\delta L_{KSVZ} = \frac{\alpha_s}{8\pi}\frac{a}{f_a}G\tilde{G} + \frac{\alpha}{8\pi}\frac{E}{N}\frac{a}{f_a}F\tilde{F}$$

where we normalised the first term as in 2.1 so that we recognise the model dependent coupling $g^0_{a\gamma} = \frac{\alpha}{2\pi f_a}\frac{E}{N}$.
As we will later see, the QCD induced axion potential is periodic with a number of inequivalent degenerate minima written in terms of the QCD anomaly factor $N_{DW} = 2N$, which has remarkable consequences in axion cosmology.

2.2.3 DFSZ axion

The DFSZ model introduces two Higgs doublets $H_u \sim (1, 2, -\frac{1}{2})$, $H_d \sim (1, 2, +\frac{1}{2})$ as well as the PQ scalar $\varphi \sim (1, 1, 0)$. Then the two Higgs couple to SM fermions in the usual Yukawa sector, and so, requiring this to be PQ invariant, fermions must have charges under $U(1)_{PQ}$:

$$L_{DSFZ} = -\lambda_u \bar{Q}_L H_u u_R - \lambda_d \bar{Q}_L H_d d_R + h.c + V(|H_u|, |H_d|, \varphi) + \lambda_H \varphi^{\dagger 2} H_u H_d + [kinetic]$$

[4] $N_Q = \chi_Q d(I_Q)T(C_Q)$ and $E_Q = \chi_Q d(C_Q)Tr(q_Q^2)$ where $d(C_Q)$ and $d(I_Q)$ denote the dimension of the colour and weak isospin representations, $T(C_Q)$ the colour index, $q_Q = T_Q^3 + Y_Q$ is the EM charge and $\chi_{Q_R} = \chi_{Q_L} = \mp 1/2$ the PQ charge depending on whether the quark bilinear $\bar{Q}_L Q_R$ couples to φ or $\varphi^\dagger$.

that has linearly independent $U(1)$ symmetres: the hypercharge and the PQ. The PQ symmetry acts on the fields as a phase rotation of charge χ_i with $i = u, d, \varphi$. The lepton sector can either couple with H_d (DSFZ-I) or $\tilde{H}_u = i\sigma H_u^*$ (DSFZ-II). We take the potential such that to ensure that the three additional fields acquire a vev:

$$\langle H_u \rangle = \frac{v_u}{\sqrt{2}} e^{ia_u/v_u} \begin{pmatrix} 1 \\ 0 \end{pmatrix} \qquad \langle H_d \rangle = \frac{v_d}{\sqrt{2}} e^{ia_d/v_d} \begin{pmatrix} 0 \\ 1 \end{pmatrix} \qquad \langle \varphi \rangle = \frac{v_\varphi}{\sqrt{2}} e^{ia_\varphi/v_\varphi}$$

The axion in this case is identified in terms of the a_i as it follows: taking in mind the infinitesimal transformation $H_{u,d}/\varphi \sim (1 + i\chi_{u,d,\varphi})H_{u,d}/\varphi$ we look at the part of PQ current containing our new fields and expand them about their v.e.v. What we obtain is

$$J_\mu^{PQ} \supset -i(\chi_\varphi \varphi^\dagger \overleftrightarrow{\partial}_\mu \varphi + \chi_u H_u^\dagger \overleftrightarrow{\partial}_\mu H_u + \chi_d H_d^\dagger \overleftrightarrow{\partial}_\mu H_d) \supset \sum_{i=\varphi,u,d} \chi_i v_i \partial_\mu a_i \equiv v_a \partial_\mu a$$

From this we read $a = \frac{1}{v_a} \sum_i \chi_i v_i a_i$ and $v_a^2 = \sum_i \chi_i^2 v_i^2$. In this way, since under a PQ rotation $a_i \to a_i + \kappa \chi_i a_i$, one finds the usual shift $a \to a + \kappa a$. To determine the PQ charges of the scalar sector, needed to express the lagrangian in terms of the axion field so defined, we impose two conditions. First we require the invariance of the operator $\varphi^{\dagger 2} H_u H_d$ under PQ tranformation, yielding the condition $\chi_u + \chi_d - 2\chi_\varphi$. Then we impose the orthogonality between the PQ current evaluated at the axion field $\sum_i \chi_i v_i \partial_\mu a_i$ and the analogue hypercharge current $\sum_i Y_i v_i \partial_\mu a_i$, corresponding to $\chi_u v_u^2 + \chi_d v_d^2 = 0$. We fix the normalisation by choosing a conventional value $\chi_\varphi = 1$ and setting $v_u/v = \sin\beta$ and $v_d/v = \cos\beta$ with $v \simeq 246 GeV$ the usual electromagnetic scale we obtain $\chi_u = 2\cos^2\beta, \chi_d = 2\sin^2\beta$. With these a trivial substitution yields $v_a^2 = \sum_i \chi_i^2 v_i^2 = v_\varphi^2 + v^2(\sin(2\beta)^2) \approx v_\varphi$ taking $v_\varphi >> v$. Then from the defining relation for a, we express $a_{u,d}$ in terms of a and select in the lagrangian, where the fields are replaced by their vevs, only the a dependent terms:

$$L_{DSFZ} \supset -(m_u \bar{u}_L u_R e^{i\chi_u \frac{a}{v_a}} + m_d \bar{d}_L d_R e^{i\chi_d \frac{a}{v_a}} + h.c.)$$

From the expansion of the exponential we get again axial current couplings between the axion and fermions in the form $m_q(a/f_a) i\bar{q}\gamma_5 q$. Again, chiral anomaly induces the $G\tilde{G}$ and $F\tilde{F}$ couplings, once removed the axion field from the mass terms via field-dependent axial transfor-

mations[5]:

$$u \to e^{-i\gamma_5 \chi_u \frac{a}{2v_a}} u \qquad\qquad d \to e^{-i\gamma_5 \chi_d \frac{a}{2v_a}} d$$

The rising anomalous term reads:

$$\delta L_{DSFZ} = \frac{\alpha_s}{8\pi}\frac{a}{f_a} G\tilde{G} + \frac{\alpha}{8\pi}\frac{E}{N}\frac{a}{f_a} F\tilde{F}$$

with $f_a = v_a/2N$ and in DSFZ-I we have $E/N = 8/3$, while in DSFZ-II $E/N = 2/3$[6].

In the DSFZ models we do have tree-level couplings between the axion and standard model fermions. Indeed chiaral rotations of the up and down quarks do not leave the fermion kinetic terms invariant, and their variation corresponds to derivative couplings of the axion to the SM fermion fields:

$$\delta(\bar{u}\not{\partial}u) = \chi_u \frac{\partial_\mu a}{2v_a}\bar{u}\gamma^\mu\gamma_5 u = \frac{1}{3}\cos^2\beta\frac{\partial_\mu a}{2f_a}\bar{u}\gamma^\mu\gamma_5 u$$

$$\delta(\bar{d}\not{\partial}d) = \chi_d \frac{\partial_\mu a}{2v_a}\bar{d}\gamma^\mu\gamma_5 d = \frac{1}{3}\sin^2\beta\frac{\partial_\mu a}{2f_a}\bar{d}\gamma^\mu\gamma_5 d$$

$$\delta(\bar{e}\not{\partial}e)_I = \chi_d \frac{\partial_\mu a}{2v_a}\bar{e}\gamma^\mu\gamma_5 e = \frac{1}{3}\sin^2\beta\frac{\partial_\mu a}{f}\bar{e}\gamma^\mu\gamma_5 e \qquad \delta(\bar{e}\not{\partial}e)_{II} = -\chi_u \frac{\partial_\mu a}{2v_a}\bar{e}\gamma^\mu\gamma_5 e = -\frac{1}{3}\cos^2\beta\frac{\partial_\mu a}{2f_a}\bar{e}\gamma^\mu\gamma_5 e$$

We conclude with remarking that both KSVZ and DFSZ models, as seen, produce the correct term necessary to solve the Strong CP problem: the main difference between them is that for DFSZ this term is induced by light quark loops calculated at low energy, rather than via the integrating out of a heavy quark.

[5] PQ invariance of the mass terms implies $\chi_{u_R} + \chi_{u_L} = \chi_u$ and $\chi_{d_R} + \chi_{d_L} = \chi_d$ so we notice that these transformations basically redefine the left and right chiral fields with a phase transformation proportional to their PQ charges.

[6] Given $n_f = 3$ the number of fermion generations we calculate for DFSZ-I:

$$N = n_f\left(\frac{1}{2}\chi_u + \frac{1}{2}\chi_d\right) = 3 \times \chi_\varphi = 3$$

$$E = n_f\left(3(\frac{2}{3})^2)\chi_u + 3(-\frac{1}{3})^2)\chi_d + (-1)^2\chi_d = 4(\chi_u + \chi_d) = 8\right.$$

instead for the DFSZ-II model, the leptons couple to the complex conjugate up-type Higgs $\tilde{H}_u$ instead than to H_d, that corresponds to changing $\chi_d \to -\chi_u$ in the last term for E.

3

Axion Cosmology

Not only do axions 'clean' QCD from the Strong CP Problem, but they figure as appealing dark matter candidates, whose relic abundance is meant to account for the present Dark Matter (DM) content $\Omega_{DM}h^2 = 0.12$. Indeed the process of 'vacuum realignment', that is the axion relaxation to the minimum of its potential, turns to be a palatable production process, generally known as *misalignment mechanism*, where the resulting energy density has the same behaviour as ordinary matter. The dependence of the axion potential and mass on the temperature of the thermal bath plays a crucial role in determining the abundance of axions generated through this mechanism, as it is displayed in 3.1. Then in 3.2 we address axion evolution. First in 3.2.1 we scan the possible initial values for the axion field, i.e. for the 'misaligned' angle, that is related to its role during the inflation era. Then in 3.2.2 we present the misalignment mechanism itself pointing out its relevance in making axion a suitable Cold Dark Matter (CDM) candidate. Furthermore (3.2.3) we give a hint about other possible CDM contributions in the form of topological defects related to the axion in a spontaneous symmetry breaking framework.

The Misalignment mechanism is not the only mechanism of production for axions. As shown in 3.3, scatterings and decays of particles in the primordial plasma can produce relativistic axions. If their decoupling occurs at high enough temperatures, they remain relativistic throughout the history of the Universe. In this case, axions are dark radiation and they are the main concern of this work.

3.1 Temperature dependence in axion potential

We previously presented the axion potential derived using chiral perturbation theory, which allowed us to determine axion properties at zero temperature. Nevertheless this approach is no more useful when the temperature reaches the critical value T_C around 160 MeV when quarks are no more confined.

Let's see how we can qualitatively guess a form for such potential. We saw that the axion field is nothing but the angular degree of freedom of a complex scalar, that undergoes global $U(1)$ SSB at scale f_a. The axion is left as the corresponding massless Goldstone boson that therefore is exhibiting a shift symmetry. Then non-perturbative processes (i.e. the instanton term) induce an axion potential by breaking this shift symmetry at a specific energy scale, which, nevertheless, being the axion still the angular degree of freedom of a complex field, must satisfy a residual discrete shift symmetry of the kind $a \to a + 2\pi f_a / N_{DW}$.[1]. The potential is therefore periodic, a choice is:

$$V(a) = f_a^2 m_a^2(T) \left[1 - \cos \frac{Na}{f_a} \right] \tag{3.1}$$

where the mass is temperature, and so time, dependent. We can assume that well above T_C such dependence can be parametrised in terms of the zero temperature mass 2.2 as:

$$m_a^2(T) \approx m_a^2 \left(\frac{T_C}{T} \right)^{\gamma} \tag{3.2}$$

with $\gamma \sim 8$. In the limit of small displacements from the potential minimum ($a/f_a << 1$), the potential can be Taylor-expanded in the quadratic $\frac{1}{2} m_a^2 a^2$.

[1] Here $N_{DW} = 2N$ is also known as the domain wall number, where N denotes the color anomaly of the PQ symmetry. Indeed a PQ rotation of the quark fields, as seen, implies an anomalous term added to the Lagrangian, that, in the case of $SU(3)$, takes the form

$$S \to S + \int d^4x \frac{g_s^2}{32\pi^2} \frac{Na}{f_a} G\tilde{G}$$

where $N\delta_{ab} = 2Tr[Q_{PQ} T_a T_b]$, depending on the fermion content of our theory. The colour anomaly basically sets the number of minima in the potential, and so the number of vacua for a. Unless otherwise stated we will set $N_{DW} = 1$.

3.2 Axion as cold Dark Matter

The temperature dependence of the axion potential and mass will be crucial in the determination of its abundance as cold dark matter relic due to misalignment mechanism. To this purpose we report for simplicity the equation[2] that the homogeneous component of the axion field in terms of $\theta_{PQ} = a/f_a$ obeys to, taking into account only the quadratic potential:

$$\ddot{\theta}_{PQ} + 3H\dot{\theta}_{PQ} + m_a^2(T)\theta_{PQ} = 0 \tag{3.3}$$

where $H = \frac{\dot{a}}{a}$ is the Hubble parameter ad now a denotes the scale factor in FLRW metric. Here we will assume to be in a radiation-dominated background where $H = \frac{1}{2t}$, needing all of this to happen before matter radiation equality in order for axions to describe dark matter. Therfore we observe that this equation resemble the motion of a harmonic oscillator with time-dependent friction and axion mass term. The change from over-damped to under-damped motion, will occur when $H \sim m_a$ and the axion field starts oscillating, thus behaving as matter-like field[3].

3.2.1 Axion as a spectator during inflation

In order to solve axion field's evolution, we need to account for initial conditions. To this purpose we explore different scenarios that rise according to whether the PQ symmetry is broken or unbroken during inflation. The temperature of the Universe during inflation can be estimated through the Gibbons-Hawking formula $T_I = H_I/2\pi$, with H_I the inflationary Hubble scale. Experimental constraints give us $T_I < 1.4 \times 10^3\ GeV$ [7]. Therefore we have two options:

[2] The motion of θ is easy to understand as the the one of a scalar field initially displaced from the minimum of its potential $\frac{f_a^2}{2} m_a^2 \theta_{PQ}^2$. The axion Lagrangian density can be written in terms of θ_{PQ} as $L_{\theta_{PQ}} = f_a^2[\frac{\dot{\theta}_{PQ}^2}{2} - \frac{m_a^2\theta_{PQ}^2}{2}]$ and the equation of motion is obtained as usual through the variation of the action in FLRW background:

$$\frac{\partial\sqrt{-g}L}{\partial\theta} - \partial_\mu \frac{\partial\sqrt{-g}L}{\partial(\partial_\mu\theta)}$$

[3] The axion field, initially displaced from its vacuum expectation value, begins to oscillate coherently across the universe as the Hubble parameter drops below the axion mass. These oscillations behave like a harmonic oscillator with minimal spatial variation and are coherent across large regions of the universe, leading to a nearly uniform field. This coherence means that the oscillations are in phase over vast distances, which is key to the axion field acting as Cold Dark Matter. Indeed in momentum space the Fourier transform of this field peaks at low momentum, corresponding to low velocities for the axions. This slow velocity characterizes axions as CDM, crucial for cosmic structure formation.

- $fa < H_I/2\pi$ and PQ symmetry is unbroken during inflation, so φ has zero vacum expectation vale. Then when the radiation temperature falls below f_a after inflation, the symmetry breaking occurs and φ acquires a vev. Upon reaching this stage, the Universe results split in casually disconnected patches, each of which selects a distinct value for the angular variable $a/fa = \theta_{PQ}$. Moreover f_a is greater than the scale of non-perturbative physics, so at this time there is no preferred value for θ_{PQ}, that is randomly selected out of a uniform distribution on $[-\pi, \pi]$ for every Hubble patch. We can think at our current Universe as composed of several patches with varying initial θ_{PQ} values that, although not initially in causal contact, now assemble the region enclosed by our Hubble horizon. To solve the equation of motion, we will need the initial value θ_i. In the post-inflationary scenario, this can be extracted from the mean value of a uniform distribution over the unit circle, reading for a quadratic potential:

$$\theta_i \equiv \sqrt{\langle \theta_{PQ} \rangle^2} = \frac{\pi}{\sqrt{3}} \simeq 1.81 \tag{3.4}$$

  Another important feature of this scenario is the rising of topological defects from the spontaneous breaking of a global symmetry, such as domain walls and cosmic strings.

- $f_a > H_I/2\pi$ and PQ symmetry is broken during inflation. Also in this framework we assist to the formation of topological defects as phase transition relics, but in this case they are later diluted by inflation. Again, causally unconnected patches with varying values of θ_{PQ} form, but inflation expands them in a way that our current observable universe has started out at the end of inflation with a single, constant value everywhere. [4]

3.2.2 Misalignment mechanism

Misalignment mechanism is a non-thermal production process that entails the oscillation of θ_{PQ} around the minimum of its potential. Indeed, as seen in the previous section, in any case the initial θ_i has stochastic origin, so we can easily suppose that at early times it is 'misaligned' with the vacuum $\theta_{PQ} = 0$. At high temperatures the axion is basically massless and the solution of 3.3 is $\theta_{PQ} = const = \theta_i$. Then when the temperature T approaches T_C, the contribution of the mass term in 3.3 becomes comparable to the expansion rate of the Universe, and the axion starts to roll toward the minimum, and then oscillates around it[5] with angular frequency

[4] This value is entirely arbitrary and uniformly distributed, however one could argue that the presence of numerous distinct Hubble patches implies that values of θ near to zero cannot be ruled out unless invoking anthropic principle.

[5] This is in analogy with coherent oscillations of the inflaton field, but with no suppression due to decay. This field drives the rapid expansion in the inflationary phase of the early Universe and, at the end of his motion,he

$m_a(T)$. It is instructive to visualize the solution in the simplified case of a scalar field with a mass m_a that is not temperature dependent. Indeed in this case the exact solution is:

$$\theta = \theta_i \left(\frac{2}{m_a t}\right)^{\frac{1}{4}} \Gamma\left(\frac{5}{4}\right) J_{\frac{1}{4}}(m_a t)$$

where Γ is the gamma function and J the Bessel's function . Depending on the relative weight of the damping term and the mass term, we clearly distinguish two regimes for this solution. Initially the system is overdamped while the Hubble parameter is dominant, but at some point, once the damping term has decayed away, it begins to oscillate because of the mass term controlling its dynamics. The oscillating behaviour is even more evident considering the latest moments of the evolution, that is taking the limit of large $m_a t$. Since for large x the Bessel's function becomes $J_{\frac{1}{4}}(x) \approx (\pi x/2)^{-1/2} \cos(x - \pi/3)$, we can parametrize the late time evolution with a slowly decaying term times a fastly oscillating one:

$$\theta(t) \approx A(t) \cos(m_a t)$$

The main difference between this scalar case and the real axion is that we have a temperature-dependent axion mass, making a bit more difficult to find the solution, but the qualitative behaviour stays the same. Now we turn to the energy density stored in this late time solution, which could be done in a clever way. Multipying 3.3 by θ_{PQ}, at this stage we can substitute θ_{PQ}^2 by its average over one oscillation, which is the energy density of axion field $\langle \theta^2 \rangle = \rho_a = f_a^2[\theta_{PQ}^2 + \frac{m_a^2 \theta_{PQ}^2}{2}]$ obtaining[8]:

$$\dot{\rho}_a = \left[\frac{\dot{m}_a}{m_a} - 3H\right]\rho_a \quad \longrightarrow \quad \rho_a = const \frac{m_a(T)}{a^3} \tag{3.5}$$

So as $\rho_a \sim a^{-3}$, θ falls off as $a^{-3/2}$. This is telling us that the axion energy density varies in terms of the scale factor in the same way as non-relativistic matter in FLRW Universe, making the misalignment axion a valid DM candidate. This is particularly evident at zero temperature since before the mass is still varying with T. On the other end, the axion number density $n_a = \rho_a / m_a(T) \sim a^{-3}$, implying that its comoving number density (i.e. the ratio of number

settles near the minimum of its potential undergoing coherent oscillations. As the inflaton oscillates, it decays into other particles, heating the universe and seeding the particles that form matter and radiation, through the 'reheating'. The coherent oscillations of the axion field, instead, do not decay, and since they act like a collection of extremely light, slow-moving particles, they contribute to the universe's energy density as cold dark matter.

density to entropy density s[6] where the entropic degrees of freedom $g_{*,s}$ can be confused with effective number of relativistic degrees of freedom g_* at high T) is fixed and so one can exploit this to evaluate the present axion amount. The initial energy density trapped in the misaligned axion field is the purely potential term $\rho_{a,i} = m_a(T_{osc})^2\theta_i^2\frac{f_a^2}{2}$, where T_{osc} determines the start of oscillations and its defined by the condition $m_a(T_{osc}) = 3H(T_{osc})$. Then the ratio between $\rho_{a,i}/m_a(T_{osc})$ and the entropy density $s(T_{osc})$ is preserved up to the current value, assuming no further entropy production. Multiplying this by the entropy density today s_0 and by m_a, we can derive the current axion energy density and its contribution to the cosmic energy budget, noticing how the result depend on the initial displacement angle θ_i. We obtain:

$$\rho_0 = \frac{1}{2}\theta f_a^2 m_a m_a(T_{osc})\frac{g_{*,s}(T_0)T_0^3}{g_{*,s}(T_o sc)T_{osc}^3}$$

Since in radiation dominated era $H^2(Tosc) \sim g_*(T_{osc})T_{osc}^4$, the solution to the condition $m_a(T_{osc}) = 3H(T_{osc})$ involves temperature dependence of $g_{*,s}$. Indeed, having in mind the temperature dependence of m_a in 3.2, we solve:

$$T_{osc} = \left(\sqrt{\frac{10}{\pi^2 g_*(T_{osc})}}m_a M_{Pl}\right)^{\frac{2}{\gamma+4}} T_C^{\frac{\gamma}{\gamma+4}}$$

We can adjust $\gamma = 8$, $T_C = 150\,MeV$, $m_a = 10\,\mu eV$ to have $T_{osc} \approx 1\,GeV$. So reasonably the oscillations will begin between the electroweak and QCD eras, when we can take the effective number of relativistic degrees of freedom to be $g_{*,s} \approx g_* = 61.75$, while the entropic degrees of freedom today is $g_{*,s} = 3.91$. The prevision for the axion contribution in terms of fraction of the total cosmic energy density is obtained dividing ρ_0 by $\rho_{tot} = 3H_0^2M_{Pl}^2$. This esteem would depend on m_a, f_a and θ_i. Using 2.2 we can relate f_a to m_a, and obtain a prediction for m_a that could match the present dark matter content[9]:

$$\Omega_a h^2 \approx 0.12\theta_i^2\left(\frac{4.7\mu eV}{m_a}\right)^{\frac{7}{6}} \approx 0.12\left(\frac{\theta_i}{2.155}\right)^2\left(\frac{9.0\,\mu eV}{m_a}\right)^{\frac{7}{6}}$$

Here the choice for θ_i comes from the average value of $\langle\theta_i\rangle^2$, considering a not exact quadratic potential, but an actual cosine[7]. The axion mass dependence $m_a^{-7/6}$ tells us that we get a smaller

[6] The entropy density is scaling with the temperature as $s(T) = \frac{2}{45\pi^2}g_{*,s}(T)T^3$

[7] The reason why this corrected value is higher than $(1.81)^2$ obtained at 3.4 is that the gradient of a cosine potential is shallower compared to a harmonic potential at large θ therefore the start of oscillations is delayed, and

dark matter density when the axion mass is heavier. This, that at first glance could seem a little counter-intuitive, can be explained remembering that the number density is set at T_{osc} and then gets diluted by the expansion until today. So the later T_{osc} occurs, the least axions get diluted and we are left with a bigger density. Then, since T_{osc} is defined when the Hubble scale drops below the mass, we see that lighter axions start oscillating later. Finally we can assert that, in order to explain dark matter, is very likely for axion particle to have a mass of order 10 μeV.

3.2.3 Topological defects from symmetry breaking

In post-inflationary scenarios the production of cold axions from misalignment discussed in the previous section is not the only Cold Dark Matter production mechanism. Additional contributions are related to the existence of topological defects.
Indeed spontaneous symmetry breaking in the early Universe is associated with phase transitions, leading to the possibility of formation of topological defects, such as domain walls and strings [10]. As seen, these are relevant only in the post inflationary scenario. Let's briefly sketch in intuitive way how these form.
At the end of the phase transition related to the spontaneous breaking of the PQ symmetry, the phase for the vacuum $a(x)/f_a$ of the PQ field is position dependent and acquires all values between $[0, 2\pi]$ in different causally uncorrelated domains. Let's observe a closed loop in physical space intersecting such regions, which is shrinking to a point. Since at the edge the phase cannot change continuosly, there must be a point within the path where this is undefined and, by continuity, the field is zero (false vacuum). In order to avoid for the path to be topologically trivially contracted, such points are aligned in a close or infinite string, called the axion string.
As the Universe expands and cools down, at some point perturbative QCD effects provide an axion potential (see 3.1) with periodicity $2\pi f_a/N$, characterised by N equivalent minima, which are related by a Z_N discrete symmetry. In different casually disconnected patches, the field assume different minima, so, in order for the transition to be smooth, there must be in between a region of false vacuum. Field configurations that interpolate in space between neighbouring vacua are domain walls.

---

so we get more axions out of them than we would in the harmonic approximation.[9]

3.3 Thermal production

If axions stay in contact with the thermal bath particles, then mutual production and annihilation, as well the decay of some massive particles coupled to the axion can lead to a population of relativistic axions. Our Universe, as tested through the cosmological data, is compatible with the degrees of freedom predicted by the SM. Therefore, any form of an additional population that is created at early times, must be very little but yet detectable by better resolved probes. Alongside $C\gamma B$ (i.e. *CMB*) and $C\nu B$, it may be possible to see a cosmic axion background *CaB* as well.

In order to create a thermal population of axions the dominant process is pion-axion conversion $N+\pi \rightarrow N+a$, where nucleons N are non-relativistic, since they came into existence only after the quark/hadron transition ($T \simeq 200 MeV$), and so the interaction rate is exponentially cut off. At higher temperatures, before QCD phase transition, there are no nucleons or pions but only quarks and gluons free in the plasma, and the dominant axion production process is photon or gluon production $a + q \rightarrow q + \gamma/G$. These interactions are relevant until the interaction rate Γ drops below the Hubble expansion rate H, then the axions decouple from the thermal bath. At this point the axion abundance is fixed by freeze-out at the decoupling temperature T_D, which occurs when $\Gamma \sim H$. Axions produced in this way are relativistic as long as $T_D > m_a$, then, once they decouple, their temperature redshifts independently from the thermal bath. If their mass is large enough ($m_a \geq 1eV$), thermal axions contribute as Hot Dark Matter (HDM), a component that behaves like matter at late times, but was initially produced while relativistic and so free-streamed during early structure formation. In this case axions would behave similarly to massive neutrinos preventing the formation of cosmic structures below the free-streaming scale. Nowadays we can state that axion is excluded as a hot dark matter candidate by the current mass bounds. Nevertheless a *CaB*, not necessarily coming from HDM contribution, is possible if the mass of the axion is negligible compared to its thermal energy for most of the cosmic history. In particular, if the axions produced at early times are still relativistic around recombination, they should show up as an additional contribution to the amount of radiation at the time of CMB formation.

In general the energy density stored in relativistic degrees of freedom can be probed at two key moments in the cosmic evolution: the Big Bang Nucleosynthesis (BBN)[8], for which the

[8] Big Bang Nucleosynthesis (BBN) is the process responsible for the synthesis of light nuclei in the early universe, beginning at a temperature scale of around 1 MeV and concluding at approximately 60 keV, lasting for about

amount of light particle is mostly relevant when Universe was one second old and at a temperature of $\sim 1\,MeV$, and the last scattering surface, namely the stage at which protons and electrons form neutral hydrogen, and photons could travel undisturbed afterward, dubbed the Cosmic Microwave Background (CMB) radiation, corresponding to $T_{CMB} \sim 0.3\,eV$ and a quite young the universe (approximately 380.000 years old).

Generically light particles that can be present in the relativistic regime with a significant cosmic abundance at the time of BBN and CMB, alongside photons and neutrinos, are address to as 'dark radiation'. Historically, the presence of this dark radiation is quantified in terms of an effective number of additional neutrino species, that we will estimate for axion across a specific stage of our early Universe. In particular the goal of this work is to evaluate thermal axion production above and below the ElectroWeak Phase Transition (EWPT).

More explicitly, the energy density of relativistic particles at the time of CMB formation can be written as

$$\rho_R(T_{CMB}) = \rho_\gamma + \rho_\nu + \rho_a = \left[1 + \frac{7}{8} N_{eff} \left(\frac{4}{11}\right)^{\frac{4}{3}}\right] \rho_\gamma \tag{3.6}$$

where the first term in the bracket is referred to photon contribution and the second one, weighted by the statistical Fermi-Dirac factor and the fourth power of the neutrino to photon temperature ratio $T_\nu/T_\gamma = (4/11)^{\frac{1}{3}}$, to neutrinos and possible dark radiation amount. Here figures the number of effective neutrino species N_{eff}: if we limit to the SM prediction, then this is naively the number of fermion generations. i.e. three. Nowadays outcomes are consistent with such prediction[9]. Nevertheless upcoming trials are meant to improve bounds on this quantity and could potentially discover a deviation from the SM, enhancing extra dark radiation components in form of relativistic species which decoupled at high temperatures, as high as the EWPT.

---

three minutes. During this period, the formation of nuclei is critically dependent on the neutron-to-proton ratio, which in turn is influenced by the decoupling of neutrons from the thermal bath. In a radiation-dominated universe, the Hubble expansion rate H scales as $H \sim \sqrt{g_\rho^*}$, where g_ρ^* is the effective number of relativistic degrees of freedom contributing to the energy density. A higher g_ρ^* implies that a greater number of relativistic particles are present in the MeV range, leading to a faster expansion rate H. So the point at which the weak interaction rate falls below the Hubble rate (i.e., when $\Gamma < H$) occurs earlier. This earlier decoupling results in a higher neutron-to-proton ratio at the time of nucleosynthesis, as neutrons have less time to decay into protons before they become bound in nuclei.

[9]BBN and CMB currently exhibit similar sensitivities in probing the effective number of neutrino species. For BBN (where the effective number of neutrino species is usually denoted by N_ν), analysis of light element abundances yields $N_\nu = 2.889 \pm 0.229$ [11, 12]. On the CMB side, the most precise measurement comes from the Planck satellite, giving $N_{Planck,eff} = 2.99 \pm 0.17$ [13], which at the moment, represent the best sensitivity available .

4

Production of hot axions above and below the EWPT

In chapter 2 we presented axion couplings to matter fields. We sum up them in two classes of interactions: couplings with gauge bosons $X = \{G, W, B\}$, that rise if the PQ symmetry is anomalous under the associated gauge group, and with SM fermions $\psi = \{Q_L, u_R, d_R, L_L, e_R\}$. We report them in the following:

$$L_a^{int} = \frac{1}{f_a}\left[aC_X\frac{\alpha_X}{8\pi}X^{a,\mu\nu}\tilde{X}_a^{\mu\nu} + \partial_\mu a C_\psi \bar{\psi}\gamma^\mu\psi\right] \tag{4.1}$$

As seen in the previous chapter, thermal axions can be produced either via scatterings or decays in the thermal bath. In particular, while both classes of interactions are relevant for scatterings, only coupling to fermions could account for production via tree-level decays if the fermion bilinear comprises fields belonging to different fermion generations, that is flavor violating couplings. The bosonic operators are suppressed by a loop factor and indeed should be understood as quantum level contributions due to the effects of the presence of some fermion that couples to the axion. In this work we focus on axion interactions with SM fermions, in particular with third generation quarks, and therefore on binary scatterings. These collisions always involve two SM fermions, the axion itself and one SM boson. At temperatures above the EWPT, this can be any of the four real component of the Higgs doublet, instead it can be a gauge field only

below the EWPT. In this chapter we aim to derive scattering cross section for these collisions. We look for the needed axion-quark couplings to select the interesting production process, for whose we list the computed cross sections (4.1 and 4.2). Detailed computations are sketched in appendix B. To be consistent with a smooth treatment of the EWPT, we expect to find the matching between the cross sections evaluated above and below this critical threshold, as showed in 4.3 The outcomes of this chapter are in agreement with the results presented in [14].

4.1 Above the EWPT

Since decays are loop and CKM suppressed in the flavor conserving case, we focus on binary scatterings. We write explicitly the axion derivative interaction terms with quarks, in the case of flavor conserving couplings:

$$L^a_{FC} = \frac{\partial_\mu a}{f_a} \sum_{i=1}^{3} \left(C_Q \bar{Q}^i_L \gamma^\mu Q^i_L + C_u \bar{u}^i_R \gamma^\mu u^i_R + C_d \bar{d}^i_R \gamma^\mu d^i_R \right) \tag{4.2}$$

where we introduced the dimensionless coefficients C_Q, C_u and C_d. It's convenient to redefine the fields rotating them by an axion dependent phase:

$$Q^i_L \to e^{iC_Q \frac{a}{f_a}} Q^i_L \qquad u^i_r \to e^{iC_u \frac{a}{f_a}} u^i_R \qquad d^i_R \to e^{iC_d \frac{a}{f_a}} d^i_R$$

As a consequence of these chiral rotations the axion couplings to gauge bosons are affected by anomalous terms while, from the quark kinetic term, we generate new axion derivative couplings that simplify the ones presented above 4.2. Finally and most important for us, the axion field appears in the Yukawa sector:

$$-L^a_{Y,FC} = e^{i(C_d - C_Q)\frac{a}{f_a}} \hat{\lambda}_d \bar{Q}_L \varphi d_R + e^{i(C_u - C_Q)\frac{a}{f_a}} \hat{\lambda}_u \bar{Q}_L \tilde{\varphi} u_R + h.c.$$

where the hatted matrices $\hat{\lambda}_{u,d}$ are diagonal in flavor space. So scattering amplitudes can depend only on two linear combinations of the three coefficients. Since we only focus on the third quark generation, we label with the top and bottom quark as $C_t \equiv -C_Q + C_u$ and $C_b \equiv -C_Q + C_d$. Then, calling their chiral components t_L, t_R and b_L, b_R, we move to mass eigenstates

exploiting the parametrization for the Higgs doublet:

$$\varphi = \begin{pmatrix} \chi_+ \\ \chi_0 \end{pmatrix} \qquad\qquad \tilde{\varphi} = i\sigma_2(\varphi^\dagger)^T = \begin{pmatrix} \chi_0^c \\ -\chi_- \end{pmatrix}$$

where $\chi_- = (\chi_+)^\dagger$ and $\chi_0^c = (\chi_0)^\dagger$. The Lagrangian becomes:

$$\begin{aligned} -L^a_{Y,FC} = {} & y_t e^{i(C_t)\frac{a}{f_a}} \left[\chi_0^c \bar{t}_L t_R - \chi_- \bar{b}_L t_R\right] + y_b e^{i(C_b)\frac{a}{f_a}} \left[\chi_+ \bar{t}_L b_R + \chi_0 \bar{b}_L b_R\right] + \\ & + y_t e^{-i(C_t)\frac{a}{f_a}} \left[\chi_0 \bar{t}_R t_L - \chi_+ \bar{t}_R b_L\right] + y_b e^{-i(C_b)\frac{a}{f_a}} \left[\chi_- \bar{b}_R t_L + \chi_0^c \bar{b}_R b_L\right] \end{aligned} \tag{4.3}$$

Since we are looking for collisions producing one axion field in final state, we can expand at first order $e^{i\frac{a}{f_a}} \approx 1 + i\frac{a}{f_a}$. From 4.3 we can read the couplings of amplitudes for scatterings involving, beside the axion, two fermions, that can be either both in the initial state or one in the initial state and the other one in the final state, and a component of the Higgs Boson[1]. Then we can evaluate the amplitudes for the various binary scatterings and derive the cross sections[2]. We list all the possible processes and the associated cross section in 4.1.

4.2 Below EWPT

As a consequence of electroweak symmetry is broken the Higgs field gets a vev rising mass terms for SM particles (see A.2.1). Then let's go back to 4.2 and consider it in mass basis. What we have is:

$$L^a_{FC} = \frac{\partial_\mu a}{f_a} \sum_{i=1}^{3} \left(C_Q \bar{u}_L \gamma^\mu u_L + C_Q \bar{d}_L \gamma^\mu d_L + C_u \bar{u}_R \gamma^\mu u_R + C_d \bar{d}_R \gamma^\mu d_R\right) \tag{4.4}$$

[1] In this basis is evident that there is no process involving SM gauge bosons. Alternatively, if we insisted on working in the basis where axion is derivatively coupled to SM fermions then we obtain all binary amplitudes to vanish as they would require a fermion chirality flip, that is not possible in the unbroken phase because we have no mass term for the fermion itself.

[2] Those are obtained via integration of the formula for the differential cross section in the center of mass (COM) frame, that we are familiar to in literature:

$$\frac{d\sigma}{d\Omega} = \frac{1}{64\pi^2 s} \frac{|p'|}{|p|} |M|^2$$

where s denotes the usual COM squared energy.

Process	*CP conjugate*	$\sigma_{ij\to ka} \times 64\pi f_a^2$
$t\bar{t} \to \chi_0 a$	$t\bar{t} \to \chi_0^c a$	$C_t^2 y_t^2$
$b\bar{b} \to \chi_0 a$	$b\bar{b} \to \chi_0^c a$	$C_b^2 y_b^2$
$t\bar{b} \to \chi_+ a$	$b\bar{t} \to \chi_- a$	$C_t^2 y_t^2 + C_b^2 y_b^2$
$t\chi_0 \to ta$	$\bar{t}\chi_0^c \to \bar{t}a$	$C_t^2 y_t^2$
$t\chi_0^c \to ta$	$\bar{t}\chi_0 \to \bar{t}a$	$C_t^2 y_t^2$
$b\chi_0 \to ba$	$\bar{b}\chi_0^c \to \bar{b}a$	$C_b^2 y_b^2$
$b\chi_0^c \to ba$	$\bar{b}\chi_0 \to \bar{b}a$	$C_b^2 y_b^2$
$t\chi_- \to ba$	$\bar{t}\chi_+ \to \bar{b}a$	$C_t^2 y_t^2 + C_b^2 y_b^2$
$b\chi_+ \to ta$	$\bar{b}\chi_- \to \bar{t}a$	$C_t^2 y_t^2 + C_b^2 y_b^2$

Table 4.1: In the first two columns we list the possible scattering processes producing axions above the EWPT. We can either have fermion/antifermion annihilations producing an axion and any of the components of the Higgs doublet or just one fermion plus a Higgs component in the initial state. For each process the scattering cross section is provided.

Specifying the chiral components for the third generation quark fields we obtain:

$$L_{3rd}^a = \frac{\partial_\mu a}{2f_a}\left[\bar{t}\gamma^\mu(C_{V,t} + C_{A,t}\gamma^5)t + \bar{b}\gamma^\mu(C_{V,d} + {}_{A,d}\,\gamma^5)b\right]$$

where we define axial and vector quark couplings as $C_{V,q} = (C_q + C_Q)$ and $C_{A,q} = (C_q - C_Q)$ with $q = u, d$ referred to third generation quarks. Nevertheless only the axial contribution is relevant since, exploiting total derivative invariance of the Lagrangian:

$$\partial_\mu a \bar{q}\gamma^\mu q = -a\partial_\mu(\bar{q}\gamma^\mu q) = 0$$

by conservation of axial vector current. Then we notice that $C_{A,t} \equiv C_t$ and $C_{A,b} \equiv C_b$. Finally the interactions we will consider are of the kind:

$$L_{3rd}^a = \frac{\partial_\mu a}{2f_a}(C_t\bar{t}\gamma^\mu\gamma^5 t + C_b\bar{b}\gamma^\mu\gamma^5 b) \tag{4.5}$$

Here we can read the axion couplings to quark, instead the quark couplings to gauge fields are the SM ones (A.2.2).

The available interactions rising from such couplings can be be split in two main types: we can either have quark-antiquark in the initial annihilation into a gauge boson plus axion, or quark scattering with a boson producing an axion in the final state. All the possible processes are listed in 4.2. Since the explicit expressions for the corresponding cross sections are too long to be displayed in the table, we report them in B. Besides the main steps for complete calculations

Process	*CP conjugate*	$\sigma_{ij\to ka}$
$q\bar{q} \to \gamma a$	SAME	B.7
$q\bar{q} \to g a$	SAME	B.8
$q\bar{q} \to h a$	SAME	B.9
$t\bar{t} \to Z^0 a$	SAME	B.5
$b\bar{b} \to Z^0 a$	SAME	B.10
$t\bar{b} \to W^+ a$	$b\bar{t} \to W^- a$	B.11
$q\gamma \to q a$	$\bar{q}\gamma \to \bar{q} a$	B.12
$qg \to q a$	$\bar{q}g \to \bar{q} a$	B.13
$qh \to q a$	$\bar{q}h \to \bar{q} a$	B.14
$tZ^0 \to t a$	$\bar{t}Z^0 \to \bar{t} a$	B.6
$bZ^0 \to b a$	$\bar{b}Z^0 \to \bar{b} a$	B.15
$tW^- \to b a$	$\bar{t}W^+ \to \bar{b} a$	B.16
$bW^+ \to t a$	$\bar{b}W^- \to \bar{t} a$	B.17

Table 4.2: In the first two columns we list the possible scattering processes producing axions below the EWPT. We can either have quark-antiquark annihilation into one gauge boson plus axion, or quark scattering with a boson rising an axion in the final state. Here $q = t, b$. For each process the scattering cross section is provided.

of cross sections are here explained for two processes, in order to outline the adopted procedure.

4.3 Matching at the EWPT

Once we have collected all the analytical expressions for cross sections above and below the EWPT, we may ask whether these actually match at this critical threshold. In particular since three out four components of the Higgs doublet correspond to the longitudinal components of the Z^0 and $W^\pm$ bosons below the EWPT, we want to connect the process involving them across this stage. Indeed a proof of consistency is to check that in the limit of vanishing masses the cross sections below EWPT coincide exactly with those above. Looking at the expressions in 4.1 and 4.2, one can easily see this is happening for[3]:

- *neutral annihilations*:

$$\sigma_{t\bar{t}\to\chi_0 a} + \sigma_{t\bar{t}\to\chi_0' a} = \sigma_{t\bar{t}\to h a} + \sigma_{t\bar{t}\to Z_L^0 a} = \frac{C_t^2 y_t^2}{32\pi f_a^2}$$

[3] As said, the Z and W components involved in the following processes are the longitudinal ones and will be therefore denoted with an index L. Indeed since cross section calculations engage the scattering amplitudes averaged over initial states, one can check that the expressions involving initial bosons that we consider here differ from the ones reported in B of a factor three.

- *neutral scatterings*

$$\sigma_{t\chi_0\to ta} + \sigma_{t\chi_0^c\to ta} = \sigma_{th\to ta} + \sigma_{tZ_L^0\to ta} =$$
$$= \sigma_{\bar{t}\chi_0^c\to\bar{t}a} + \sigma_{\bar{t}\chi_0\to\bar{t}a} = \sigma_{\bar{t}h\to\bar{t}a} + \sigma_{\bar{t}Z_L^0\to\bar{t}a} = \frac{C_t^2 y_t^2}{32\pi f_a^2}$$

- *charged annihilations:*

$$\sigma_{t\bar{b}\to\chi_+ a} + \sigma_{b\bar{t}\to\chi_- a} = \sigma_{t\bar{b}\to W_L^+ a} + \sigma_{b\bar{t}\to W_L^- a} = \frac{C_t^2 y_t^2 + C_b^2 y_b^2}{32\pi f_a^2}$$

- *charged scatterings*

$$\sigma_{t\chi_-\to ba} + \sigma_{b\chi_+\to ta} = \sigma_{tW^-\to ba} + \sigma_{bW^+\to ta} =$$
$$= \sigma_{\bar{t}\chi_+\to\bar{b}a} + \sigma_{\bar{b}\chi_-\to\bar{t}a} = \sigma_{\bar{t}W_L^+\to\bar{b}a} + \sigma_{\bar{b}W_L^-\to\bar{t}a} = \frac{C_t^2 y_t^2 + C_b^2 y_b^2}{32\pi f_a^2}$$

5

Tracking the number density

The equation ruling the axion number density evolution with time is the following Boltzmann equation, whose derivation is presented in C:

$$\frac{d}{dt}n_a + 3Hn_a = \sum_S \bar{\Gamma}_s(n_a^{eq} - n_a) \tag{5.1}$$

where H is the Hubble parameter. We underline that this equation has been derived under the assumption of kinetic equilibrium for the axion, and also of chemical equilibrium for bath particles. The collision operator on the RHS involves the sum over thermally averaged scattering cross sections that are linked to the quantities we previously evaluated:

$$\bar{\Gamma}_S = \frac{g_i g_j}{32\pi^4 n_a^{eq}} T \int_{s_{min}}^{\infty} ds \frac{\lambda(s, m_i, m_j)}{\sqrt{s}} \sigma_{ij\to ka}(s) K_1(\frac{\sqrt{s}}{T}) \tag{5.2}$$

where $\lambda(s, m_i, m_j) = [s - (m_i + m_j)^2][s - (m_i - m_j)^2]$ and the minimum center of mass energy is $s_{min} = Max((m_i + m_j)^2, m_k^2)$ depending on the process. $K_n(z)$ are the modified Bessel function of the second kind. As it is common in literature, we switch our unknown to $Y_a = n_a/s$ and our evolution variable to $x = m/T$, where m is the haviest mass involved in the process and T the thermal bath temperature [1]. The equation that we are going to solve

[1] We have that the LHS is $\dot{n_a} + 3Hn_a = a^{-3}(\dot{a^3 n_a}) = s(\dot{n_a/s}) = s\dot{Y_a}$, supposing entropy in conserved in a cohomoving volume. Also, to perform the change of variable we have in mind that $\frac{dx}{dt} = -\frac{m}{T^2}\frac{dT}{dt} =$

numerically is finally:

$$sHx\frac{dY_a}{dx} = \left(1 - \frac{1}{3}\frac{d\ln g_s^*}{dlnx}\right)\left(\sum_S \gamma_{a,S}\right)\left(1 - \frac{Y_a}{Y_{eq}}\right) \tag{5.3}$$

with $\gamma_{a,S} \equiv n_a^{eq}\bar{\Gamma}_S$.
The main focus of section 5.1 is to depict $\gamma_{a,S}$ as function of the temperature T for the various processes across the EWPT.

5.1 Thermally averaged cross sections

In order to analyze quantities that are function of the temperature alone, we remove the dependence on the other parameters in $\gamma_{a,S}$ through the definition:

$$\gamma_S(T) = \frac{f_a^2\gamma_{a,S}}{C_{t,b}^2 y_{t,b}^2} \qquad or \qquad \gamma_S(T) = \frac{f_a^2\gamma_{a,S}}{C_t^2 y_t^2 + C_b^2 y_b^2} \tag{5.4}$$

respectively for all neutral and charged scatterings involving third generation quarks t and b. The quantity γ_S involves an integral that can be always computed numerically in a specific temperature range, and so we evaluate it for each process above and below EWPT accounting for the playing temperatures.
In particular we take as reference threshold the critical temperature corresponding to the Higgs vev $v \sim 245\ GeV$. Then for cross sections above the EWPT γ_S is easy to compute analytically: for each of them we get a dependence $\sim T^6$. Then all results are summed up to obtain $\sum_{S,above}\gamma_S \equiv \gamma_{above}$ and displayed in a logarithmic plot as a function T. This is done for a temperature range $[10^4, 245]\ GeV$ in 5.1.

$-\frac{x}{T}[-HT/(1+\frac{1}{3}\frac{dlog(g_s^*)}{dlogT})]$ and $dlogT = -dlogx$

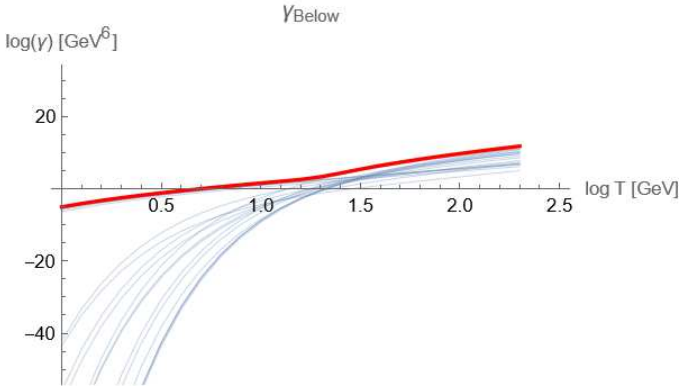

Figure 5.2: Plot of $\log_{10}(\gamma)$ as a function of $\log_{10}(T)$ after electroweak symmetry breaking for a T range of $[245, 1]\ GeV$. Thin blue lines are referred to each single process in 4.2 summing up to the total rate in red.

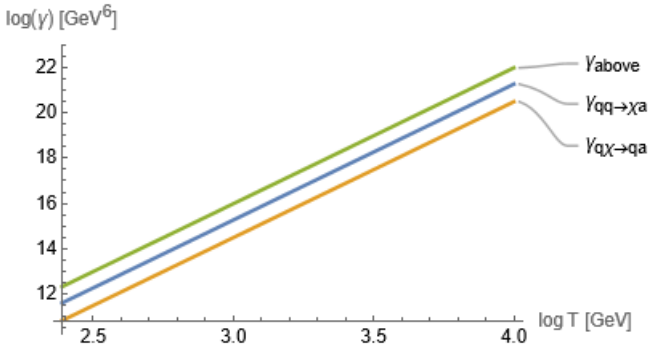

Figure 5.1: Plot of $\log_{10}(\gamma)$ as a function of $\log_{10}(T)$ before electroweak symmetry breaking for a T range of $[245, 10^4]\ GeV$. We plot the rate for each single process where the component of the Higgs doublet is in the initial state (orange) or in the final state (blue), and the total rate (green) accounting for all scatterings in 4.1.

For cross sections below the EWPT the integral 5.2 is too complicated to be solved analytically, but we are able to find a numerical solution: therefore we evaluate it for temperatures in a range of $[1, 245]\ GeV$ for every process listed in 4.2. Then we sum them up to $\sum_{S,below} \gamma_S \equiv \gamma_{below}$. A logarithmic plot for γ_{below} is shown in 5.2 . Finally the total rates γ_{above} and γ_{below} calculated for scattering processes, respectively, above and below the EWPT, are expected to connect smoothly at this threshold: this is easy visualised in 5.3. Here we considered processes involved in the matching that we presented in 4.3, where the yukawa couplings have been introduced for rates above the EWPT and the axion-quark couplings have been set to one.

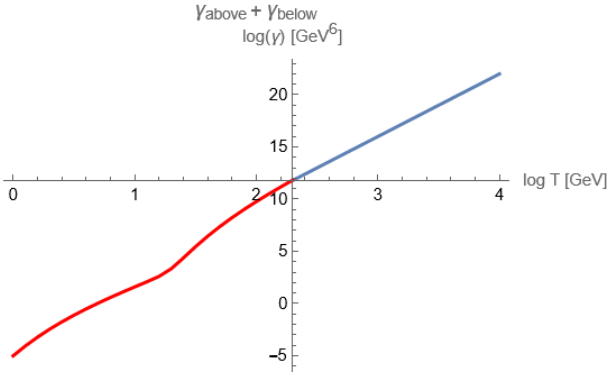

Figure 5.3: Matching of rates above and below the electroweak phase transition. The total rate for interactions involving massive bosons below this threshold smoothly connects with their counterparts in the unbroken phase. All axion-quark couplings have been set to one.

In the following we will switch on separately the top- and bottom-axion couplings and evaluate the total rates imposing $C_t = 1$ or $C_b = 1$ respectively.

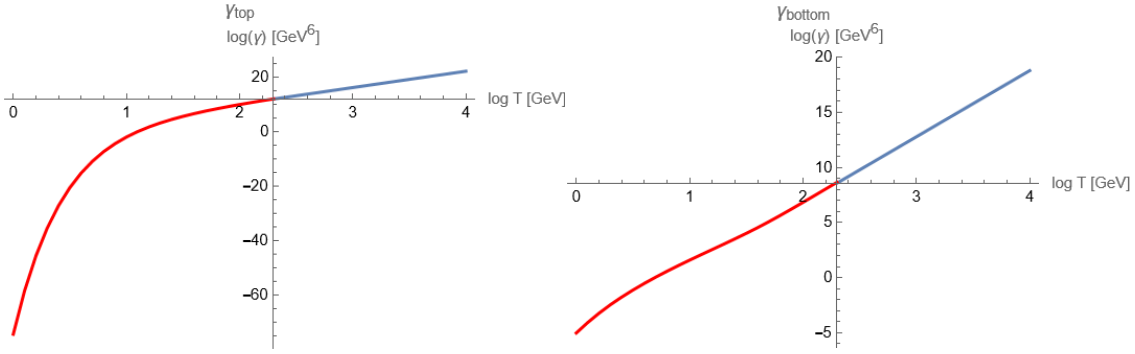

(a) (b)

Figure 5.4: Matching of rates above and below the electroweak phase transition for top-axion coupling (a) and for bottom-axion coupling (b).

5.2 Evaluation of ΔN_{eff}

The rates that we obtained in the previous section are needed to solve the Boltzmann equation 5.3. Therefore we perform interpolations of such total rates and plug these into the equation. This is then numerically solved. The numerical solution is evaluated from an initial temperature $T_i = 10^4\ GeV$ and assuming the initial abundance of axions to be zero down to the EWPT stage ($T_c \simeq 245\ GeV$), using the above EWPT interpolated rate, and then down to the lower temperature of $T_f = 1\ GeV$ with an initial thermal abundance of axions at T_c, exploiting the

results obtained below the EWPT. The very same result is obtained considering a single rate across the EWPT and solving the equations from T_i down to a temperature T_f. In particular we derive solutions for bottom and top axion couplings separately, that we set to one, depending on the axion suppressing scale f_a.

This results need to be connected to our relevant physical observable, that is ΔN_{eff}.
We previously discussed the effective number of neutrinos N_{eff} that is related to the radiation energy density $\rho_R = \rho_\gamma + \rho_\nu + \rho_a$, which includes any relativistic particle with a non-negligible contribution, by 3.6. What we are interested in is the deviation from the predicted value, that accounts only for neutrinos contribution, due to axion dark radiation. This defines:

$$\Delta N_{eff} = N_{eff} - N_{eff}^{SM} = \frac{8}{7}\left(\frac{11}{4}\right)^{4/3}\frac{\rho_a}{\rho_\gamma} \tag{5.5}$$

Since we derived the Boltzmann equations for the axion comoving number density $Y_a = n_a/s$, we connect ΔN_{eff} to this quantity [2]:

$$\Delta N_{eff} \simeq 74.8449\, Y_a^{4/3} \tag{5.6}$$

We notice that this last step required converting the asymptotic comoving number density into an asymptotic comoving energy density, thus we made the further assumption of *chemical* equilibrium also for axion particle. This implies the expressions for the number density and the energy density being the equilibrium ones:

$$n_a = \frac{\zeta(3)}{\pi^2}T^3 \qquad \rho_a = \frac{\pi^2}{30}T^4$$

that are valid for Bose-Einstein (BE) statistics.

[2] Given that the entropy density is $s = \frac{2\pi^2}{45}g_s^* T^3$ and the axion number density reads $n_a = \frac{\zeta(3)}{\pi^2}T^3$, we can invert both and find two expression for T: one will be inserted in $\rho_\gamma = \frac{2\pi^2}{30}T^4 = \frac{2\pi^2}{30}\left(\frac{45s}{2\pi^2 g_s^*}\right)^{4/3}$ while the other in $\rho_a = \frac{\pi^2}{30}T^4 = \frac{\pi^2}{30}\left(\frac{\pi^2 n_a}{\zeta(3)}\right)^{4/3}$. Combining the two into ΔN_{eff} and the the considering value of $g_s^* = 43/11$ at recombination, we obtain its relation to Y_a.

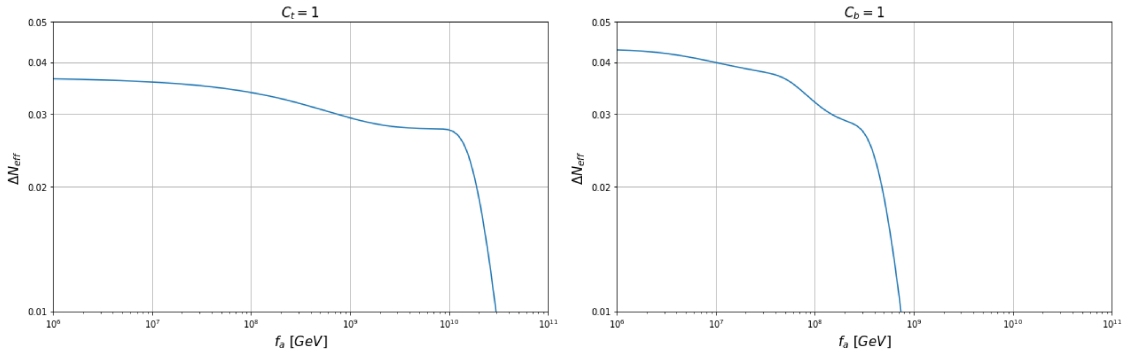

(a) (b)

Figure 5.5: ΔN_{eff} as function of f_a for top and bottom axion coupling separately

Given this is easy to evaluate ΔN_{eff}. The results are shown in 5.5a and 5.5b for top-axion and bottom-axion couplings respectively as a function of the scale f_a.
The general behaviour is that the signal increases as f_a decreases, reflecting the fact that the axion decouples at lower temperatures, where the number of degrees of freedom in thermal equilibrium is smaller, and yields a bigger ΔN_{eff}. Indeed this can be easily understood observing that the axion decouples from the thermal bath when its interaction rate drops below the Hubble expansion rate. For smaller f_a, the axion-quark interactions are stronger, leading to decoupling at lower temperatures. Consequently, the axion remains in thermal equilibrium for a longer period, contributing more significantly to the radiation density and thus increasing ΔN_{eff}. We set $C_i = 1$ in our equations, effectively examining the results as a function of f_a/C_i. The clear conclusion is that larger couplings keep the axion in thermal equilibrium down to lower temperatures, resulting in a larger axion relic density and a higher ΔN_{eff}.
However, this increase in ΔN_{eff} does not continue indefinitely. The plateau observed in the figure arises because, at some point, even though the interaction rate continues to increase as f_a decreases, the comoving number density of axions saturates. This saturation occurs when the decoupling temperature reaches a regime where the thermal bath is dominated by particles that are already non-relativistic, limiting further increase in the axion number density and thus in ΔN_{eff}.
We also observe that for $f_a < 10^9\ GeV$ processes involving the axion-bottom coupling become efficient and provide a larger ΔN_{eff} compared to the axion-top case. The top quark, due to its larger mass, decouples from the thermal bath earlier compared to the bottom quark and thus the overall ΔN_{eff} turns to be smaller. Nevertheless, because the top mass (or equivalently the top Yukawa coupling) is larger, and the cross section is proportional to the mass, the suppres-

sion of ΔN_{eff} at larger f_a is less pronounced.
In summary: when f_a is large, the axion-top quark interaction dominates because of the larger cross-section, but since the top quark decouples earlier, the axion contribution to ΔN_{eff} remains smaller. As f_a decreases, axion-bottom quark interactions become more significant. Since the bottom quark decouples later than the top quark, this results in a larger ΔN_{eff} because the axion remains coupled to the thermal bath for a longer period. For very low f_a , the axion continues to interact with quarks down to even lower temperatures. However as the bottom quark decouples, no further increase in ΔN_{eff} is observed, leading to the saturation of Y_a and the formation of a plateau.

6

Towards a Phase Space analysis

As seen, interactions in the thermal bath dump relativistic axion particles into the early Universe in the form of dark radiation. If such processes occur rapidly enough compared to the expansion rate of the Universe, these may even lead to thermal equilibrium, until at some point the Universe become so cold and diluted that particles cannot interact anymore and they just free-stream uninterrupted. The goal of our discussion is to estimate their contribution to the energy density stored in relativistic degrees of freedom at the time of CMB formation, quantified by ΔN_{eff}. To this purpose in chapter 5 we exploited the formalism of the Boltzmann equation for the number density, but in this section we aim to lay the foundations to a more accurate analysis that could improve our predictions. Indeed solving ordinary differential equations that track a given moment of the distribution function allows to predict the amount of dark radiation with a certain accuracy, but these are based upon some assumptions that are not always justified. In what follows we will portray a formalism based entirely on a phase space analysis, presented in a model independent way in [1], and apply it to the specific case of axion production across the EWPT. We will build an integro-differential Boltzmann equation that allows to track the particle distribution in the phase space without the assumption of reaching a thermal profile, as happens for ordinary methods. We list the main novelties of this approach, displayed in [1].

- **Non-thermalized relics**: starting form initial conditions at early times with no additional dark radiation, if the interaction strength is insufficient, these particles might not have thermalized in the early Universe but still exist in measurable quantities today. Our

approach takes into account parameter space regions in which they never reaches thermalization;

- **Decoupling epoch**: the decoupling of particles is neither instantaneous nor momentum-independent. Methods based on ordinary differential equations already go beyond the instantaneous decoupling, but they still need to assume the phase space distribution (PSD) to be thermal after decoupling. In [1] is shown how different momenta decouple at different times and such difference in the decoupling temperature for the various momentum bins originates distortions of the PSD from the thermal profile;

- **Quantum statistical effects**: while adopting ordinary differential equations describing the evolution of number or energy densities, at some point one is forced to employ the Maxwell-Boltzmann statistics, neglecting quantum statistics of dark radiation particles. This assumption is never needed in a formalism where the original integro-differential equations are employed;

- **Feedback on the thermal bath**: while on one side dark radiation keeps being produced, on the other side, thermal bath particles lose energy. So we would like to account for the whole system. That's why we rather deal with a system of equations: an extra Boltzmann equation that takes into consideration the changes in the thermal bath's energy density[1] completes our framework.The right hand side of this equation has a collision term quantifying the energy exchanged with the dark radiation sector alongside its evolution due the Hubble expansion.

6.1 Derivation of the Theoretical Framework

In appendix C we presented the Boltzmann equation C.1 in simple form. If we evaluate the Liouville operator for dark radiation what we obtain is:

$$\omega \frac{df_a(k,t)}{dt} = C[f(k,T)] \tag{6.1}$$

with the $C[f(k,T)]$ being the collision operator C.3 that encodes the dynamics mediating the interaction processes. As said, the radiation energy density ρ_B evolves, both because of the energy exchanged between visible and dark sectors and of the dilution due to expansion. What

[1] As we believe SM interactions are enough efficient to ensure thermalization at early times, it is sufficient to monitor the primordial bath's energy density without delving into phase space this time.

we can do is to integrate both sides of Boltzmann equation for the axion obtaining:

$$\frac{d\rho_a}{dt} + 4H\rho_a = g_a \int \frac{d^3k}{(2\pi)^3}\omega\frac{df_a}{dt} = g_a \int \frac{d^3k}{(2\pi)^3}C[f_a(k,t)]$$

and this quantity has to be, with the opposite sign, equal to the right-hand side of the equation accounting for the red-shift of the bath energy density. So the evolution of thermal bath with density ρ_B and pressure p_B is encoded by:

$$\frac{d\rho_B}{dt} + 3H(\rho_B + p_B) = -\left(\frac{d\rho_a}{dt} + 4H\rho_a\right) = -g_a \int \frac{d^3k}{(2\pi)^3}C[f_a(k,t)] \tag{6.2}$$

With these two (6.1 and 6.2) we track the evolution of the dark radiation PSD for axion and the bath energy density. To complete the system we need one more equation and this is the Friedmann equation for the Hubble rate $H \equiv \dot{a}/a$, where $a(t)$ is the FLRW scale factor, for which we assumes that there is no other contribution to the energy density besides the ones from the thermal bath and the dark radiation. The final system is:

$$\begin{cases} \omega\frac{df_a(k,t)}{dt} = C[f(k,t)] \\ \frac{d\rho_B}{dt} + 3H(\rho_B + p_B) = -g_a \int \frac{d^3k}{(2\pi)^3}C[f_a(k,t)] \\ H = \sqrt{\frac{\rho_B+\rho_a}{3M_{\rm Pl}^2}} \end{cases} \tag{6.3}$$

Energy density ρ_B and pressure p_B are related via the equation of state $p_B = w_B\rho_B$.

Once collisions have stopped happening at a significant rate, the phase space evolution is just due to free-streaming and the dark radiation energy density scales $\sim a^{-4}$ as the photon energy density (at temperatures below the electron mass). Thus once we are well below the MeV scale, the ratio $\frac{\rho_a}{\rho_\gamma}$ reaches a constant value, and this ratio is crucial to quantify the amount of additional radiation, as shown by 5.5.

6.1.1 Collision term

We now focus on the collision operator for binary scatterings of the kind $B_1B_2 \to B_3a$. We account for the relativistic dispersion for dark radiation $\omega = k$ and factor out the only term

involving the PSD, so we have:

$$\frac{df_a(k,t)}{dt} = C(k,t)\left(1 - \frac{f_a(k,t)}{f_{eq}(k,t)}\right)$$

where we denote with $f_{eq}(k,t)$ the equilibrium PSD for axion without chemical potential. For binary scatterings of the kind $B_1B_2 \to B_3a$ we have:

$$C_{B_1B_2\to B_3a} = \frac{1}{2\omega}\int d\Pi_1 d\Pi_2 d\Pi_3 (2\pi)^4 \delta^4(p_1+p_2-p_3-k)|\mathcal{M}_{B_1B_2\to B_3a}|^2 f_{B_1} f_{B_2}(1 \pm f_{B_3})$$

We report here the analytical result for the collision operator derived in [15] for a generic massive particle wirh mass m_a in the final state and we specify it for the axion dark radiation. We first remember the definition for the Mandelstam variables $s = (p_1+p_2)^2 = (p_3+k)^2$ and $t = (p_1-p_3)^2 = (p_2-k)^2$. In the center of momentum frame of the collision, initial state particles and final state particles have opposite momenta with equal modulus:

$$p_{12} = \frac{\sqrt{\lambda(s,m_1,m_2)}}{2\sqrt{s}} \quad and \quad k_{3a} = \frac{\sqrt{\lambda(s,m_3,m_a)}}{2\sqrt{s}}$$

with the usual $\lambda(s,m_i,m_j) = [s-(m_i+m_j)^2][s-(m_i-m_j)^2]$. With some tricks one can rewrite the integration measure as:

$$d\Pi_1 d\Pi_2 d\Pi_3 (2\pi)^4 \delta^4(p_1+p_2-p_3-k) = \frac{g_1 g_2 g_3}{128\pi^3 k}\frac{ds dt d\varepsilon_3}{\sqrt{\lambda(s,m_3,m_a)}}$$

So the collision term becomes:

$$C(T,k) = \frac{g_1 g_2 g_3}{256\pi^3 \omega k}\int_{s_{min}}\frac{ds}{\sqrt{\lambda(s,m_3,m_a)}}\int_{\varepsilon_3^-}^{\varepsilon_3^+} d\varepsilon_3 \int_{t_{min}}^{t_{max}} dt |M(t,s)|^2 f_1 f_2 \tag{6.4}$$

with $s_{min} = Max((m_1+m_2)^2,(m_3+m_a)^2)$ and we denote with ε_3 the energy for the bath particle in the final state. The integration over $d\varepsilon_3$ has boundaries that come from the values of s in the frame in which the axion has four-momentum (ω,k), and they are found by solving the equation:

$$s = m_3^2 + m_a^2 + 2(\omega\varepsilon_3^{\pm} \mp k(\sqrt{\varepsilon_3^{\pm 2} - m_3^2}))$$

The variable t in the COM frame is:

$$t = m_1^2 + m_a^2 - 2(\sqrt{m_1^2 + p_{12}^2}\sqrt{m_a^2 + k_{3a}^2} - \cos(\theta_{1a})p_{12}k_{3a}) \tag{6.5}$$

and the maximum and minimun value for t are found setting for the scattering angle in the COM frame $\cos(\theta_{1a}) = -1$ and $\cos(\theta_{1a}) = +1$ respectively. Then, as it is reasonable, if we assume equilibrium distributions for bath particle B_1, B_2 and B_2, it is easy to perform the integral over ε_3 analytically. We can exploit the conservation of energy to write $f_1^{eq}(p_1)f_2^{eq}(p_2) = e^{-(\varepsilon_1+\varepsilon_2)/T} = e^{-(\varepsilon_3+\omega)/T}$ and performing the integration we obtain:

$$C(T,k) = \frac{g_1 g_2 g_3}{256\pi^3}\frac{Te^{-\omega/T}}{\omega k}\int_{s_{min}}\frac{ds}{\lambda(s,m_3,m_a)}(e^{-\varepsilon_3^-/T} - e^{-\varepsilon_3^+/T})\int_{t_{min}}^{t_{max}} dt|\mathcal{M}(t,s)|^2$$

Now we are ready to take $m_a \to 0$ in the case of dark radiation. We have that ε_3^+ goes to infinity while ε_3^- remains finite, so that, performing the limit we obtain:

$$\lim_{m_a\to 0}\varepsilon_3^- = \frac{s-m_3^2}{4k} + \frac{km_3^2}{s-m_3^2}$$

and so:

$$C(T,k) = \frac{g_1 g_2 g_3}{256\pi^3}\frac{Te^{-k/T}}{k^2}\int_{s_{min}}\frac{ds}{s-m_3^2}e^{-\left(\frac{s-m_3^2}{4k}+\frac{km_3^2}{s-m_3^2}\right)/T}\int_{t_{min}}^{t_{max}} dt|\mathcal{M}(t,s)|^2 \tag{6.6}$$

with

$$t_{min/max} = m_1^2 - \frac{2(s-m_3^2)}{\sqrt{4s}}\left(\sqrt{m_1^2+p_{12}^2} \pm p_{12}\right)$$

Finally this has to feed the system:

$$\begin{cases} \frac{df_a(k,t)}{dt} = C(k,T(t))\left(1 - \frac{f_a(k,t)}{f_{eq}(k,t)}\right) \\ \frac{d\rho_B}{dt} + 3H(1+w_B)\rho_B = -g_a\int\frac{d^3k}{(2\pi)^3}kC(k,T(t))\left(1-\frac{f_a(k,t)}{f_{eq}(k,t)}\right) \\ H = \sqrt{\frac{\rho_B+\rho_a}{3M_{\rm Pl}^2}} \end{cases} \tag{6.7}$$

As the collision operator in temperature dependent we can also employ this last as evolution

variable [2]:

$$\begin{cases} \frac{df_a(k,T)}{d(\log T)} = -\frac{C(k,T)}{H}\left(1 - \frac{f_a(k,T)}{f_{eq}(k,T)}\right) \\ \frac{d\rho_B}{d(\log T)} = 3(1+w_B)\rho_B + \frac{g_a}{H}\int \frac{d^3k}{(2\pi)^3} kC(k,T)\left(1 - \frac{f_a(k,T)}{f_{eq}(k,T)}\right) \\ H = \sqrt{\frac{\rho_B+\rho_a}{3M_{\rm Pl}^2}} \end{cases} \tag{6.8}$$

where we can safely take the equilibrium distribution being the Maxwell Boltzmann[3] $f_{eq,MB}(k,T) = e^{-\frac{k}{T}}$.

6.1.2 System Setup

In this section, we present the key setup for deriving the numerical solution [4] and its relation to ΔN_{eff}. We rewrite 6.7 in a more convenient way following the formalism adopted in [1]. First we employ as time variable the scale factor $a(t)$, in particular denoted with a_I the scale factor at a temperature $T_I = 10^4\ GeV$ we use the dimensionless ratio $A \equiv a/a_I$. Then we introduce the comoving momentum:

$$q \equiv \frac{ka}{a_I T_I} = \frac{kA}{T_I}$$

and the comoving energy density of the thermal bath and axions:

$$R_B \equiv \frac{\rho_B A^4}{T_I^4} \qquad\qquad R_a \equiv \frac{\rho_B A^4}{T_I^4}$$

In this way we scale out the effect of the Hubble expansion since the physical momentum for dark radiation scales like a^{-1} and the energy density for radiation-like fluid is proportional to a^{-4}. The comoving energy density for axion can be computed at each value of A integrating

[2] We used for the change of variable the following $\frac{d(\log T)}{dt} = -H$

[3] Alternatively we can think of accounting for the bosonic nature of axion, i.e. the fact that multiple particles can occupy the same quantum state , via the Bose Einstein distribution:

$$f_{eq,BE}(k,T) = \frac{1}{e^{-\frac{k}{T}} - 1}$$

At high temperatures, we can think of the particles as widely spread out in phase space, so that the probability of multiple particles occupying the same quantum state is low: the -1 in the denominator becomes negligible and the formula reduces to the classical MB one.

[4] A preliminary attempt at a numerical procedure is provided in D.2

the PSD:

$$R_a = \frac{g_a}{2\pi^2} \int dq q^3 f_a(q, A) \tag{6.9}$$

The Boltzmann system that we plug in our code is finally:

$$\begin{cases} \frac{df_a(q,A)}{dlogA} = \frac{C(q,A)}{H(A)} \left(1 - \frac{f_a(q,A)}{f_{eq}(q,A)}\right) \\ \frac{dR_B}{dlogA} + (3w_B - 1)R_B = -\frac{g_a}{H(A)} \int \frac{dqq^3}{2\pi^2} C(q,A) \left(1 - \frac{f_a(q,A)}{f_{eq}(q,A)}\right) \\ H = \sqrt{\frac{R_B + R_a}{3M_{\rm Pl}^2}} \frac{T_I^2}{A^2} \end{cases} \tag{6.10}$$

This is an integro-differential system. Indeed the first equation ruling the temporal evolution of f_a contains on the right-hand side the Hubble parameter: this is determined by the third equation and so it is set by the energy content of the universe. This results from the integral of f_a over momentum for dark radiation 6.9 and from the second equation for the bath energy density, that is also integro-differential.

We write a code to solve the system numerically and extract ΔN_{eff}. The first step consists in evaluating the collision operator using 6.6 for all the processes considered in the previous section, that is all the scattering amplitudes $|\mathcal{M}(t,s)|^2$ reported in appendix D.1. The integral is numerically solved for a range of momenta and temperatures, these last depending on whether the corresponding process occurs above or below the EWPT. The sums of all rates above and below the threshold are then interpolated in two dimensions, resulting in the function $C(k, T)$, that enters the 6.10. This selects the above-EWPT interpolating function for values of the temperature T higher than 245 GeV and returns the below-EWPT one otherwise.

To model the phase space distribution, the momentum space is divided into discrete intervals called momentum bins. Each bin represents a range of momenta, and the code calculates the value of $f_a(q, A)$ within each bin, allowing to capture the continuous spectrum of dark radiation in a simple way. By summing over these bins, we can compute quantities like the total energy of axion dark radiation. To connect the values of the temperature T to the variable A one can invert:

$$R_B(A) = \frac{\pi^2}{30} g_\rho^*(T) \left(\frac{T}{T_I}\right)^4 A^4 \tag{6.11}$$

that comes from the usual formula for relativistic energy density.

The initial distribution is assumed to be zero, indicating no axion dark radiation at the start,

and the initial comoving energy density is:

$$R_B(A=1) = \frac{\pi^2}{30} g^*_\rho(T_I)$$

corresponding to the thermal bath at the initial temperature T_I. The system needs to be integrated starting from $A_I = 1$ up to values of the scale factor A_F corresponding to a temperature T_F below the electron mass ($\sim 0.5\,MeV$)[5], so that the effective number of relativistic degrees of freedom does not change afterward, i.e. $g_\rho(T << T_F) = \text{const}$, and therefore the ratio ρ_a/ρ_B stays constant across the expansion of the Universe.

Rewriting the axion and photon energy densities in 5.5 in terms of the comoving ones extracted from our solution we obtain the final formula:

$$\Delta N_{eff} = \frac{8}{7}\left(\frac{11}{4}\right)^{\frac{4}{3}} \frac{R_a(A_F)}{2R_B(A_F)/g^*_\rho(T_F)} \tag{6.12}$$

where the 2 factor comes from the two photon polarization and $g^*_\rho(T_F)$ denotes the number of relativistic degrees of freedom at the considered end temperature.

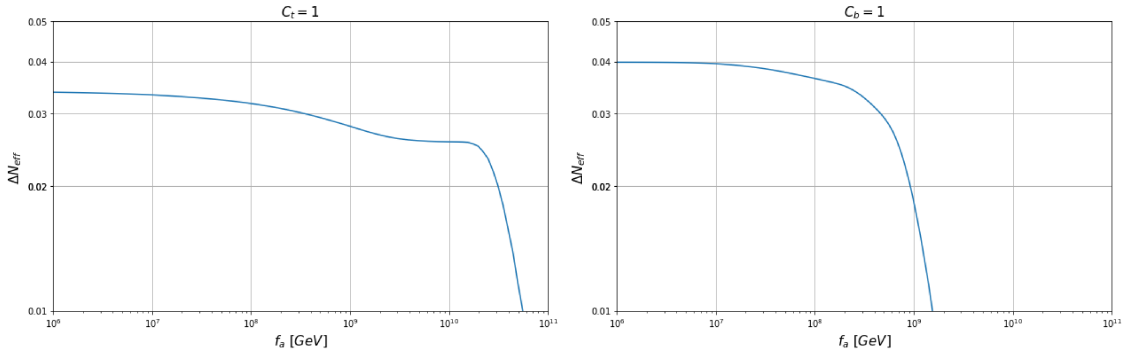

(a) (b)

Figure 6.1: ΔN_{eff} as function of f_a for top and bottom axion coupling separately, derived with the phase-space approach.

In figures 6.1a and 6.1b we show the results for ΔN_{eff} as a function of the axion scale f_a in the case we switch on top-axion and bottom-axion couplings separately. The overall beahaviour

[5] Far above the QCD phase transition (QCDPT), axions can be produced efficiently through scatterings with quarks, but as the temperature of the Universe lowers below the GeV scale, these interactions turn to be irrelevant since quarks become confined into hadrons. So the idea is to consider a rate function $C(q, A)$ that switches between the interpolated integrals valid above and below $T_{EWPT} = 245\ GeV$ and is set to zero once 1 GeV is exceeded.

reflects the one already found for ΔN_{eff} with the canonical formalism, but there are some key differences between the two approaches. Indeed, as said, the comoving number density formalism typically assumes that the axions reach thermal equilibrium with the primordial bath. On the other hand, by directly solving the equation for the distribution function, we might capture the additional non-thermal axion production that the number density approach misses. Hence higher values for ΔN_{eff} may derive from considering non-thermal behaviour of the PSD and accounting for out-of-equilibrium axion interactions, particularly at high values of f_a, when the interactions are not strong enough to mantain full thermal equilibrium, but yet contribute to the overall axion abundance. Indeed there is an extension of the plot to slightly larger values of f_a, suggesting that smaller couplings give a significant contribution to non-thermal production. This is likely due to the more precise handling of the distribution function, which accounts for the gradual decoupling of axions rather than assuming a sharp transition. Also with this approach, we note that ΔN_{eff} remains higher for bottom quark interactions due to his longer period of coupling.

6.2 Conclusions

The effective number of neutrino species N_{eff} leads to observable consequences in the CMB temperature and polarization anisotropy, making it a powerful observable to probe extensions of the SM containing new light degrees of freedom, such as the axion. Indeed, axions produced via scatterings with thermal bath particles can contribute to the radiation energy density of the universe, if they remain relativistic, at the time of recombination. As mentioned, current measurements of N_{eff} are consistent with the SM prediction. However, future observations of the CMB aim to improve bounds on this quantity: this introduces the possibility of detecting deviations from the SM due to extra dark radiation components in the form of relativistic axions produced at high temperatures. Nowadays, the best sensitivity we have comes from Planck satellite ($\sigma(N_{eff}) \simeq 0.17$), yet in the near future, we expect to move further, up to $\sigma(N_{eff}) \simeq 0.05$ due to the Simons Observatory [16] or $\sigma(N_{eff}) \simeq 0.03$ with Cosmic Microwave Background 'Stage 4' ($CMB - S4$) [17],[18]. There are also futuristic proposals [19] with the target $\sigma(N_{eff}) \simeq 0.0014$.

Motivated by these advancements, we evaluate the amount of axion dark radiation produced in the Early Universe across the stage of EWPT in terms of ΔN_{eff}, with the hope that ongoing and future cosmological probes will provide valuable data to test these predictions.

After investigating the scattering processes involving third generation quarks, our results depend on two couplings, C_t and C_b. In our analysis, we switch on separately the bottom and top axion couplings, setting them to one. This corresponds to examining the results as function of f_a/C_i, which quantifies the strength of axion-quark interaction. The scattering amplitudes and cross sections contribute to the interaction rate that appears on the right hand side of our equations.

First, we adopt the canonical approach, which solves the Boltzmann equation for the axion number density. This provides an estimate for ΔN_{eff} as a function of the axion energy scale f_a (figures 5.5b and5.5a). Smaller f_a values, corresponding to larger axion-quark couplings, mean stronger interactions that keep axion in thermal equilibrium with the primordial bath for longer time, leading to a greater amount of axion dark radiation and, consequently, a bigger ΔN_{eff}. Roughly speaking, this increasing behaviour is significant as long as the axion decoupling temperature is high enough to produce the fermions involved in the scatterings, i. e. top and bottom quarks. Beyond this point, ΔN_{eff} changes slowly with interaction strength as the axion comoving number density saturates. Since the top quark is heavier, and so it decouples from the thermal bath earlier compared to the bottom quark, processes involving the axion-

bottom coupling provide a larger ΔN_{eff}. On the other hand, given that the cross section is proportional to the mass, the interaction rate is larger for the top quark, making axion production relevant even at larger f_a. The results obtained with this method chapter are in agreement with the ones presented in [14]. It is worth to notice that we are evaluating axion production without accounting for the backreaction on the energy density. The thermal bath evolves according to the Hubble expansion and changes in the effective number of relativistic degrees of freedom as the temperature evolves, but without any direct energy transfer from axion production.

In the last part of this work, we enlightened how a phase-space formalism, which tracks the evolution of the axion distribution function while accounting for feedback from the thermal bath, could be applied to the case of axion production across the EWPT. This can be done by plugging the expressions for the scattering amplitudes, calculated in this work and shown in D.1, into the equations derived in 6.1. With a numerical approach based on such calculations, future works may reveal a more refined trend for ΔN_{eff}, offering a slightly different picture. Our results (figures 6.1b and 6.1a) indicate a plot for ΔN_{eff} that is extending across a tiny wider range of f_a values, suggesting that axion production is relevant even at higher f_a, or equivalently smaller couplings, where the canonical method might underestimate the contribution. The last method can portray regimes where interactions are significant but not strong enough to maintain full thermal equilibrium and axions are produced in smaller quantities but that can still contribute significantly to dark radiation. Furthermore, we rely on the fact that both the axion abundance and the evolution of the primordial plasma are self-consistently accounted for, as well as the ability to resolve momentum-specific details, that are averaged out in the canonical number density approach. This potentially gives us a more complete description. For this reasons, we believe that this formalism could provide a more accurate prediction for the contribution of axion dark radiation to ΔN_{eff}, which is crucial in the light of the upcoming high-precision CMB measurements.

The comparison between the results obtained with the two different methods is visualised 6.2a and 6.2b, which shows different plots at higher f_a but the same behaviour for stronger couplings, when the thermal equilibrium is ensured. Here we also portray the trend for ΔN_{eff} both obtained with accounting for the bosonic nature of axion, i. e. considering a Bose Einstein equilibrium distribution and the derived statics, than with using the classical approximation, i. e. the Maxwell Boltzamnn. The deviation of the values obtained with the phase-space approach

with respect to the number density one at higher f_a is shown in 6.3a and 6.3b [6]

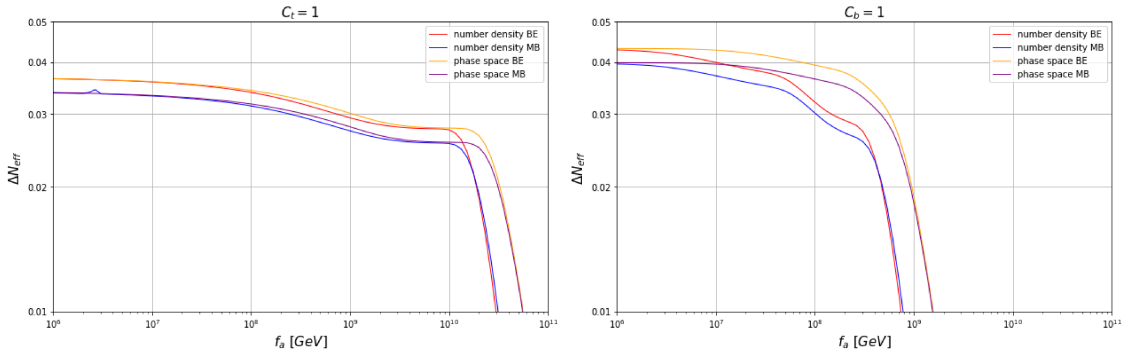

(a) (b)

Figure 6.2: Comparison of trends for ΔN_{eff} as function of f_a, for top and bottom axion coupling separately, derived with the number density and the phase-space approach, cosidering the Maxwell-Boltzamnn or the Bose-Enstein as axion equilibrium distribution.

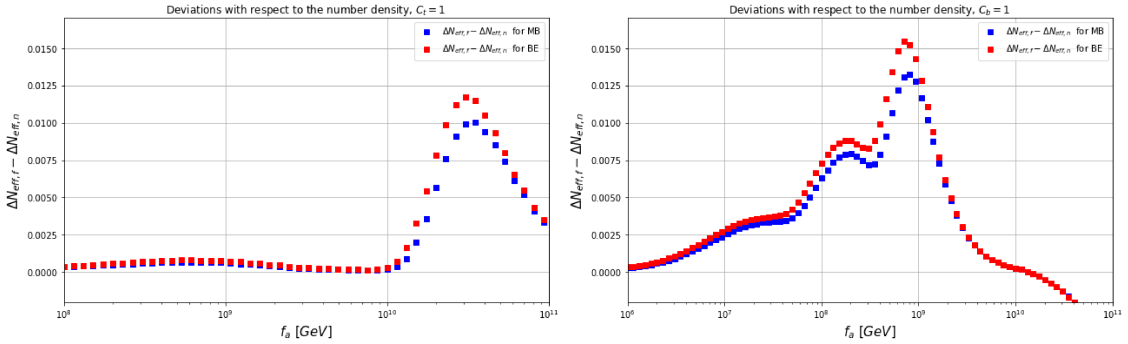

(a) (b)

Figure 6.3: Deviation of ΔN_{eff} evaluated with the phase space approach , with respect to the number density result, for the MB (blue) and the BE (red) cases as function of f_a.

We finally precise that the results obtained in this last chapter for ΔN_{eff} should be considered preliminary and require further validation. In this sense our analysis lays the foundation for a more refined study to fully capture the dynamics of axion production across the EWPT.

[6] Since the bottom quark, being lighter, decouples later than the top quark, axion interactions involving bottom quarks persist until a lower temperature. This makes any minor changes in the axion abundance, coming from non-thermal production mechanisms, more significant for the bottom quark. Consequently, the effects captured in the phase-space approach could lead to a more pronounced enhancement in ΔN_{eff} for the bottom quark compared to the top quark.

A

The Standard Model of particle physics

This section is devoted to the main features of the Standard Model of particle physics, which is the most comprehensive and empirically validated theory of fundamental interactions by now. It is built upon the framework of gauge theories and it is based on the group $G_{SM} = SU(3)_c \times SU(2)_L \times U(1)_Y$[1]. In the first part we review the path to our modern theoretical picture of the strong interactions, introducing quarks and QCD, whose Lagrangian is presented in 1.1 and 1.2. The second paragraph resumes the main steps in the construction of our current model for electroweak interactions.

A.1 About QCD

In order to explain their rich spectrum, elementary constituents of strongly interacting particles were introduced: the quarks (Gell-Mann and Zweig, 1963). Mesons were interpreted as quark-antiquark bound states, and baryons as bound states of three quarks. At first, three species of quarks were assumed (up, down, and strange), then the discovery of additional particles pointed out the existence of other three species (charm, bottom, and top). We refer to this characterization as *flavor*. However this model presented two issues. Indeed free particles

[1] Here $SU(3)_c$ is the symmetry group of strong 'colored' interactions, i.e. QCD, $SU(2)_L$ is the weak isospin that only regards left-handed particles since right-handed are not subjected to weak interactions; the subscript Y to $U(1)_Y$ denotes the hypercharge, that, as we will see, is related to the electric charge and weak isospin.

with fractional charge[2] were not observed. Then, despite being spin 1/2 particles (which are meant to obey Fermi-Dirac statistics) , in order to explain the spectrum of baryons, it seemed unavoidable to assume their quarks wavefunction to be symmetric under the interchange of quantum numbers. To recover the agreement with Fermi-Dirac statistics, an additional quantum number was introduced, the color: if baryon wavefunctions are antisymmetric in color and symmetric in spin and flavor, then are antisymmetric overall. This color is nothing but the charge for a new internal $SU(3)$ simmetry, and quarks corresponds to its fundamental representation. Denoting them as q_i, with $i = 1, 2, 3$ being the color index, the invariance of hadron wavefunctions under $SU(3)$ allows only the combinations: $\bar{q}_i q_j$, $\varepsilon^{ijk} q_i q_j q_k$, and $\varepsilon_{ijk} \bar{q}^i \bar{q}^j \bar{q}^k$. This means that physical hadrons are singlets under color and the only admitted ones are mesons, baryons, and antibaryons, as observed. Finally the bosons associated to the $SU(3)$ gauge field are called gluons. QCD Lagrangian (1.2) has been discussed in chapter 1.1.

A.2 Electroweak interactions

A unified and experimentally correct description of weak and electromagnetic interactions is realized by the model, introduced by Glashow, Weinberg and Salam, of spontaneously broken gauge theory $SU(2)_L \times U(1)_Y \to U(1)_{em}$.

A.2.1 The Bosonic sector

Let's start with a theory with $SU(2)$ and $U(1)$ gauge simmetries (the latter needed since otherwhise SSB would lead to a system with no massless photon). To operate SSB, we introduce a complex scalar field in the spinor representation of $SU(2)$ and charge $+1/2$ under $U(1)$ symmetry, so that its complete gauge transformation is

$$\varphi \to e^{i\alpha^a \tau^a} e^{i\beta/2} \varphi$$

where $\tau^a = \sigma^2/2$ denotes the generators of $SU(2)$ (σ^a are Pauli matrices).

The covariant derivative of φ is

$$D_\mu \varphi = (\partial_\mu - igA^a_\mu \tau^a - \frac{i}{2} g' B_\mu)\varphi \tag{A.1}$$

[2] To have baryons with integer charges, we need to assign to quarks fractional electric charge: $+2/3$ for u, c, t and $-1/3$ for d, s, b.

with A^a_μ and B_μ, respectively, the $SU(2)$ and $U(1)$ gauge bosons, and different coupling constants g and g'. The gauge bosons sector reads:

$$L_{GB} = -\frac{1}{2}A^{a\mu\nu}A^a_{\mu\nu} - \frac{1}{2}B^{\mu\nu}B_{\mu\nu} + (D_\mu\varphi)^\dagger D_\mu\varphi - V(\varphi^\dagger\varphi)$$

where $A^a_{\mu\nu}$ and $B_{\mu\nu}$ are the field strength tensors making up the kinetic term for $SU(2)$ and $U(1)$.
Exploiting the unitary gauge, we can write $\varphi = \frac{1}{\sqrt{2}}(0,\ v + h(x))^T$, were $h(x)$ is a real scalar field known as Higgs boson and $v = \mu/\sqrt{\lambda}$ is the minimum of the scalar potential $V(\varphi^\dagger\varphi)$. From the kinetic term of the scalar field $(D_\mu\varphi)^\dagger D_\mu\varphi$ evaluated at its vacuum expectation value $\langle\varphi\rangle = \frac{1}{\sqrt{2}}(0\ v)^T$ one derives:

$$L_{GB} \supset \frac{1}{2}\frac{v^2}{4}\left[g^2(A^1_\mu)^2 + g^2(A^2_\mu)^2 + (-gA^3_\mu + g'B_\mu)^2\right]$$

We can identify the following vector bosons

$$W^\pm_\mu = \frac{1}{\sqrt{2}}(A^1_\mu \mp iA^2_\mu) \qquad Z^0_\mu = \frac{1}{\sqrt{g^2+g'^2}}(gA^3_\mu - g'B_\mu) \qquad A_\mu = \frac{1}{\sqrt{g^2+g'^2}}(gA^3_\mu + g'B_\mu)$$

with $m_W = \frac{v}{2}g$ and $m_Z = \frac{v}{2}\sqrt{g^2+g'^2}$, while the fourth orthogonal to Z^0_μ stays massless. One can rewrite the expressions introducing the weak mixing angle θ_w as the angle that appears in the change of basis from (A^3, B) to (Z^0, A), that is such that $\cos\theta_w = \frac{g}{\sqrt{g^2+g'^2}}$ and $\sin\theta_w = \frac{g'}{\sqrt{g^2+g'^2}}$.
Exploiting the unitary gauge we can also see that expanding the scalar potential we get a mass term and self interactions for h field:

$$V(\varphi^\dagger\varphi) = \mu^2\varphi^\dagger\varphi - \lambda(\varphi^\dagger\varphi)^2 \quad\longrightarrow\quad \frac{1}{2}m_h^2h^2 - \lambda v h^3 - \frac{1}{4}\lambda h^4$$

where $m_h = \sqrt{\lambda}v$ denotes the mass of the Higgs boson.
Finally we note that the expansion of the kinetic energy for the scalar in unitary gauge, besides rising the gauge boson mass terms, yields the interactions of the Higgs with other bosons:

$$L_{GB} = \frac{1}{2}(\partial_\mu h)^2 + \left[m_W^2W^{\mu+}W^-_\mu + \frac{1}{2}m_Z^2Z^\mu Z_\mu\right]\cdot\left(1+\frac{h}{v}\right)^2$$

A.2.2 Gauge couplings to fermions

The couplings of gauge bosons to fermions rise from the fermionic kinetic term. Let's first write the covariant derivative for a fermion belonging to $SU(2)$ and with charge Y under $U(1)$, in terms of the mass eigenstate fields:

$$D_\mu = \partial_\mu - i\frac{g}{\sqrt{2}}(W^+_\mu T^+ + W^-_\mu T^-) - i\frac{g}{\cos\theta_w}Z_\mu(T^3 - \sin\theta_w{}^2 Q) - iA_\mu Q \qquad \text{(A.2)}$$

with $T^\pm = \frac{1}{2}(T^1 \pm iT^2) = \frac{1}{2}(\sigma^1 \pm i\sigma^2)$, and $Q = T^3 + Y$(where T^1, T^2 and T^3 denote the $SU(2)$ generators). We need to specify the quantum numbers of the fermion fields accounting for the fact that the W boson couples only to left-handed helicity states of quarks and leptons. So we assign the left-handed fermion fields to doublets of $SU(2)$: $E_L = \begin{pmatrix} \nu_L \\ e_L \end{pmatrix}$ and $Q_L = \begin{pmatrix} u_L \\ d_L \end{pmatrix}$, while making the right-handed fermion fields singlets under this group u_R, d_R, e_R.
Writing for the covariant derivative the expression A.2, we recover from the kinetic term $\sum_\psi \psi i\not{D}\psi$ the Lagrangian for the electro-weak interactions of quarks and leptons:

$$\begin{aligned} L_K = {} & \bar{E}_L i\not{\partial} E_L + \bar{e}_L i\not{\partial} e_L + \bar{Q}_L i\not{\partial} Q_L + \bar{u}_R i\not{\partial} u_R + \bar{d}_R i\not{\partial} d_R \\ & + g(W^+_\mu J^{\mu-} + W^-_\mu J^{\mu+} + Z^0_\mu J^\mu_Z) + eA_\mu J^\mu_{EM} \end{aligned}$$

where

$$\begin{aligned} J^{\mu+} &= \frac{1}{\sqrt{2}}(\bar{\nu}_L\gamma^\mu e_L + \bar{u}_L\gamma^\mu d_L) \\ J^{\mu-} &= \frac{1}{\sqrt{2}}(\bar{e}_L\gamma^\mu \nu_L + \bar{d}_L\gamma^\mu u_L) \\ J^\mu_Z &= \frac{1}{\cos\theta_w}\sum_\psi \left[\bar{\psi}\gamma^\mu\left(\frac{T^3_\psi}{2} - Q_\psi \sin^2\theta_w\right)\psi + \bar{\psi}\gamma^\mu\gamma^5(-\frac{T^3_\psi}{2})\psi\right] \\ J^\mu_{em} &= \sum_\psi \bar{\psi}\gamma^\mu\psi Q_\psi \end{aligned}$$

A.2.3 Fermion mass term: the Yukawa sector

Since the left- and right-handed components of our fermion fields have different gauge quantum numbers, a simple mass term would violate gauge invariance. Therefore we must again invoke the scalar field φ realizing spontaneous symmetry breaking. We should recall that there

are known to be three generations of quarks and leptons, so that in flavor space we organize the matter fields in triplets, for instance $u_{L,R} = (u,\ c,\ t)^T_{L,R}$. So in the following discussion we will denote with i the flavour index for each of them, running from 1 to 3.
We can write the following gauge invariant lagrangian:

$$L_m = -\lambda_e^{ij}\bar{E}_L^i\varphi e_R^j - \lambda_d^{ij}\bar{Q}_L^i\varphi d_R^j - \lambda_u^{ij}\bar{Q}_L^i\tilde{\varphi}u_R^j + h.c.$$

Where we define $\tilde{\varphi}^a = \varepsilon^{ab}\varphi_b^\dagger$. After SSB this sector reads:

$$L_m = -\frac{h+v}{\sqrt{2}}(\lambda_e^{ij}\bar{e}_L^i e_R^j + \lambda_d^{ij}\bar{d}_L^i d_R^j + \lambda_u^{ij}\bar{u}_L^i u_R^j)$$

where the λ^{ij}s are complex flavour mixing matrices, violating CP.
These can be decomposed by mean of unitary matrices U_q and W_q such that $\lambda_q = U_q D_q W_q^\dagger$, where D_q is a diagonal matrix with positive eigenvalues. Then performing a change of variables $q_R^i = W_q^{ij}q_R^j$ and $q_L^i = U_q^{ij}q_L^j$, that is converting the quark fields to the basis of mass eigenstates, the previous expression reads:

$$L_m = -\left(1+\frac{h}{v}\right)\left[m_e^i\bar{e}_L^i e_R^i + m_d^i\bar{d}_L^i d_R^i + m_u^i\bar{u}_L^i u_R^i\right]$$

so that the quark masses are defined as $m_q^i = \frac{1}{\sqrt{2}}y_q^i v$, where $D_q^{ii} \equiv y_q^i$. In this basis, the mass terms and Higgs couplings are diagonal in flavor and conserve P, C and T.
However because of unitarity of U_q and W_q matrices, this change of basis does not affect all the other SM sectors but the charged weak interactions that mix u_L and d_L. Indeed the current that couples with the W^+ boson takes the form:

$$J^{\mu+} \supset \frac{1}{\sqrt{2}}\bar{u}_L^i\gamma^\mu(U_u^\dagger U_d)_{ij}d_L^j = \frac{1}{\sqrt{2}}\bar{u}_L^i\gamma^\mu V_{ij}d_L^j$$

where V_{ij} is the Cabibbo-Kobayashi-Maskawa (CKM) matrix, whose off-diagonal terms allow weak-interaction transitions between quark generations. It is worth to say that V is a general unitary 3×3 matrix. Therefore it has 9 parameters, that is 3 rotation angles (i.e. the number of parameters of an $O(3)$ element) and 6 complex phases. Through rotation of quarks,[3] 5 out of 6 phases can be removed. The remaing phase, that makes some couplings of the W to quarks

[3] If quarks are rotated by an overall phase, the Lagrangian stays invariant: the baryonic number is indeed a symmetry, associated to a coherent phase shift in all the quark fields.

complex, is a source of CP violation in electroweak sector.
By sake of simplicity, we assumed no ν_R and no mass for neutrinos, implying no transitions between leptons of different generations.[4]

[4]Since one can exploit any unitary matrix in order to represent the neutrinos in the mass basis, we are free to choose $U_\nu = U_e^\dagger$.

B

Scattering Cross Sections

In this section we specify the procedure to compute the cross sections for the examined scatterings and give their result in the case below-EWPT. Being dark radiation, we will neglect the axion mass in our discussion. Let's first give some useful ingredients. Considering a process of the kind $1 + 2 \to 3 + a$ we define the Mandelstam variables in terms of the involved four-momenta:

$$s = (p_1 + p_2)^2 = (p_3 + k)^2 \qquad t = (p_1 - p_3)^2 = (p_2 - k)^2 \qquad u = (p_1 - k)^2 = (p_2 - p_3)^2$$

with the usual constraint $s + t + u = \sum_i m_i^2$. The Lorentz invariant cross section is:

$$\sigma_{1+2\to 3+a} = \frac{1}{4I} \int |\bar{M}|^2 d\Phi^{(2)} \tag{B.1}$$

where $|\bar{M}|^2$ is the cross section averaged squared amplitude, and I is the flux factor, that in its manifest Lorentz invariant expression reads:

$$I = \sqrt{p_1^2 \cdot p_2^2 - m_1^2 m_2^2} = \frac{s}{2} \sqrt{1 - \frac{2(m_1^2 + m_2^2)}{s} + \frac{(m_1^2 - m_2^2)^2}{s^2}} \tag{B.2}$$

The phase space for final state particles reads:

$$d\Phi^{(2)} = (2\pi)^4 \delta^4(p_1 + p_2 - p_3 - k) \frac{dp_3}{(2\pi)^3 2E_3} \frac{dk}{(2\pi)^3 E_k} \equiv (2\pi)^4 \delta^4(p_1 + p_2 - p_3 - k) d\Pi_3 d\Pi_a \tag{B.3}$$

Since we are free to perform the integral over the phase space in any frame as long as the final result is given in a manifest Lorentz invariant form, we give the expression for $d\Phi^{(2)}$ in the center of mass (COM) frame:

$$d\Phi^{(2)}_{COM} = \frac{d\Omega}{32\pi^2} \left(1 - \frac{m_3^2}{s}\right) \tag{B.4}$$

Now we proceed to sketch the computations to derive some specific binary scatterings cross section both above and below the EWPT as a function of the variable s, that allow us to outline a general procedure.

Above EWPT

Let's focus on $t\bar{t} \to \chi_0 a$, then the result can be easily generalised to all the scatterings presented in 4.1. We remind that here all particle are taken massless. Using the coupling $i y_t C_t \frac{a}{2f_a} \chi_0 \bar{t}(1 - \gamma^5) t$ extrapolated from 4.2, the amplitude for this process is simple:

$$\bar{M}_{t\bar{t} \to \chi_0 a} = \frac{y_t C_t}{2f_a} \bar{v}(p_2)(1 - \gamma^5) u(p_1)$$

We then the square, average and sum over initial and final polarizations this expression. Here the resulting fermionic trace can be easily solved exploiting known properties of γ-matrices obtaining finally:

$$|\bar{M}|^2 = \frac{1}{2} \times \frac{1}{2} \frac{y_t^2 c_t^2}{4f_a^2} \times 8 p_1 \cdot p_2$$

Since the particle are massless $2p_1 \cdot p_2 = s$ and the cross section formula presented above gets simplified. Combining these facts one can check our final expression:

$$\sigma_{t\bar{t} \to \chi_0 a} = \frac{1}{64\pi} \frac{y_t^2 c_t^2}{f_a^2}$$

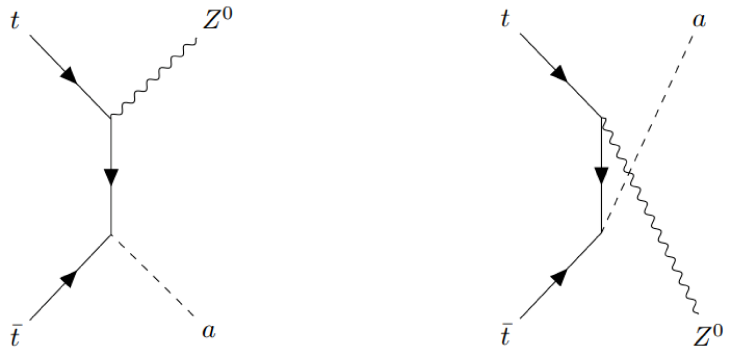

Figure B.1: Feynmann diagrams for the process $\bar{t}t \to Z^0 a$ including t and u channel contributions.

B.1 Scattering cross sections below the EWPT

In this section we will present the analytical results obtained for the cross sections of axion scattering with third generation quarks below the EWPT. Firstly we give the computations details for two of them to outline the general framework: $\bar{t}t \to Z^0 a$, that is a process where we have two initial quarks and one boson in the final state, and $tZ^0 \to ta$, that provides an example for the case where the boson is in the inial state.

B.1.1 $\bar{t}t \to Z^0 a$

If we draw the Feynmann diagrams for this process, we see that it comprises the contribution of t and u channels, that is a general feature for the considered scatterings of this kind. We derived the axion-quarks couplings in 4.5, whereas we read the coupling of the quarks-Z vertex in A.2.2 where the axial and vector coefficients need to be specified for the top quark. The amplitude therefore reads:

$$iM_{\bar{t}t\to Z^0 a} = \frac{g}{\cos\theta_w}\frac{C_t}{2f_a}\varepsilon^*_\mu(p_3)k_\nu\bar{v}(p_2)\left[\gamma^\nu\gamma^5\frac{i(\not{p}_1 - \not{p}_3 + m_t)}{t-m_t^2}i\gamma^\mu\left(\frac{1}{4} - \sin^2\theta_w\frac{2}{3} - \frac{1}{4}\gamma^5\right) + \left(\frac{1}{4} - \sin^2\theta_w\frac{2}{3} - \frac{1}{4}\gamma^5\right)\frac{i(\not{p}_1 - \not{k} + m_t)}{u-m_t^2}\gamma^\nu\gamma^5\right]u(p_1)$$

The squared amplitude reads:

$$|\bar{M}|^2_{\bar{t}t\to Z^0 a} = \frac{1}{4}\frac{g^2}{\cos^2\theta_w 4f_a^2}\left(-g_{\mu\alpha} + \frac{p_{3\mu}p_{3\alpha}}{m_z^2}\right)k_\nu k_\beta T^{\mu\nu\alpha\beta}$$

where we have already performed the sum over polarization vectors and denoted with $T^{\mu\nu\alpha\beta}$ the trace over Dirac indices:

$$T^{\mu\nu\alpha\beta} = Tr\Bigg[(\not{p_1} + m_t)\left(\gamma^\mu(g_V + g_A\gamma^5)\frac{i(\not{p_1} - \not{p_3} + m_t)}{t - m_t^2}\gamma^\nu\gamma^5 + \gamma^\nu\gamma^5\frac{(\not{p_1} - \not{k} + m_t)}{u - m_t^2}\gamma^\mu(g_V + g_A\gamma^5)\right)$$
$$(\not{p_2} - m_t)\left(\gamma^\nu\gamma^5\frac{(\not{p_1} - \not{p_3} + m_t)}{t - m_t^2}\gamma^\mu(g_V + g_A\gamma^5) + \gamma^\mu(g_V + g_A\gamma^5)\frac{(\not{p_1} - \not{k} + m_t)}{u - m_t^2}\gamma^\nu\gamma^5\right)\Bigg]$$

where we absorbed in g_V and g_A the axial and vector coefficients. We evaluate this trace using Dirac algebra and contract all the indices, then rearrange our expression for $|\bar{M}|^2$ in terms of Mandelstam variables[1]. In particular, setting for $\cos\theta_w = m_w^2/m_z^2$ we have:

$$|\bar{M}|^2_{\bar{t}t\to Z^0 a} = -\frac{1}{4}\frac{g^2 m_Z^2}{m_W^2 4 f_a^2}\frac{1}{(9m_z^4(m_t^2 - t)(m_t^2 - u)}(2m_t^2(18m_t^6 m_Z^2 - 59m_t^4 m_Z^4 - 9m_t^4 m_Z^2 t - 9m_t^4 m_Z^2 u +$$
$$59m_t^2 m_Z^4 t + 59m_t^2 m_Z^4 u - 18m_t^2 m_Z^2 tu - 32m_W^2 m_Z^4 + 64m_W^2 m_Z^2 s - 32m_W^2 s^2 + 40m_W m_Z^6 - 80m_W m_Z^4 s +$$
$$40m_W m_Z^2 s^2 - 17m_Z^4 t^2 - 25m_Z^4 tu - 17m_Z^4 u^2 + 9m_Z^2 t^2 u + 9m_Z^2 tu^2)$$

Then we use Mandelstam relation $u = 2m_t^2 + m_Z^2 - t - s$ to rewrite this espression as a function of t and s only. Having defined θ the scattering angle in the COM frame, we express t in terms of s and θ:

$$t_{COM} = m_t^2 - \frac{(s - m_Z^2)}{2\sqrt{s}}\left(\sqrt{s} - \sqrt{s - 4m_t^2}\cos\theta\right)$$

and we plug it in the expression for $|\bar{M}|^2$. We are now ready to perform the integration in the COM frame exploiting the B.4, where we set $m_3 \equiv m_Z$. Finally accounting for the flux of this process:

$$I_{\bar{t}t\to Z^0 a} = \frac{s}{2}\sqrt{1 - \frac{4m_t^2}{s}}$$

we find a Lorentz invariant expression for the cross section:

$$\sigma_{\bar{t}t\to Z^0 a} = \frac{C_t^2 g^2 m_t^2}{1152\pi f_a^2 m_W^2 m_Z^2}\frac{(s - m_Z^2)}{s^{3/2}\sqrt{s - 4m_t^2}}\left(4\sqrt{\frac{s}{s - 4m_t^2}}\tanh^{-1}\left(\sqrt{1 - \frac{m_t^2}{s}}\right)(-m_Z^2(9m_t^2 + 40m_W^2)\right.$$
$$\left. + 32m_W^4 + 17m_Z^4) + 9m_Z^2(s - 2m_Z^2))\right) \tag{B.5}$$

[1] This is done by mean of FeynCalc Mathematica Package

B.1.2 $tZ^0 \to ta$

Figure B.2: Feynmann diagrams for the process $tZ^0 \to ta$ including s and u channel contributions.

The amplitude accounting for s and u channel contributions is the following:

$$iM_{tZ^0\to ta} = \frac{g}{\cos\theta_w}\frac{C_t}{2f_a}\varepsilon_\mu(p_2)k_\nu\bar{v}(p_1)\left[\gamma^\nu\gamma^5\frac{i(\not{p}_1+\not{p}_2+m_t)}{s-m_t^2}i\gamma^\mu\left(\frac{1}{4}-\sin^2\theta_w\frac{2}{3}-\frac{1}{4}\gamma^5\right)+\left(\frac{1}{4}-\sin^2\theta_w\frac{2}{3}-\frac{1}{4}\gamma^5\right)\frac{i(\not{p}_1-\not{k}+m_t)}{u-m_t^2}\gamma^\nu\gamma^5\right]u(p_1)$$

and the unpolarized squared amplitude therefore reads:

$$|\bar{M}|^2_{tZ^0\to ta} = \frac{1}{6}\frac{g^2}{\cos^2\theta_w 4f_a^2}\left(-g_{\mu\alpha}+\frac{p_{2\mu}p_{2\alpha}}{m_z^2}\right)k_\nu k_\beta S^{\mu\nu\alpha\beta}$$

with:

$$S^{\mu\nu\alpha\beta} = Tr\left[(\not{p}_1+m_t)\left(\gamma^\mu(g_V+g_A\gamma^5)\frac{i(\not{p}_1+\not{p}_2+m_t)}{t-m_t^2}\gamma^\nu\gamma^5+\gamma^\nu\gamma^5\frac{(\not{p}_1-\not{k}+m_t)}{u-m_t^2}\gamma^\mu(g_V+g_A\gamma^5)\right)(\not{p}_3+m_t)\left(\gamma^\nu\gamma^5\frac{(\not{p}_1+\not{p}_2+m_t)}{t-m_t^2}\gamma^\mu(g_V+g_A\gamma^5)+\gamma^\mu(g_V+g_A\gamma^5)\frac{(\not{p}_1-\not{k}+m_t)}{u-m_t^2}\gamma^\nu\gamma^5\right)\right]$$

Analogously to the previous case we can solve this and express the result in terms of s, t and u [2]:

$$|\bar{M}|^2_{tZ^0\to ta} = \frac{1}{6}\frac{g^2 m_Z^2}{m_W^2 4f_a^2}\frac{1}{9m_Z^4(m_t^2-s)(m_t^2-u)} 2m_t^2(18m_t^6 m_Z^2 - 59m_t^4 m_Z^4 - 9m_t^4 m_Z^2 s - 9m_t^4 m_Z^2 u + 59m_t^2 m_z^4 s + 59m_t^2 m_Z^4 u - 18m_t^2 m_Z^2 su - 32m_W^4 m_Z^4 + 64m_W^4 m_Z^2 t - 32m_W^4 t^2 + 40m_W^2 m_Z^6 - 80m_W^2 m_Z^4 t + 40m_W^2 m_Z^2 t^2 - 17m_Z^4 s^2 - 25m_Z^4 su - 17m_Z^4 u^2 + 9m_Z^2 s^2 u + 9m_Z^2 su^2) \quad I$$

Then we apply again the Mandelstam trick and introduce the scattering angle θ in the COM. This time the kinematics of the process yields the following relation between t and s:

$$t_{COM} = m_Z^2 - \frac{(s-m_t^2)}{\sqrt{s}}\left(\frac{s+m_Z^2-m_t^2}{2\sqrt{s}} - \frac{\sqrt{[s-(m_t-m_z)^2][s-(m_t+m_Z)^2]}}{2\sqrt{s}}\cos\theta\right)$$

Since the top quark is in the final state we set $m_3 = m_1 \equiv m_t$ and $m_2 = m_Z$ in B.4 and B.2. After integration, our final Lorentz invariant expression reads:

$$\begin{aligned}\sigma_{tZ^0\to tZ} =& \frac{C_t^2 g^2}{3456\pi f_a^2}\frac{m_t^2(s-m_t^2)}{s^2 m_W^2 m_Z^2\sqrt{(m_t^2-m_Z^2+s^2)^2-4m_t^2 s}}\Bigg(\frac{-2s^2\left(-m_Z^2\left(9m_t^2+40m_W^2\right)+32m_W^4+17m_Z^4\right)}{+\sqrt{m_t^4-2m_t^2\left(m_Z^2+s\right)+\left(m_Z^2-s\right)^2}} \\ &\log\left(\frac{m_t^2+\sqrt{\left(s-(m_t-m_z)^2\right)\left(s-(m_t+m_z)^2\right)}-m_z^2+s}{m_t^2-\sqrt{\left(s-(m_t-m_Z)^2\right)\left(s-(m_t+m_Z)^2\right)}-m_Z^2+s}\right)+3s\left(m_Z^2\left(3m_t^2+40m_W^2\right)- \\ &32m_W^4-8m_Z^4+(m_t-m_Z)(m_t+m_Z)\left(32m_W^4-40m_W^2m_Z^2+17m_Z^4\right)+9m_Z^2s^2\Bigg)\end{aligned} \tag{B.6}$$

B.2 Other cross sections

Now we present the cross sections for the remaining processes. First we list the ones where we have two fermions in the initial state and one gauge boson in the final state. In the following $q = t, b$.

$$\sigma_{\bar{q}q\to\gamma a} = \frac{Q_q^2 e^2 C_q^2}{4\pi f_a^2}\frac{m_q^2}{(s-4m_q^2)}\tanh^{-1}\left(\sqrt{1-\frac{4m_q^2}{s}}\right) \tag{B.7}$$

[2] We can check that our calculation is satisfying crossing symmetry property. Indeed in order to obtain $M_{tZ^0\to ta}$ we need to replace in the matrix for the previous process $M_{\bar{t}t\to Z^0 a}$ the momenta $p_2 \to -p_3$ and $p_3 \to -p_2$, that corresponds to switch $t \to s$. Then, once accounted for the different polarization in the initial state and for an overall minus sign since we are crossing one fermion field, this can be clearly seen if we compare the two expressions.

$$\sigma_{\bar{q}q\to ga} = \frac{g_s^2 C_q^2}{9\pi f_a^2}\frac{m_q^2}{(s-4m_q^2)}\tanh^{-1}\left(\sqrt{1-\frac{4m_q^2}{s}}\right) \tag{B.8}$$

$$\sigma_{\bar{q}q\to ba} = \frac{y_q^2 C_q^2}{64\pi f_a^2}\frac{(s-m_b^2)}{s(s-4m_q^2)}\left(\sqrt{s(s-4m_q^2)} - 4m_t^2\tanh^{-1}\left(\sqrt{1-\frac{4m_q^2}{s}}\right)\right) \tag{B.9}$$

$$\begin{aligned}\sigma_{\bar{b}b\to Z^0 a} =& \frac{C_b^2 g^2 m_b^2}{1152\pi f_a^2 m_W^2 m_Z^2}\frac{(s-m_Z^2)}{s^{3/2}\sqrt{s-4m_b^2}}\left(4\sqrt{\frac{s}{s-4m_b^2}}\tanh^{-1}\left(\sqrt{1-\frac{m_b^2}{s}}\right)(-m_Z^2(9m_b^2+4m_W^2)\right.\\ &\left.+8m_W^4+5m_Z^4)+9m_Z^2(s-2m_Z^2))\right)\end{aligned} \tag{B.10}$$

$$\begin{aligned}\sigma_{t\bar{b}\to W^+ a} =& \frac{g^2\left(s-m_W^2\right)}{128\pi s f_a^2 m_W^2\left(-2m_b^2\left(m_t^2+s\right)+m_b^4+\left(s-m_t^2\right)^2\right)}\left(c_b^2 m_b^2((s-2m_W^2)\right.\\ &\sqrt{-2m_b^2\left(m_t^2+s\right)+m_b^4+\left(s-m_t^2\right)^2}+2s\left(-m_b^2+m_t^2+2m_W^2\right)\\ &\coth^{-1}\left(\frac{m_b^2-m_t^2+s}{\sqrt{-2m_b^2\left(m_t^2+s\right)+m_b^4+\left(s-m_t^2\right)^2}}\right))+c_t^2 m_t^2((s-2m_W^2)\\ &\sqrt{-2m_b^2\left(m_t^2+s\right)+m_b^4+\left(s-m_t^2\right)^2}+2s\left(m_b^2-m_t^2+2m_W^2\right)\\ &\coth^{-1}\left(\frac{-m_b^2+m_t^2+s}{\sqrt{-2m_b^2\left(m_t^2+s\right)+m_b^4+\left(s-m_t^2\right)^2}}\right))-4sc_b m_b^2 c_t m_t^2\\ &(\coth^{-1}\left(\frac{m_b^2-m_t^2+s}{\sqrt{-2m_b^2\left(m_t^2+s\right)+m_b^4+\left(s-m_t^2\right)^2}}\right)+\\ &\coth^{-1}\left(\frac{-m_b^2+m_t^2+s}{\sqrt{-2m_b^2\left(m_t^2+s\right)+m_b^4+\left(s-m_t^2\right)^2}}\right))\end{aligned} \tag{B.11}$$

Finally the cross sections of scatterings involving bosons in the initial state are shown:

$$\sigma_{q\gamma\to qa} = \frac{Q_q^2 C_q^2 e^2}{32\pi f_a^2}\frac{m_q^2}{s^2(s-m_q^2)}\left(2s^2\log\left(\frac{s}{m_q^2}\right)-3s^2+4m_q^2 s-m_q^4\right) \tag{B.12}$$

$$\sigma_{qg\to qa} = \frac{C_q^2 g_s^2}{192\pi f_a^2}\frac{m_q^2}{s^2(s-m_q^2)}\left(2s^2\log\left(\frac{s}{m_q^2}\right) - 3s^2 + 4m_q^2 s - m_q^4\right) \tag{B.13}$$

$$\begin{aligned}\sigma_{qb\to qa} =& \frac{C_q^2 y_q^2}{64\pi f_a^2}\frac{s-m_t^2}{s[(m_q^2-m_b^2+s)^2-4m_q^2 s]}\Big[(-m_b^2+m_q^2+s)\sqrt{[s-(m_b-m_q)^2][s-(m_b+m_q)^2]}- \\ & 2sm_q^2\log\left(-\frac{\sqrt{[s-(m_b-m_q)^2][s-(m_b+m_q)^2]}+s-m_b^2+m_q^2}{\sqrt{[s-(m_b-m_q)^2][s-(m_b+m_q)^2]}-s+m_b^2-m_q^2}\right)\Big]\end{aligned} \tag{B.14}$$

$$\begin{aligned}\sigma_{bZ^0\to ba} =& \frac{C_b^2 g^2}{3456\pi f_a^2}\frac{m_b^2(s-m_b^2)}{s^2 m_W^2 m_Z^2\sqrt{(m_b^2-m_Z^2+s)^2-4m_b^2 s]}}\Bigg(\frac{-2s^2\left(-m_Z^2\left(9m_b^2+4m_W^2\right)+80m_W^4+5m_Z^4\right)}{\sqrt{m_b^4-2m_b^2\left(m_Z^2+s\right)+\left(m_Z^2-s\right)^2}} \\ & \log\left(\frac{m_b^2+\sqrt{\left(s-(m_b-m_z)^2\right)\left(s-(m_b+m_z)^2\right)}-m_Z^2+s}{m_b^2-\sqrt{\left(s-(m_b-m_Z)^2\right)\left(s-(m_b+m_Z)^2\right)}-m_Z^2+s}\right)+3s(m_Z^2(3m_b^2+4m_W^2)- \\ & 8m_W^4-4m_Z^4)+(m_b^2-m_Z^2)(-4m_W^2m_Z^2+8m_W^4+5m_Z^4)+9s^2m_Z^2\Bigg)\end{aligned} \tag{B.15}$$

$$\begin{aligned}\sigma_{tW^-\to ba} =& \frac{g^2\left(s-{m_b}^2\right)}{384\pi {m_W}^2 s^2\left(\left({m_t}^2-{m_W}^2+s\right)^2-4{m_t}^2 s\right)}\Big(\sqrt{{m_t}^4-2{m_t}^2\left({m_W}^2+s\right)+\left({m_W}^2-s\right)^2} \\ & \left({c_b}^2{m_b}^2\left({m_t}^4+{m_t}^2\left({m_W}^2-2s\right)-2{m_W}^4+{m_W}^2 s+s^2\right)+2c_b c_t {m_b}^2{m_t}^2\right. \\ & \left.\left(-{m_t}^2+{m_W}^2+3s\right)+{c_t}^2{m_t}^2\left({m_b}^2\left({m_t}^2-{m_W}^2-3s\right)+s({m_t}^2-\right.\right. \\ & \left.\left.{m_W}^2+s)\right))+2c_t^2 m_t^2 s^2\log\left(\frac{{m_t}^2-\sqrt{{m_t}^4-2{m_t}^2\left({m_W}^2+s\right)+\left({m_W}^2-s\right)^2}-{m_W}^2+s}{{m_t}^2+\sqrt{{m_t}^4-2{m_t}^2\left({m_W}^2+s\right)+\left({m_W}^2-s\right)^2}-{m_W}^2+s}\right) \\ & \left(2c_b{m_b}^2+c_t\left(-{m_b}^2+{m_t}^2-2{m_W}^2\right)\right)\Big)\end{aligned} \tag{B.16}$$

$$\sigma_{bW^+\to ta} = \frac{g^2\left(s-{m_t}^2\right)}{384\pi {m_W}^2 s^2\left(\left({m_b}^2-{m_W}^2+s\right)^2-4{m_b}^2 s\right)}\Big(\sqrt{{m_b}^4-2{m_b}^2\left({m_W}^2+s\right)+\left({m_W}^2-s\right)^2}$$
$$\left({c_t}^2{m_t}^2\left({m_b}^4+{m_b}^2\left({m_W}^2-2s\right)-2{m_W}^4+{m_W}^2 s+s^2\right)+2c_t c_b {m_t}^2{m_b}^2\right.$$
$$\left.\left(-{m_b}^2+{m_W}^2+3s\right)+{c_b}^2{m_b}^2\left({m_t}^2\left({m_b}^2-{m_W}^2-3s\right)+s\left({m_b}^2-\right.\right.\right.$$
$$\left.\left.\left.{m_W}^2+s\right)\right)\right)+2c_b^2 m_b^2 s^2\log\left(\frac{{m_b}^2-\sqrt{{m_b}^4-2{m_b}^2\left({m_W}^2+s\right)+\left({m_W}^2-s\right)^2}-{m_W}^2+s}{{m_b}^2+\sqrt{{m_b}^4-2{m_b}^2\left({m_W}^2+s\right)+\left({m_W}^2-s\right)^2}-{m_W}^2+s}\right)$$
$$\left(2c_t{m_t}^2+c_b\left(-{m_t}^2+{m_b}^2-2{m_W}^2\right)\right)\Big) \tag{B.17}$$

C

Boltzmann equation

The Boltzmann equation represents a fundamental tool to track the evolution of particles in the Early Universe. In this section we will derive it for the number density and adjust it for the case of binary scatterings.
Given the distribution function $f(x^\mu, p^\mu)$ for our particle, that in general will depend on its spacetime position and its four momentum, we can generically write the Boltzamann equation as:

$$L[f] = C[f] \tag{C.1}$$

On the left hand side we have the Liouville operator L, that represents the evolution for f due to spacetime geometry: denoted with λ the affine parameter which parametrizes the particle's trajectory in the spacetime, it reads[1]:

$$L[f(x^\mu, p^\mu)] = \frac{dx^\mu}{d\lambda}\frac{\partial f}{\partial x^\mu} + \frac{dp^\mu}{d\lambda}\frac{\partial f}{\partial p^\mu} = \left(p^\mu \frac{\partial}{x^\mu} - \Gamma^\mu_{\nu\rho} p^\nu p^\rho \frac{\partial}{\partial p^\mu}\right) f$$

[1] We used the fact that for the physical four-momentum $p^\mu = \frac{dx^\mu}{d\lambda}$ we have the geodesic equation:

$$\frac{dp^\mu}{d\lambda} + \Gamma^\mu_{\nu\rho} p^\nu p^\rho = 0$$

where $\Gamma^\mu_{\nu\rho} = \frac{1}{2} g^{\mu\gamma}\left(\frac{\partial g^{\gamma\nu}}{\partial x^\rho} + \frac{\partial g^{\gamma\rho}}{\partial x^\nu} - \frac{\partial g^{\nu\rho}}{\partial x^\gamma}\right)$ is the affine connection.

In a homogeneous and isotropic Universe, f turns out to depend only on the time and the modulus of the momentum, or alternatively on the whole energy, i.e. $f(t, E)$. Then in a FLRW metric the Liuoville operator becomes[2]:

$$L[f(t,E)] = E\frac{\partial f}{\partial t} - Hp^2\frac{\partial f}{\partial E}$$

where $H = \frac{\dot{a}}{a}$ is the Hubble parameter. Since we need an equation for the number density, we integrate both sides of C.1 in d^3p, and simultaneously multiply by $\frac{g}{(2\pi)^3}$ and divide by E. Then we require a little bit of work[3] to obtain:

$$\dot{n}(t) + 3Hn(t) = \frac{g}{(2\pi)^3}\int d^3p\frac{C[f(t,E)]}{E} \tag{C.2}$$

The right hand side takes into account all the possible interactions. Indeed C is known as the collision operator: we immediately see from C.2 that if we have $C = 0$, meaning that the particle does not interact in any way, than the RHS vanishes and the equation yields $n(t) \sim a^{-3}$, as we expect in an expanding universe. We are interested in tracking the number density of axions $n_a(t)$ involved in collisions of the kind $1 + 2 \to 3 + a$, so the collision operator reads:

$$\begin{aligned} RHS = \int d\Pi_1 d\Pi_2 d\Pi_3 d\Pi_a (2\pi^4)\delta^4(p_1 + p_2 - p_3 - k)[|\mathcal{M}|^2_{12\to 3a} f_1 f_2 (1 \pm f_3)(1 + f_a) - \\ |\mathcal{M}|^2_{3a\to 12} f_3 f_a (1 \pm f_1)(1 \pm f_2)] \end{aligned} \tag{C.3}$$

where $d\Pi_i = \frac{d^3p_i}{(2\pi)^3 2E_i}$ and $|\mathcal{M}|^2$ denotes the squared amplitude that is not yet averaged over the initial polarizations. The terms of the kind $1 \pm f_i$ account for quantum correction due to

[2] For a FLRW metric we have $\Gamma^0_{ij} = a\dot{a}\delta_{ij}$, $\Gamma^i_{0j} = \Gamma^i_{j0} = \frac{\dot{a}}{a}$

[3] The first term of the LHS is immediate:

$$\frac{g}{(2\pi)^3}\int d^3p\frac{\partial f(t,E)}{\partial t} = \frac{\partial}{\partial t}\left(\frac{g}{(2\pi)^3}\int d^3p f(t,E)\right) = \dot{n}(t)$$

Instead exploiting $EdE = pdp$ and integrating by parts, the second term can be rearranged as:

$$\frac{g}{(2\pi)^3}\int d^3p H\frac{p^2}{E}\frac{\partial f}{\partial E} = \frac{g}{(2\pi)^3}\int dpH\frac{p^4}{E}\frac{\partial f}{\partial E}\int d\Omega = \frac{g}{(2\pi)^3}\int dpHp^3\frac{\partial f}{\partial p}\int d\Omega = -3H\frac{g}{(2\pi)^3}\int dpp^2\int d\Omega = -3Hn(t)$$

the statistics of the involved particles[4]. Neglecting them and supposing temporal invariance so that $|\mathcal{M}|^2_{12\to 3a} = |\mathcal{M}|^2_{3a\to 12}$, the expression simplifies to:

$$RHS = \int d\Pi_1 d\Pi_2 d\Pi_3 d\Pi_a (2\pi^4)\delta^4(p_1 + p_2 - p_3 - k)|\mathcal{M}|^2_{12\to 3a}(f_1 f_2 - f_3 f_a)$$

If we assume kinetic equilibrium is reached, meaning that collisions occur rapidly compared to the time-scale under which conditions for our particles are changing, we can use for the phase space distribution the equilibrium one, that becomes $f = \frac{1}{exp((E-\mu)/T)\pm 1} \simeq e^{-(E-\mu)/T}$ once neglected quantum statistics. The chemical potential can be taken to be $\mu_i \simeq 0$ whenever also chemical equilibrium is reached, meaning that both forward and backward reactions for particle i are efficient. This is the condition of thermodynamic equilibrium, that we will suppose for particles 1, 2, and 3 in the thermal bath to solve our equation. Exploiting this assumption plus the conservation of energy, the term $f_1 f_2 - f_3 f_4 = f_1^{eq} f_2^{eq}(1 - n_a(t)/n_a^{eq})$. In a compact form we have:

$$\dot{n}_a(t) + 3Hn_a(t) = C_{1+2\to 3+a}(n_a^{eq} - n_a(t))/n_a^{eq} \tag{C.4}$$

We stress that this equation has been derived under the assumption of *kinetic* equilibrium (as well as a MB profile) for the axion particle.

C.1 Collision operator for scatterings

For a scattering $1 + 2 \to 3 + a$, where we take particles 1 and 2 to be in thermal equilibrium, we obtained the following term in the collision operator:

$$C_{1+2\to 3+a} = \int d\Pi_1 d\Pi_2 d\Pi_3 d\Pi_a (2\pi^4)\delta^4(p_1 + p_2 - p_3 - k) f_1^{eq} f_2^{eq} |\mathcal{M}|^2_{1+2\to 3+a} \tag{C.5}$$

Here the squared matrix element is summed over both initial and final polarizations, without taking any average. We can express the cross section formula B.1 in terms of Lorentz invariant relative velocity between the particles 1 and 2, defined as:

$$v_{12} = \frac{\sqrt{(p_1 \cdot p_2)^2 - m_1^2 m_2^2}}{p_1 \cdot p_2} = \frac{\lambda^{1/2}(s, m_1, m_2)}{p_1 \cdot p_2} \tag{C.6}$$

[4]Phase space 'cells' for final states may be already occupied, and fermions and bosons are less and more likely to occupy the same states, respectively. This leads to Pauli-blocking (− sign) and Bose-enhancement (+ sign) phenomena [15].

where $s = (p_1 + p_2)^2$ and $\lambda(x, y, z) = [x - (y+z)^2][x - (y-z)^2]$. Indeed provided that the flux can be written as $I = p1 \cdot p_2 v_{12}$ and accounting for the phase space B.3, the Lorentz invariant cross section reads:

$$\sigma_{1+2\to 3+a} = \frac{1}{g_1 g_2} \frac{1}{4p_1 \cdot p_2 v_{12}} \int d\Pi_3 d\Pi_a |\mathcal{M}|^2_{1+2\to 3+a} (2\pi)^4 \delta^4(p_1 + p_2 - p_3 - k) \qquad \text{(C.7)}$$

where we divided by an overall factor of $g_1 g_2$ because here the squared amplitude is not averaged. Then the C.5 can be written in terms of a thermally avraged cross section as it follows:

$$C_{1+2\to 3+a} = 2 g_1 g_2 \int d\Pi_1 d\Pi_2 f_1^{eq} f_2^{eq} \lambda^{1/2}(s, m_1, m_2) \sigma_{1+2\to 3+4} \qquad \text{(C.8)}$$

The integration measure is in polar coordinates is:

$$d\Pi_1 d\Pi_2 = \frac{|\vec{p_1}|^2 d|\vec{p_1}| d\Omega_1}{(2\pi)^3 2E_1} \frac{|\vec{p_2}|^2 d|\vec{p_2}| d\Omega_2}{(2\pi)^3 2E_2} = \frac{|\vec{p_1}||\vec{p_2}|}{32\pi^4} dE_1 dE_2 d\cos\theta \qquad \text{(C.9)}$$

Here the integration over three out of four angular variables has been trivially performed and we have identified the fourth one with the angle θ between the initial momenta. Moreover since the particles are on-shell $E_i dE_i = p_i d|\vec{p_i}|$. Now it is convenient to perform the following change of variables:

$$E_+ = E_1 + E_2 \qquad E_- = E_1 - E_2 \qquad s = m_1^2 + m_2^2 + 2(E_1 E_2 - |\vec{p_1}||\vec{p_2}| \cos\theta)$$

leading to the measure:

$$d\Pi_1 d\Pi_2 d\cos\theta = \frac{dE_+ dE_- ds}{128\pi^4}$$

while the integration region ($E_1 \geq m_1, E_2 \geq m_2, |\cos\theta| \leq 1$) is delimited by:

$$s \geq s_{min} = (m_1^2 + m_2^2) \qquad E_+ = \sqrt{s} \qquad \frac{|E_- - E_+(m_1^2 - m_2^2)/s|}{(E_+^2 - s)^{1/2}} \leq \frac{\lambda^{1/2}(s, m_1, m_2)}{s}$$

Since the product $f_1^{eq} f_2^{eq} = e^{-E_+/T}$ depends on E_+ the integration over dE_- is straightforward:

$$C_{1+2\to 3+a} = \frac{g_1 g_2}{32\pi^4} \times \int_{s_{min}} ds \frac{1}{s} \lambda(s, m_1, m_2) \sigma_{1+2\to 3+a}(s) \int_{\sqrt{s}} dE_+ e^{-E_+/T} (E_+^2 - s)^{1/2}$$

Integration over dE_+ yields a Bessel function, leading to our final expression for the collision operator:

$$C_{1+2\to 3+a} = \frac{g_1 g_2}{32\pi^4} T \int_{s_{min}} ds \frac{1}{\sqrt{s}} \lambda(s, m_1, m_2) \sigma_{1+2\to 3+a}(s) K_1(\sqrt{s}/T) \tag{C.10}$$

Combining this last and C.4 we finally obtain 5.1.

D

Code Implementation for Boltzmann System Solution

This appendix complements Section 6.1.2 of Chapter 6, where the solution to the Boltzmann system 6.7 for axion dark radiation across the EWPT, using the phase-space approach, is derived.

In the first section, we list all the analytic expressions for the amplitudes $|\mathcal{M}(s,t)|^2$ for the scatterings considered in this work, which contribute to the collision rate 6.6. Following that, we provide the main steps of the code that we used to derive numerical solution for 6.10. Additionally, we provide some insights into the phase-space analysis.

D.1 Scattering amplitudes

The generic expression for the amplitude of a process above the EWPT involving a quark $q = t, b$ is:

$$|\mathcal{M}|^2_{q\bar{q}\to\chi a} = C_q^2 y_q^2 s/(4f_a^2) \qquad |\mathcal{M}|^2_{q\chi\to qa} = -C_q^2 y_q^2 t/(2f_a^2) \tag{D.1}$$

On the other hand we have the following amplitudes below the EWPT:

$$|\mathcal{M}|^2_{q\bar{q}\to\gamma a} = \frac{Q_q^2 C_q e^2 m_q^2 s^2}{f_a^2(m_q^2-t)(s+t-m_q^2)} \qquad |\mathcal{M}|^2_{q\gamma\to qa} = -\frac{Q_q^2 C_q^2 e^2 m_q^2 t^2}{f_a^2(m_q^2-s)(s+t-m_q^2)} \tag{D.2}$$

$$|\mathcal{M}|^2_{q\bar{q}\to ga} = \frac{4C_q^2 g_s^2 m_q^2 s^2}{f_a^2 9(m_q^2 - t)(s + t - m_q^2)} \qquad |\mathcal{M}|^2_{q\gamma\to qa} = -\frac{C_q^2 g_s^2 m_q^2 t^2}{f_a^2 6(m_q^2 - s)(t + s - m_q^2)} \tag{D.3}$$

$$\begin{aligned} |\mathcal{M}|^2_{q\bar{q}\to ba} &= \frac{y_q^2 C_q^2}{32 f_a^2} \frac{8(m_b^4 m_q^2 - m_b^2 s(m_q^2 + t) + s(m_q^4 - 2m_q^2 t + t(s + t)))}{(m_q^2 - t)(m_b^2 + m_q^2 - s - t)} \\ |\mathcal{M}|^2_{qb\to qa} &= -\frac{y_q^2 C_q^2}{16 f_a^2} \frac{8(m_b^4 m_q^2 - m_b^2 t(m_q^2 + s) + t(m_q^4 - 2m_q^2 s + s(t + s)))}{(m_q^2 - s)(m_b^2 + m_q^2 - t - s)} \end{aligned} \tag{D.4}$$

$$\begin{aligned} |\mathcal{M}|^2_{t\bar{t}\to Z^0 a} &= -\frac{g^2 C_t^2 m_Z^2}{16 f_a^2 m_W^2} \Big(2m_t^2 (9m_t^4 (2m_Z^4 - m_Z^2 s) + 9m_t^2 (m_Z^4 (s + 4t) + 2m_Z^2 st) + \\ &32m_W^4 (m_Z^2 - s)^2 - 40m_W^2 (m_Z^3 - m_Z s)^2 + 17m_Z^8 - 2m_Z^6 (17s + 9t) + m_Z^4 (17s^2 + 27st + 18t^2) - \\ &9m_Z^2 st(s + t)) \Big) \frac{1}{9m_Z^4 (m_t^2 - t)(mt^2 + m_Z^2 - s - t)} \\ |\mathcal{M}|^2_{tZ^0\to ta} &= \frac{g^2 C_t^2 m_Z^2}{24 f_a^2 m_W^2} \Big(2m_t^2 (9m_t^4 (2m_Z^4 - m_Z^2 t) + 9m_t^2 (m_Z^4 (t + 4s) + 2m_Z^2 ts) + \\ &32m_W^4 (m_Z^2 - t)^2 - 40m_W^2 (m_Z^3 - m_Z t)^2 + 17m_Z^8 - 2m_Z^6 (17t + 9s) + m_Z^4 (17t^2 + 27ts + 18s^2) - \\ &9m_Z^2 ts(t + s)) \Big) \frac{1}{9m_Z^4 (m_t^2 - s)(mt^2 + m_Z^2 - t - s)} \end{aligned} \tag{D.5}$$

$$
\begin{aligned}
|\mathcal{M}|^2_{b\bar{b}\to Z^0 a} &= -\frac{g^2 C_b^2 m_Z^2}{16 f_a^2 m_W^2}\Big(2m_b^2(9m_b^4(2m_Z^4 - m_Z^2 s) + 9m_b^2(m_Z^4(s+4t) + 2m_Z^2 st) + \\
&8m_W^4(m_Z^2 - s)^2 - 4m_W^2(m_Z^3 - m_Z s)^2 + 5m_Z^8 - 2m_Z^6(5s+9t) + m_Z^4(5s^2 + 27st + 18t^2) - \\
&9m_Z^2 st(s+t))\Big)\frac{1}{9m_Z^4(m_b^2 - t)(mb^2 + m_Z^2 - s - t)} \\
|\mathcal{M}|^2_{bZ^0\to ba} &= \frac{g^2 C_b^2 m_Z^2}{24 f_a^2 m_W^2}\Big(2m_b^2(9m_b^4(2m_Z^4 - m_Z^2 t) + 9m_b^2(m_Z^4(t+4s) + 2m_Z^2 ts) + \\
&8m_W^4(m_Z^2 - t)^2 - 4m_W^2(m_Z^3 - m_Z t)^2 + 5m_Z^8 - 2m_Z^6(5t+9s) + m_Z^4(5t^2 + 27ts + 18s^2) - \\
&9m_Z^2 ts(t+s))\Big)\frac{1}{9m_Z^4(m_b^2 - s)(mb^2 + m_Z^2 - t - s)}
\end{aligned}
\tag{D.6}
$$

$$
\begin{aligned}
|\mathcal{M}|^2_{t\bar{b}\to W^+ a} &= \frac{g^2}{8fa^2 m_W^2(t - m_b^2)(-m_b^2 - m_W^2 + s + t)}\Big(C_b^2 m_b^2((-m_b^2 - m_W^2 + s + t)(m_W^2(m_b^2 + \\
&m_t^2 - 2(s+t)) + s(t - m_t^2) + 2m_W^4)) + C_t^2 m_t^2((t - m_b^2)(m_W^2(m_b^2 + m_t^2 - s - 2t) + s(-m_t^2 + \\
&s+t))) + 2C_b m_b^2 C_t m_t^2 (s - m_W^2)^2\Big) \\
|\mathcal{M}|^2_{tW^-\to ba} &= \frac{-g^2}{12fa^2 m_W^2(s - m_b^2)(-m_b^2 - m_W^2 + t + s)}\Big(C_b^2 m_b^2((-m_b^2 - m_W^2 + t + s)(m_W^2(m_b^2 + \\
&m_t^2 - 2(t+s)) + t(s - m_t^2) + 2m_W^4)) + C_t^2 m_t^2((s - m_b^2)(m_W^2(m_b^2 + m_t^2 - t - 2s) + s(-m_t^2 + \\
&t+s))) + 2C_b m_b^2 C_t m_t^2 (t - m_W^2)^2\Big)
\end{aligned}
\tag{D.7}
$$

As done for the corresponding cross sections (4.3), a good check is ensuring that in the limit of vanishing masses the scattering amplitudes below EWPT involving the longitudinal components of massive gauge bosons coincide exactly with those above. This is easy to see:

- *neutral annihilations*:

$$
|\mathcal{M}|^2_{t\bar{t}\to\chi_0 a} + |\mathcal{M}|^2_{t\bar{t}\to\chi_0' a} = |\mathcal{M}|^2_{t\bar{t}\to ha} + |\mathcal{M}|^2_{t\bar{t}\to Z_L^0 a} = \frac{C_t^2 y_t^2 s}{2f_a^2}
$$

- *neutral scatterings*

$$|\mathcal{M}|^2_{t\chi_0\to ta} + |\mathcal{M}|^2_{t\chi_0'\to ta} = |\mathcal{M}|^2_{th\to ta} + |\mathcal{M}|^2_{tZ_L^0\to ta} =$$
$$= |\mathcal{M}|^2_{\bar{t}\chi_0'\to \bar{t}a} + |\mathcal{M}|_{\bar{t}\chi_0\to \bar{t}^2 a} = |\mathcal{M}|^2_{\bar{t}h\to \bar{t}a} + |\mathcal{M}|^2_{\bar{t}Z_L^0\to \bar{t}a} = \frac{-C_t^2 y_t^2 t}{f_a^2}$$

- *charged annihilations:*

$$|\mathcal{M}|^2_{t\bar{b}\to \chi_+ a} + |\mathcal{M}|^2_{b\bar{t}\to \chi_- a} = |\mathcal{M}|^2_{t\bar{b}\to W_L^+ a} + |\mathcal{M}|^2_{b\bar{t}\to W_L^- a} = \frac{(C_t^2 y_t^2 + C_b^2 y_b^2)s}{2f_a^2}$$

- *charged scatterings*

$$|\mathcal{M}|^2_{t\chi_-\to ba} + |\mathcal{M}|^2_{b\chi_+\to ta} = |\mathcal{M}|^2_{tW^-\to ba} + |\mathcal{M}|^2_{bW^+\to ta} =$$
$$= |\mathcal{M}|^2_{\bar{t}\chi_+\to \bar{b}a} + |\mathcal{M}|^2_{\bar{b}\chi_-\to \bar{t}a} = |\mathcal{M}|^2_{\bar{t}W_L^+\to \bar{b}a} + |\mathcal{M}|^2_{\bar{b}W_L^-\to \bar{t}a} = \frac{-(C_t^2 y_t^2 + C_b^2 y_b^2)t}{f_a^2}$$

D.2 The Code

In this section we point out how Python could be used to model the evolution of the dark radiation phase space distribution (PSD) due to interactions with the thermal bath, which involves numerically solving an integro-differential system. Python is particularly well-suited for this task due to its extensive ecosystem of scientific libraries, such as NumPy and SciPy, which enable efficient numerical computations, differential equation solving, and data manipulation. The combination of these tools makes Python a convenient and powerful choice for complex physical simulations, such as tracking the behavior of dark radiation over time.

The first step is deriving the collision rate 6.6 for all scattering amplitudes presented in the previous section. While for amplitudes above the EWPT, this integral is analitically solvable, for the ones below the solution has to be fully numeric.
In what follows the `create_rate_function(Msq, m1, m2, m3, g1, g2, g3)` takes as input arguments a symbolic expression for the amplitude $|\mathcal{M}(t,s)|^2$, alongside the associated masses and degrees of freedom. It returns a `create_rate_function(T,p)` that can be evaluated at a given temperature and momentum.

```python
import numpy as np
import sympy as sp
from scipy.integrate import quad
import matplotlib.pyplot as plt
from scipy.interpolate import RectBivariateSpline

# symbolic variables
t,s= sp.symbols('t, s')

# Function to evaluate t_max and t_min
def calculate_tmin_tmax(s_val, m1, m2, m3):
    lamb = (s_val - (m1 + m2)**2) * (s_val - (m1 - m2)**2)
    k12 = np.sqrt(lamb / (4 * s_val))
    tmax = m1**2 - 2 * (s_val - m3**2) / np.sqrt(4 * s_val) *
    (np.sqrt(m1**2 + k12**2) - k12)
    tmin = m1**2 - 2 * (s_val - m3**2) / np.sqrt(4 * s_val) *
    (np.sqrt(m1**2 + k12**2) + k12)
    return tmin, tmax

# Function to create the rate
def create_rate_function(Msq, m1, m2, m3, g1, g2, g3):
    Msq_func = sp.lambdify((t, s), Msq, 'numpy')

    def rate_function(T, p):

        def integrand_s(s_val):
            # Calcola tmin e tmax
            tmin, tmax = calculate_tmin_tmax(s_val, m1, m2, m3)

            # Integrand with respect to t
            def integrand_t(t_val):
                return Msq_func(t_val, s_val)

```

```
            # Numerically integrate over t
            integral_t_val, _ = quad(integrand_t, tmin, tmax, limit=1000)

            # Calculates E3
            E3 = ((s_val-m3**2)/(4 * p))+((p * m3**2)/(s_val-m3**2))

            # Integrand with respect to s
            return np.exp(-E3 / T) * integral_t_val / (s_val - m3**2)

        # Calculate smin
        smin = max((m1 + m2)**2, m3**2)

        # Numerically integrate over s
        Integral, _ = quad(integrand_s, smin, np.inf, limit=1000)


        # Final rate
        rate = (g1 * g2 * g3 / (256 * np.pi**3)) * (T * np.exp(-p / T)
        / p**2) * Integral

        return rate

    return rate_function
```

The integral 6.6 can be solved for each process and evaluated for values of temperature T and momentum k. The temperature covers the range $[1, 245]$ GeV, for the sum of rates valid below the EWPT, and $[245, 10000]$ GeV for the ones above. The momentum, instead, has to be taken in a logarithmic spaced interval, such as $\frac{k}{T} \in [10^{-4}, 10^{3}]$ GeV, to carefully select the relevant momenta. Then the rate values obtained in this way can be interpolated over a grid $[T, k/T]$ using `RectBivariateSpline`, resulting in two functions. Finally the rate $C(k, T)$ that enters the right hand side of the first two equations in the system 6.7 can be defined in terms of an `if` statement that switches between the interpolated functions obtained above and below 245 GeV and is set it to zero once 1 GeV is exceeded:

```
def unified_interpolation(T, k):
    if T > 245:
        return rate_interpolated_above(T, k/T)
    if  245 >= T >= 1:
        return  rate_interpolate_below(T,k/T)
    else :
        return np.zeros_like(rate_interpolated_below(T, k/T))
```

The top and bottom-axion couplings have been set to one: $C_{t,b} = 1$. In what follows we report the definitions of all the quantities and constants that feed the Boltzmann system. The letter X is denotes generically dark radiation, in our case standing for axions. The value the temperature of the thermal bath T can be obtained the evolution variable A through an iterative implementation. A key ingredient for the definition of the relationship $T(A)$ is the function for the evolution of the effective number of the energy density degrees of freedom `g_star_rho_interp(T)`. This comes from interpolation of tabulated data of T and $g_\rho^*(T)$. The same procedure is adopted for the function for the equation of state parameter evolution `w_B_fun(T)`.

```
# Constants
M_pl = 2.4 * (10**18)  # Planck mass
T_I = 10**4  # High-temperature scale
g_X = 1.0  # Placeholder for degrees of freedom of dark radiation

# Function C(q, A)
def C(q, A,T, fa):
    k=q*T_I/A
    T_A=T
    result=unified_interpolation(T_A,k)#
   # print(f"C_rate result for T={T_A}, k={k}: {result}")

    if result is None:
        raise ValueError("The unified_interpolation returned None.")
    return result.flatten()/ (fa**2)

```

```
# Function for the equilibrium distribution of X
def f_eq_X(q, A, T):
    k=q*T_I/A
    T_A=T
    return   np.exp(- k / T_A) #MB 1 / (np.exp(k / T_A) - 1)#BE


# Function to calculate R_X(A)
def R_X(f_X, q_bins):
    return (g_X / (2 * np.pi**2)) * np.trapz(q_bins**3 * f_X, q_bins)
```

Finally the code provided below is designed to track how the distribution of axion dark radiation changes due to scatterings with thermal bath particles as the universe expands, specifically across the Electro-Weak Phase Transition. The momentum space is divided into logarithmically spaced intervals, referred to as momentum bins. This binning approach allows the model to compute the distribution function across a wide range of energies, providing a detailed picture of how dark radiation evolves. By summing over these bins, the code performs the necessary integrals to calculate quantities such as the energy density of the axions and the thermal bath.

To carry out these integrals, the `trapz` function from the NumPy library is employed, which uses the trapezoidal rule for numerical integration. This method is particularly effective for integrating discrete data points, which is common in simulations involving momentum bins. Additionally, the `odeint` function from SciPy's integration module is used to solve the system of differential equations over a range of scale factors, starting from an initial condition where dark radiation is absent. This allows the model to dynamically evolve the dark radiation distribution as the universe expands.

```
import numpy as np
from scipy.integrate import odeint

# Function C(q, A)
def C(q, A,T, fa):
    k=q*T_I/A
    T_A=T
```

```
    result=unified_interpolation(T_A,k)#
   # print(f"C_rate result for T={T_A}, k={k}: {result}")

    if result is None:
        raise ValueError("The unified_interpolation_2 returned None.")
    return result.flatten()/ (fa**2)

# Function for the equilibrium distribution of X
def f_eq_X(q, A, T):
    k=q*T_I/A
    T_A=T
    return   np.exp(- k / T_A) #1 / (np.exp(k / T_A) - 1)#



# Function to calculate R_X(A)
def R_X(f_X, q_bins):
    return (g_X / (2*( np.pi**2))) * np.trapz((q_bins**3)* f_X, q_bins)

T_values=[]
# System of differential equations
def derivatives(y, logA, N_q, q_bins, fa):
    A = np.exp(logA)
    f_X = y[:N_q]
    R_B = y[N_q]

    R_X_val = R_X(f_X, q_bins)

    TT=1/A
    for i in range(7):
        TT = ( R_B /(np.pi**2/30 * g_star_rho_interp(TT)) )**(1./4.)
        *T_I /A
      #print(TT)
```

```
    T_values.append(TT)
    # Calculate R_X(A)


    # Update Hubble parameter H
    H = np.sqrt((R_B + R_X_val) / (3 * (M_pl**2))) * (T_I**2 / A**2)

    # Differential equations for f_X
    d_f_X_dlogA = np.zeros(N_q)
    for i, q in enumerate(q_bins):
        C_val = C(q, A, TT, fa)
        d_f_X_dlogA[i] =(C_val / H) * (1 - f_X[i] / f_eq_X(q, A, TT))



    integrand = q_bins**3 * (1 - f_X / f_eq_X(q_bins, A, TT)) *
    C(q_bins, A,TT, fa) / H
    integral = np.trapz(integrand, q_bins)
    dR_B_dlogA =  - (3 * w_B_fun(TT) - 1) * R_B- (g_X / (2 * np.pi**2))
    * integral

    return np.concatenate([d_f_X_dlogA, [dR_B_dlogA]])
# Number of momentum bins
N_q = 64

# Define logarithmically spaced bins
q_bins = np.logspace(np.log10(0.005), np.log10(20), N_q)


# Set initial conditions
initial_f_X = np.zeros(N_q)  # Initial f_X(q, A)
initial_R_B = g_star_rho_interp(T_I) *np.pi**2/30 # Initial R_B
initial_conditions = np.concatenate([initial_f_X, [initial_R_B]])
```

```
74
75  # Define the range for integration
76  logA_start =0
77  logA_end =  np.log10(T_I/2e-6)
78
79  A_steps= np.logspace(0,logA_end,100)
80
81
82  # Extract results for a fixed value of fa
83  solution = odeint(derivatives, initial_conditions, np.log(A_steps),
84  args=(N_q, q_bins, 10**6), atol=1e-6, rtol=1e-6, hmax=0.01)
85
86
87  f_X_solution = solution[:, :N_q]
88  R_B_solution= solution[:, N_q]
89  R_X_solution= R_X(f_X_solution, q_bins)
90
91
92  DeltaN_eff=8/7 * ((11/4)**(4/3))*(R_X_solution[-1]/(2*(R_B_solution[-1])
93  /g_star_rho_interp(T_values[-1]))
94  print(DeltaN_eff)
```

We show the results for the PSD $f_X(q, \mathcal{A})$, where the scale factor is given at given temperature $\mathcal{A}(T)$, as function of the cohomoving momentum in figure D.1, both rescaled in a convenient way in order to compare the shape of the PSD at given temperatures[1].Here we use a definition for the dark radiation temperature[2], that does not rely upon the assumption of thermalization,

[1] The multiplicative factor $(g_X/2\pi^2)q^3$ is needed to identify the integrand whose integral leads to the dimensionless comoving energy density R_X. Indeed we divide by the quantity R_X to compare the PSD at different moments. Initially, before the production processes become efficient, the value of f_X is rather small, and it grows later on. Thus we are comparing the shape of the PSD at different times and not the overall normalization. The choice of the variable on the horizontal axis is also convenient because we want to investigate when we achieve thermalization.

[2] Applying this to the expression for f_{eq}, one finds that the dark radiation temperature is equal to the one of the thermal bath, i.e. $T_X = T$.

extracted from the PSD as its second moment [1]:

$$T_X(A) = \frac{T_I}{A}\Big(\frac{\int dqq^4 f_X(q,A)}{\int dqq^2 f_X(q,A)}\Big)^{1/2}(2\sqrt{3})^{-1}$$

We compare the $f_X(q,A)$ with the reference thermal distribution, for which we take the MB type: $f_{eq,X}(q,A) = \exp\left(T_I q/(A T_X(A))\right)$. We notice that already at early-times the PSD, that appears to be higher and skewed towards higher momenta, reaches a thermal profile, for lower values of f_a, such that the interactions are efficient. This is likely due to the enhanced production rates in the unbroken phase, where quarks are massless and there is no thermal suppression. As the temperature drops and the EWPT occurs, the quarks gain their masses and the Universe gets less dense, leading to a lower production. Finally, the late-time PSD, when axion production has ceased, is the free-streaming one. Nevertheless also smaller couplings , i.e. values of f_a such that thermalization is never or barely achieved, could give a contribution to non-thermal axion production. Furthermore this approach could possibly capture momentum-specific behaviours, that in general are neglected in the canonical number density approach, that averages over all momentum modes and tends to smooth out the variations.

We conclude by stating that the computational implementation sketched in this appendix should be considered preliminary and requires further validation as well as the employment of more accurate numerical methods to ensure robustness and precision.

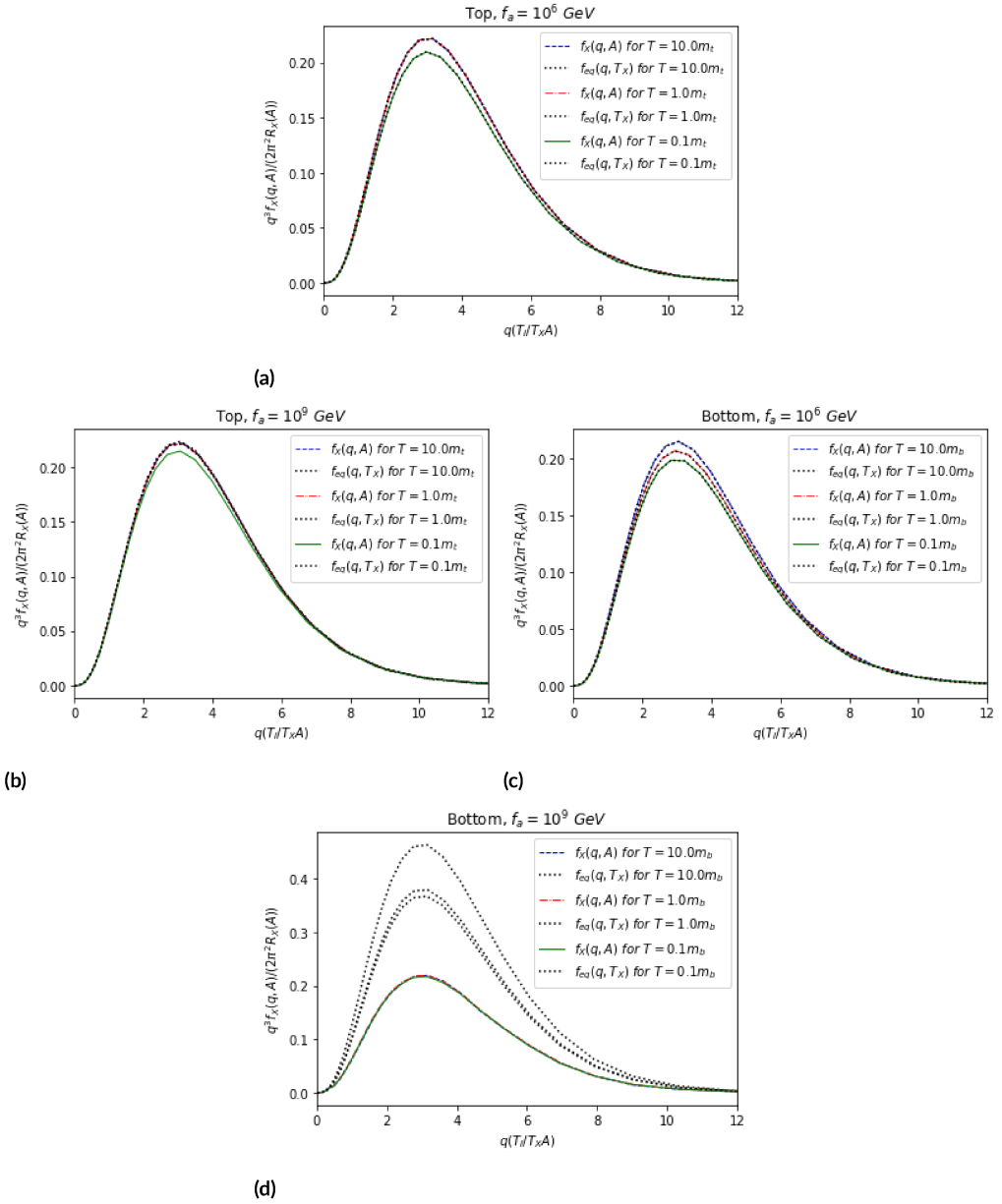

Figure D.1: Plots of f_X as a function of the comoving momentum for production via top- and bottom-axion couplings (with $f_a = 10^6, 10^9$). Various colors correspond to different scale factor values, i. e. different bath temperature T. We compare them with the thermal distribution with temperature $T_X(A)$ (dotted black lines).

References

[1] F. D'Eramo, F. Hajkarim, and A. Lenoci, "Dark radiation from the primordial thermal bath in momentum space," *Journal of Cosmology and Astroparticle Physics*, vol. 2024, no. 03, p. 009, 2024.

[2] R. Peccei, "Discrete and global symmetries in particle physics," in *Broken Symmetries: Proceedings of the 37. Internationale Universitätswochen für Kern-und Teilchenphysik, Schladming, Austria, February 28–March 7, 1998*. Springer, 2007, pp. 1–50.

[3] J. S. Bell and R. W. Jackiw, "A *pcac* puzzle: $\pi^0 \to \gamma\gamma$ in the σ-model," *Nuovo cimento*, vol. 60, no. CERN-TH-920, pp. 47–61, 1969.

[4] K. Fujikawa, "Path-integral measure for gauge-invariant fermion theories," *Physical Review Letters*, vol. 42, no. 18, p. 1195, 1979.

[5] A. Hook, "Tasi lectures on the strong cp problem and axions," *arXiv preprint arXiv:1812.02669*, 2018.

[6] L. Di Luzio, M. Giannotti, E. Nardi, and L. Visinelli, "The landscape of *qcd* axion models," *Physics Reports*, vol. 870, pp. 1–117, 2020.

[7] D. J. Marsh, "Axion cosmology," *Physics Reports*, vol. 643, pp. 1–79, 2016.

[8] E. Kolb, *The early universe*. CRC press, 2018.

[9] C. A. O'Hare, "Cosmology of axion dark matter," *arXiv preprint arXiv:2403.17697*, 2024.

[10] A. Gangui, "Cosmology from topological defects," in *AIP Conference Proceedings*, vol. 668, no. 1. American Institute of Physics, 2003, pp. 226–262.

[11] O. Pisanti, G. Mangano, G. Miele, and P. Mazzella, "Primordial deuterium after luna: concordances and error budget," *Journal of Cosmology and Astroparticle Physics*, vol. 2021, no. 04, p. 020, 2021.

[12] T.-H. Yeh, J. Shelton, K. A. Olive, and B. D. Fields, "Probing physics beyond the standard model: limits from bbn and the cmb independently and combined," *Journal of Cosmology and Astroparticle Physics*, vol. 2022, no. 10, p. 046, 2022.

[13] P. Collaboration, N. Aghanim, Y. Akrami, M. Ashdown, J. Aumont, C. Baccigalupi, M. Ballardini, A. Banday, R. Barreiro, N. Bartolo *et al.*, "Planck 2018 results. vi. cosmological parameters," 2020.

[14] F. Arias-Aragón, F. D'Eramo, R. Z. Ferreira, L. Merlo, and A. Notari, "Production of thermal axions across the electroweak phase transition," *Journal of Cosmology and Astroparticle Physics*, vol. 2021, no. 03, p. 090, 2021.

[15] F. D'Eramo and A. Lenoci, "Lower mass bounds on fimp dark matter produced via freeze-in," *Journal of Cosmology and Astroparticle Physics*, vol. 2021, no. 10, p. 045, 2021.

[16] P. Ade, J. Aguirre, Z. Ahmed, S. Aiola, A. Ali, D. Alonso, M. A. Alvarez, K. Arnold, P. Ashton, J. Austermann *et al.*, "The simons observatory: science goals and forecasts," *Journal of Cosmology and Astroparticle Physics*, vol. 2019, no. 02, p. 056, 2019.

[17] K. N. Abazajian, P. Adshead, Z. Ahmed, S. W. Allen, D. Alonso, K. S. Arnold, C. Baccigalupi, J. G. Bartlett, N. Battaglia, B. A. Benson *et al.*, "Cmb-s4 science book," *arXiv preprint arXiv:1610.02743*, 2016.

[18] K. Abazajian, A. Abdulghafour, G. E. Addison, P. Adshead, Z. Ahmed, M. Ajello, D. Akerib, S. W. Allen, D. Alonso, M. Alvarez *et al.*, "Snowmass 2021 cmb-s4 white paper," *arXiv preprint arXiv:2203.08024*, 2022.

[19] N. Sehgal, S. Aiola, Y. Akrami, K. Basu, M. Boylan-Kolchin, S. Bryan, S. Clesse, F.-Y. Cyr-Racine, L. Di Mascolo, S. Dicker *et al.*, "Cmb-hd: an ultra-deep, high-resolution millimeter-wave survey over half the sky," *arXiv preprint arXiv:1906.10134*, 2019.

[20] M. Dine, "Tasi lectures on the strong cp problem," *arXiv preprint hep-ph/0011376*, 2000.

[21] R. D. Peccei, "*The Strong CP Problem and Axions*," 2006.

[22] D. V. S. M. E. Peskin, *An Introduction to Quantum Field Theory*. CRC Press Taylor & Francis Group, 2018.

[23] A. Caputo and G. Raffelt, "Astrophysical axion bounds: The 2024 edition," *arXiv preprint arXiv:2401.13728*, 2024.

[24] P. Sikivie, "Axion cosmology," in *Axions: Theory, Cosmology, and Experimental Searches*. Springer, 2008, pp. 19–50.

[25] P. Gondolo and G. Gelmini, "Cosmic abundances of stable particles: Improved analysis," *Nuclear Physics B*, vol. 360, no. 1, pp. 145–179, 1991.

[26] R. Z. Ferreira and A. Notari, "Observable windows for the qcd axion through the number of relativistic species," *Physical Review Letters*, vol. 120, no. 19, p. 191301, 2018.

[27] F. Nicolas, P. Stefano *et al.*, "Dark matter freeze-in production in fast-expanding universes," *JCAP*, vol. 2, 2018.

[28] F. D'Eramo, R. Z. Ferreira, A. Notari, and J. L. Bernal, "Hot axions and the ho tension," *Journal of Cosmology and Astroparticle Physics*, vol. 2018, no. 11, p. 014, 2018.

[29] W. Von Schlippe, "Relativistic kinematics of particle interactions," *University of Utah*, 2002.

[30] L. Husdal, "On effective degrees of freedom in the early universe," *Galaxies*, vol. 4, no. 4, p. 78, 2016.

[31] F. D'Eramo, "Axions in the early universe," *SciPost Physics Proceedings*, no. 12, p. 005, 2023.